The Pennsylvania State University

The Graduate School

Department of Mechanical and Nuclear Engineering

PASSIVE, ITERATIVE, AND REPETITIVE CONTROL FOR

FLEXIBLE DISTRIBUTED PARAMETER SYSTEMS

A Thesis in

Mechanical Engineering

by

Haiyu Zhao

Submitted in Partial Fulfillment
of the Requirements
for the Degree of

Doctor of Philosophy

December 2005

The thesis of Haiyu Zhao has been reviewed and approved* by the following:

Christopher D. Rahn
Professor of Mechanical Engineering
Thesis Adviser
Chair of Committee

Kon-Well Wang
William E. Diefenderfer Chaired Professor of Mechanical Engineering

Qian Wang
Assistant Professor of Mechanical Engineering

Farhan Gandhi
Associate Professor of Aerospace Engineering

H. J. Sommer III
Professor of Mechanical Engineering
Interim Head of the Department of Mechanical and Nuclear Engineering

*Signatures are on file in the Graduate School.

Abstract

Many engineering structures have distributed parameter models governed by partial differential equations. Without damping, distributed flexible structures are not stable due to the infinite number of resonances at natural frequencies. Bounded sinusoidal inputs at these frequencies can cause unbounded response. This thesis shows that Passive Control, Iterative Learning Control (ILC), and Repetitive Learning Control (RLC) can be designed to reduce tracking or regulation errors in response to bounded, periodic inputs. Distributed flexible strings, beams, membranes, plates, axially moving materials, electrostatic microbridges, and flexible whisker contact imagers are studied.

Passive control using distributed or boundary damping is proven to stabilize the response of strings, beams, membranes, and plates. Damping ensures bounded response to bounded distributed and boundary inputs. Distributed viscous or Kelvin-Voigt material damping can guarantee pointwise or strong boundedness for strings and beams and weak boundedness for membranes and plates. Translational damping on one boundary stabilizes strings and beams. Damping on part of the boundary can also weakly stabilize the forced response of membranes and plates, provided the damped and undamped boundary normals satisfy certain conditions. For example, damping on half and one side of the boundary is sufficient for circular and rectangular domains, respectively.

Iterative Learning Control provides precise tension and speed control of axially moving material systems to enable high speed processing of paper, plastics, fibers, and

films. PD tension/speed control is proven to ensure strong and weak boundedness of distributed displacement and tension, respectively, in a single span axially moving material system. ILC provides the same theoretical result with half the speed error and 30% of the tension error of PD control using the same control effort.

Repetitive Learning Control is applied to an electrostatic microbridge and a repetitive contact imager. Electrostatic microactuators are used extensively in MEMS sensors, RF switches, and microfluidic pumps. Due to high bandwidth operation, however, reduction of residual vibration using feedback control is difficult to implement. Feedforward RLC is designed, proven stable, and simulated for an electrostatic microbridge under a periodic desired spatial/time trajectory. High residual stresses in the microbridge mean that bending stiffness can be neglected and a pinned string model with uniform loading is appropriate. Squeeze film damping ensures boundedness of the distributed transverse displacement. Offline RLC processing of the average displacement as measured by capacitive sensing updates a waveform generator's parameters. Simulations show a 36% reduction in midspan overshoot under repetitive control.

Repetitive contact imaging uses a flexible whisker attached to a two axis robot through a load cell. Assuming small deformations and rotations, the pitch axis decouples from yaw. The yaw axis, under PD control, sweeps periodically back and forth across the object while the pitch axis, under RLC, maintains a uniform contact force. Once the RLC converges, the 3D contact points can be determined using an elastica algorithm. RLC is proven stable based on a distributed parameter beam model and experimentally shown to outperform PD control with 75% reduction in the moment error.

Table of Contents

List of Tables

List of Figures

Acknowledgments

My deepest gratitude is due to my advisor Dr. Christopher D. Rahn for his unwavering guidance, support, patience, and encouragement he has shown me during my time here at the Penn State. I thank my other committee members, Drs. Kon-Well Wang, Qian Wang, and Farhan Gandhi, for their insightful commentary on my work. I am also grateful to all of my labmates, for inspiration and enlightening discussions on a wide variety of topics.

I take this opportunity to express my love and sincere thanks to my parents - Motian Zhao and Guilan Liu, for their endless love and support. They teach me the value of hard work by their own examples and provide me enormous support throughout my life.

Chapter 1

Introduction

Vibration reduces the perceived quality, productivity, and efficiency of many mechanical systems, causing defects, fatigue failure, limiting production speeds during manufacturing, and producing a potential dangerous and uncomfortable operating environment. Passive and active control have been extensively used to reduce vibration in a variety of applications, including smart structures, web handling, manufacturing, and robotics.

1.1 Methods of Vibration Control

Passive control involves modification of the mass, damping, and stiffness of the system to make the system less responsive to its vibratory environment. The idea is based on changing or adding to the basic structure passive elements, such as masses, dampers, and springs. These elements simply react passively in opposition to the accelerations, velocities, or deflections imposed upon them by vibration [48].

Unlike passive control, active control systems require external power and electromechanical, electrohydraulic, or electropneumatic actuators. Sensors detect the vibration and the control algorithm, often implemented using a microprocessor, produces control signals that are power amplified before being sent to the actuators.

Semi-active control is independent of any external power supply. The energy required by semi-active devices is low power and can often be stored in a battery. In addition, semi-active control devices are essentially passive devices where stiffness and damping can be adjusted in real time.

While passive vibration control is usually adequate, active vibration control holds potential for high performance. Innovations in piezoelectric film technology and modeling as well as the rapid advancements in computers have made active vibration control systems more cost efficient and effective than previously possible.

1.2 Vibration Control of Distributed Parameter Systems

At the scale of most mechanical applications, the material composing the system components acts as a continuum. Components that do not deform appreciably under the applied loading may be approximated as rigid bodies. The remaining components are modeled by partial differential equations (PDEs) and a set of boundary conditions due to dependence on both spatial and time variables. These are called distributed parameter systems (DPSs).

One control design method for DPSs is to apply distributed actuation throughout the continuum, requiring an infinite number of actuators and sensors [12]. F dell'Isola *et al.* [22] design devices for passive electric damping of structural vibrations by distributed piezoelectric transducers and electric networks. The use of few actuators and sensors located on the boundary of the system provides a more practical alternative. This approach, known as boundary control, results in control strategies that are often simple, physically motivated, and easy to implement and tune. There are many examples of

boundary controllers for strings [25, 56], cantilevered beams [10, 15], cables [4], rotors [42], and flexible link robots [21].

One common approach to determine the stability of flexible distributed parameter systems is to discretize the PDE using Galerkin [1], FEM [62], or finite difference approximations [49]. The system reduces to a finite set second order differential equations (ODEs) with mass, damping, and stiffness matrices. Many control design tools exist for discretized ODE models such as H_∞ control [26]. The system is exponentially and hence bounded input and bounded output (b.i.b.o.) [17] stable if the stiffness matrix is positive definite (no rigid body modes) and the damping matrix satisfies complete or pervasive damping conditions [31].

A substantial difficulty in the design of discretized model-based controllers is the choice of the discretization order. Reduction of the infinite dimensional continuum model to a finite dimensional (N^{th} order) discrete model neglects the effect of modes above a cut-off frequency. With sufficient system damping, these higher-order modes can be neglected if the controller rolls off (*i.e.* the controller gain drops sharply) at high frequency. However, if N is too small, it will result in the spillover instability [43]. There are two types of spillover: observation spillover and control spillover. The former entails the contamination of sensor output through the residual mode dynamics, while in the latter, the residual modes are excited by feedback control which is designed for a low-order model, senses and actuates higher-order modes, rendering them unstable [5]. Spillover can be avoided by reducing the control gain. However, this often results in poor performance. On the other hand, if N is too large, it will result in a high-order

controller that can be difficult and costly to implement. If the design of controllers is based on the actual DPS, it will not have eliminate spillover instabilities.

Transform techniques can be used to analyze the stability of DPSs. Yang and Mote [65] apply the root locus method to predict the controller stability of an axially moving string system. Yang *et al.* [63, 64] also present a frequency domain stability criteria for the closed-loop system stability of DPSs.

Discretization may be the only option for DPSs with complex geometry or built-up assemblies. Many manufacturing, aerospace, HVAC (Heating, Ventilation, and Air Conditioning), acoustic, robotic, transportation, and power transmission applications, however, have the geometric simplicity that make PDE models the most accurate and concise representation of the system dynamics.

Unlike discretization, distributed parameter methods require extensive hand derivations that become prohibitively difficult with the increasing number and complexity of the underlying PDEs. Thus, the most relevant applications for this approach consist of a few simple components (*e.g.* rigid bodies, second order components (strings, cables, rods, and membranes), and fourth order components (beams and plates)) that are simply connected.

Control design based on DPSs eliminates control spillover instabilities. The physical displacement, slope, and curvature of the continuum constitute the state variables rather than numerically generated node displacements or modes. Thus, the system model closely links to the underlying mechanics. Unfortunately, the relatively few boundary control techniques (*e.g.* Lyapunov theorem [36], functional analysis [28], and semi-group theory [25]) have not yet been developed for DPSs. Most boundary controllers proposed

are standard, linear, damper-like controllers designed for simple linear PDE models. The stability of these controllers is analyzed by combining Lyapunov theorem, functional analysis, and semi-group theory.

The Lyapunov approach used in this dissertation generally allows the designer to choose actuators but not sensors. The control law resulting from Lyapunov analysis of a distributed system may require measurement of position, slope, curvature, and/or shear and their time derivatives, for example. Position and slope can be measured using laser or eddy current displacement probes. Strain gages or load cells measure curvature and shear. Distributed sensing using spatially varying piezoelectric film [14] or high-speed video can provide full state feedback including distributed position, slope, curvature, and shear measurements. In many cases, filtered backwards differenced signals can substitute for velocity measurements.

1.3   Stability

For damped DPSs, there are no simple conditions for exponential or b.i.b.o. stability. First, the type of damping (*e.g.* viscous or Kelvin-Voigt [8]) and whether it is on the boundary or globally or locally distributed must be defined. Second, one must define boundedness based on either an $\mathcal{L}_2$ spatial norm (weak) or pointwise (strong) displacement measure. Finally, the input distribution (point, distributed, or boundary) must be specified.

The design and stability proof for the controllers discussed in the dissertation is based on the energy multiplier method [38, 46, 56] wherein the time derivative of a positive Lyapunov functional is shown to be bounded by negative functional [36].

Equalities and inequalities are extensively used in the proofs, leading to sufficient and therefore conservative results.

1.4 Objective of This Research

The main purpose of this research is to develop passive, iterative, repetitive controller that provide b.i.b.o. stability for flexible DPSs. First, the energy multiplier method establishes the boundedness of damped continua in response to distributed and boundary inputs. Distributed viscous and material damping and boundary damping are analyzed. Second, for periodic inputs/disturbance, iterative learning control (ILC) and repetitive learning control (RL) are developed for several applications.

The first application is ILC tension and speed control of an axially moving material. During the manufacture of continuous materials (paper, foil, plastic, fabric, wire, and yarn) the vibration, tension, and speed of the moving material is regulated to ensure product quality and maximize productivity. In web handling, the web can vibrate out-of-plane (transverse direction) due to aerodynamic and roller eccentricity excitation. Steering the web to maintain centerline tracking involves control of lateral web vibration. Longitudinal tension/speed/vibration control allows aggressive speed trajectories (*e.g.* stop/start motion) without breaking the web.

The second application is RLC of an MEMS electrostatic microbridge. Electrostatic microactuators are used extensively in MEMS sensors, RF switches, and microfluidic pumps. Due to high bandwidth operation, however, reduction of residual vibration using feedback control is difficult to implement. Feedforward techniques such as RLC can be implemented using high speed ADC and programmable waveform generators.

Finally, RLC for a contact imager is developed and experimentally tested. Repetitive contact imaging uses a flexible whisker attached to a two axis robot through a load cell. Assuming small deformations and rotations, the pitch axis decouples from yaw. The yaw axis, under PD control, sweeps periodically back and forth across the object while the pitch axis, under RLC, maintains a uniform contact force. Once the RL controller converges, the 3D contact points can be determined using an elastica algorithm.

1.4.1 BIBO Stability of Distributed Flexible Systems

Many engineering applications have DPS models governed by PDEs. One dimensional continua such as strings and beams and two dimensional continua such as membranes and plates accurately model systems with sufficiently simple geometry. Often forcing of unknown but bounded magnitude disturbs the system and the boundedness of the response comes into question. Without damping, flexible structures are not stable due to the many resonances corresponding to natural frequencies in the system. Bounded sinusoidal inputs at these frequencies can cause unbounded response.

Recently, researchers have made progress in the stability analysis of DPSs. Cavalcanti and Oquendo [16] show exponential and polynomial decay for a partially viscoelastic nonlinear wave equation subject to nonlinear and localized frictional damping. Cheng [18] proves the continuity of the input/output map for boundary control systems through the system transfer function. Komornik [38] and Lagnese [40] use the multiplier method to prove the boundary stabilization of membranes and plates. Guesmia [27] provides decay estimates when integral inequalities can not be applied due to the lack of dissipativity.

The energy multiplier method [66, 67] based on Lyapunov theorem is applied in this dissertation to prove bounded response to distributed inputs for damped strings, beams, membranes, and plates.

Viscoelastic material behavior, frictional interaction between contacting surfaces, or movement through a dissipative fluid cause damping in flexible structures. Distributed (viscous and material) and boundary (viscous) damping are analyzed here [8]. Viscous damping forces are produced when the structure moves through fluid and are proportional to transverse velocity $\dot{w}$ where $w(x,t)$ is the material transverse displacement. Kelvin-Voigt damping is due to material viscoelasticity and proportional to material strain rate: $\dot{w}_{xx}$ for strings, $\dot{w}_{xxxx}$ for beams, $\nabla \dot{w}$ for membranes, and $\Delta \dot{w}$ for plates.

1.4.2 Iterative Learning Velocity and Tension Control for Axially Moving Materials

Precise velocity and tension control prevents registration and tension nonuniformities that may lead to product failure or defects in axially moving material systems (*e.g.* high speed processing of paper, plastics, films, and fibers). Ebler *et al.* [24] summarize the use of load cell and dancer arm sensors for web handling. Boulter [13] provides a self-tuning control scheme for tension regulation in the frequency domain. Koc *et al.* [37] combine LPV control and H_∞ control to reject disturbances introduced by velocity variations and improve robustness to roll radius and inertia variations. Lu *et al.* [45] develop robust control algorithms for tape transport using a H_∞ mixed sensitivity approach within a disturbance observer architecture. Pagilla *et al.* [51] propose a feedback controller with an observer for average web tension. Baumgart *et al.* [9] present an

observer-based robust nonlinear feedback controller for tape transport systems that does not require tension measurements.

These controllers are based on a finite dimensional approximation of the full order distributed parameter model of axially moving materials. They neglect higher order modes that can be sensed and excited by the controller, resulting in spillover instabilities [5]. Controllers based on distributed parameter models can be designed to overcome the spillover instability problem and ensure stability of all modes [56]. Using this approach, Nagarkatti *et al.* [50] apply control torques to rollers at the boundaries of a distributed axially moving material domain to regulate speed and tension and prove strong exponential stability using the energy multiplier method [66].

Axially moving material systems are often subject to periodic disturbances. Stop/ start motion trajectories associated with intermittent material usage and roller eccentricity produce periodic prescribed material displacements that can excite longitudinal dynamics, causing large tension and web breaks.

Iterative learning control (ILC) has the potential to reduce tension variations due to periodic disturbances. While ILC has been applied to many discrete control problems [2], it has only recently been applied to distributed parameter models [55].

1.4.3   Repetitive Control of an Electrostatic Microbridge Actuator

Microelectromechanical systems (MEMS) are used in a wide variety of commercial, military, and industrial products. Electrostatic, thermal, electromagnetic, and

piezoelectric mechanisms, due to scalability and fabrication simplicity, are used exten-sively for actuation in many applications. MEMS accelerometers use electrostatic actua-tion for self-test. MEMS gyros use piezoelectric actuation to provide a sinusoidal driving force for angular rate measurement. Piezoelectric and electrostatic actuators are used for RF switches. In all of these cases, the actuator is used to impart a prescribed motion to the system. The prescribed motion is either repeated many times (*e.g.* switch) or is a purely periodic trajectory (*e.g.* gyro). Due to squeeze film and Couette damping, the vibration response of MEMS devices decays passively in response to inputs [56, 66]. With sufficient damping, residual vibration is suppressed but the response may be too slow. Thus, active control has the potential to greatly improve the performance of MEMS actu-ators. Iterative learning and repetitive control, in particular are feedforward techniques that have great potential for MEMS applications [23, 30, 55, 68]. These approaches can reduce vibration response resulting from periodic inputs using only feedforward control so high bandwidth real-time control is not required.

Researchers have modeled MEMS using lumped parameter, finite element, and partial differential equation models. Hung and Senturia [32] derive efficient low order models of MEMS based on fully meshed numerical analysis methods. Pamidighantam *et al.* [52] use a lumped parameter model to derive expressions for pull-in voltage of electrostatically actuated clamped and cantilevered beams. Lam and Darling [41] use an Euler-Bernoulli finite element model to calculate the stiction force of cantilever beams. Collenz *et al.* [20] investigate the large deflections of beams under electrostatic loads using a FEM model based on a sequential field-coupling approach. Liu *et al.* [44] derive mechanical and optical models of a surface micromachined variable optical attenuator

and verify the static and dynamic models using a FEM approach. A unified modeling approach can be found in Lyshevski [47] and Pelesko and Bernstein [53]. Krylov and Maimon [39] study the transient nonlinear dynamics of an electrostatically actuated microbeam that includes distributed nonlinear input and nonlinear squeeze film damping.

The simple geometries (*e.g.* beams and plates) of MEMS actuators motivate the use of distributed parameters, partial differential equation models (see *e.g.* [39]). These models capture the full distributed response of the system without FEM truncation of higher order modes. Controllers based on PDE models also produce physically motivated controllers that do not have spillover instabilities [5]. Unfortunately, stability proofs are significantly complicated and few tools exist for analysis of PDE systems. A number of researches, however, have developed Lyapunov-based Energy Multiplier methods for PDE systems under static and dynamic feedback. The challenge in this approach is to determine implementable (*i.e.* finite number of physically realizable sensors and actuators) controllers with proven stability based on the distributed model.

The control theoretical treatments of MEMS systems are very limited. The control of microelectrical machines is considered in [32]. Bamieh *et al.* [7] propose a distributed control scheme for spatially invariant systems. Balogh *et al.* [6] design a Lyapunov-based boundary controller for 2D channel flows. Senouci-Bereksi [11] designs and implements a nonlinear controller for magnetostrictive beam vibration.

1.4.4 Repetitive Contact Imaging

There are many robotic applications requiring obstacle avoidance and/or object identification in unstructured environments. Underwater crawlers used for mine counter

measures, for example, need sensors to identify mines. In the harsh and murky surfzone environment where these crawlers operate, delicate or optical sensors cannot be used. Limited communication bandwidth requires information-dense shape sensing.

Many researchers use flexible whiskers to measure contacted object shape. Kaneko *et al.* [35] extract contact position from the rotational compliance of an active flexible whisker. Russell [57] uses tip contact of an array of curved passive whiskers to measure the surface contours of concave and convex objects. Ueno *et al.* [61] determine contact distance (range) by measuring natural frequency changes in a vibrating whisker with a torque sensor. Scholz and Rahn [58] use an active whisker to measure two dimensional profiles of contacted objects based on an elastica whisker model. Clements and Rahn [19] use a two axis robot and flexible whisker to measure three dimensional profiles of contacted objects.

A significant challenge in contact sensing using flexible whiskers is to collect sufficient data to accurately resolve the contacted object shape. This can be achieved by using repeated contact with the object with a specified spacing [19] or by sliding the whisker across the object [58]. The approach used in [19] produces accurate contact points but can be prohibitively time consuming for high resolution sensing. The sweep method used in [58] produces only 2D slices of the contacted object profile. To measure 3D object shapes by sliding the whisker across the object requires accurate regulation of the contact force during sliding. This is a challenging control problem even for rigid-linked robots and has yet to be solved for a flexible whisker system.

The feedforward techniques of iterative learning and repetitive control, however, have recently been extended to flexible systems [23, 55, 68, 69]. For the contact sensing

application, the whisker can be repeatedly swept across the object and the results from the previous sweep can be used to update the control input for the next sweep. Thus, after a few relatively fast sweeps across the object, the whisker follows the object contour while maintaining a constant contact force. The data from the last, most accurate sweep can then be processed using the elastica model to determine the 3D contact points [19, 58].

1.5 Thesis Organization

The dissertation is organized in five main chapters. Chapter 2 discuss as b.i.b.o. stability for one and two dimensional DPSs. Chapter 3 presents ILC for axially moving material systems. In Chapter 4, RLC is analyzed for electrostatic microbridge. Chapter 5 shows a repetitive contact imager with experiment results. Conclusions, contributions, and future work are addressed in Chapter 6.

Chapter 2

BIBO Stability of Distributed Flexible Systems

2.1 Mathematical Preliminaries

The following definitions, equalities, and inequalities are extensively used in the dissertation and are presented without proof (see [3, 29, 34] for details). Throughout the chapter, for a 2D domain, we assume that it is an open, bounded, connected, Lipschitz domain with boundary Γ.

2.1.1 Definitions

1. **Gradient, divergence, Laplacian operator, and biharmonic operator**: x_1 and x_2 are two axes of 2-dimensional Cartesian coordinates, $\nabla w = \left(\mathbf{i}\frac{\partial}{\partial x_1} + \mathbf{j}\frac{\partial}{\partial x_2} \right) w$ is the gradient of w, $\nabla \cdot \mathbf{r} = \mathbf{i} \cdot \frac{\partial \mathbf{r}}{\partial x_1} + \mathbf{j} \cdot \frac{\partial \mathbf{r}}{\partial x_2}$ is the divergence of $\mathbf{r}$, where w is a scalar and $\mathbf{r}$ is a vector, $\Delta = \nabla \cdot \nabla$ is Laplacian operator, and $\Delta^2 = \Delta\Delta$ is biharmonic operator.

2. **Inner product**: $\mathbf{a} \cdot \mathbf{b} = ab\cos\theta$, where θ is the angle between the two vectors.

3. **Open set and closed set**: Let $A \subseteq V$, a normed linear space. The set A is open if for every $\mathbf{a} \in A$, there is a radius $r > 0$ such that $B(\mathbf{a}, r) \subseteq A$, where $B(\mathbf{a}, r) = \{\mathbf{a} \in V \mid \|\mathbf{a}\| < r\}$. The set A is closed in V if its complement $V - A$ is open in V.

4. $\mathcal{L}_2$ **norm**: The inner product induces a natural norm $\|f\| = \sqrt{\langle f, f \rangle}$, denoted by $\|f\|_{\mathcal{L}_2}$. $\mathcal{L}_p(\Omega)$ is the linear space of measurable functions $v : \Omega \to \mathbb{R}$, such that $\|v\|_{\mathcal{L}_p(\Omega)} = \{\int_\Omega |v(x)|^p \, dx\}^{1/p} < \infty$. $\mathcal{L}_\infty$ is given by the essential supremum. More precisely, $|f|_\infty = \text{ess sup } |f|$.

5. **Lipschitz continuous**: A function v defined on Ω is said to be Lipschitz continuous if for some constant c, $|v(x) - v(y)| \le c \|x - y\|$ $\forall x, y \in \Omega$.

6. **Disjoint**: Two sets A_1 and A_2 are disjoint if their intersection $A_1 \cap A_2 \equiv \varnothing$, where $\varnothing$ is the empty set.

2.1.2 Equalities

The Divergence Theorem applies to vector fields $V = P(x_1, x_2)\mathbf{i} + Q(x_1, x_2)\mathbf{j}$ as follows

$$\int_\Omega \left(\frac{\partial P}{\partial x_1} + \frac{\partial Q}{\partial x_2} \right) dx = \int_\Gamma (Pdx_2 - Qdx_1). \tag{2.1}$$

The normal derivative of $w(\mathbf{x}, t)$ is defined as

$$\frac{\partial w}{\partial n} = \nabla w \cdot \mathbf{n} \quad on \; \Gamma, \tag{2.2}$$

where $\mathbf{n}$ is the unit-normal vector to Γ pointing toward the exterior of Ω.

The following integral equalities apply to $w \in H^1(\Omega)$ and $v \in H^2(\Omega)$

$$\int_\Omega \Delta v \, w \, dx = \int_\Gamma \frac{\partial v}{\partial n} w d\Gamma - \int_\Omega \nabla v \cdot \nabla w \, dx, \tag{2.3}$$

$$\int_\Omega \mathbf{r} \cdot \nabla w \, dx = \int_\Gamma (\mathbf{r} \cdot \mathbf{n}) w d\Gamma - \int_\Omega (\nabla \cdot \mathbf{r}) \, w dx. \tag{2.4}$$

The divergence of products can be calculated as follows:

$$\nabla \cdot (w\mathbf{a}) = w\nabla \cdot \mathbf{a} + (\nabla w) \cdot \mathbf{a}, \tag{2.5}$$

$$\nabla (\mathbf{a} \cdot \mathbf{b}) = \mathbf{a} \times (\nabla \times \mathbf{b}) + \mathbf{b} \times (\nabla \times \mathbf{a}) + (\nabla \cdot \mathbf{a}) \mathbf{b} + (\nabla \cdot \mathbf{b}) \mathbf{a}, \tag{2.6}$$

where $\mathbf{r}$, $\mathbf{a}$, and $\mathbf{b}$ are vectors.

2.1.3 Inequalities

The nonlinear damping inequality

$$(\mathbf{a} \cdot \mathbf{b}) \leq \delta |\mathbf{a}|^2 + \frac{1}{\delta} |\mathbf{b}|^2. \tag{2.7}$$

2.1.3.1 One Dimensional

Pointwise integral inequality

$$w^2(x,t) \leq L \int_0^L w_x^2(x,t)\, dx, \forall x \in (0,L). \tag{2.8}$$

Weak integral inequality

$$\int_0^L w^2(x,t)\, dx \leq L^2 \int_0^L w_x^2(x,t)\, dx, \tag{2.9}$$

$$\forall w(x,t) \in H = \left\{ a | a \in H^1(0,L),\ a(0) = 0 \right\}.$$

2.1.3.2 Two Dimensional

The Poincaré inequality

$$\int_{\Omega} w^2 dx \leq m_1 \int_{\Omega} |\nabla w|^2 dx \tag{2.10}$$

holds $\forall w \in H^2(\Omega)$ with $w = 0$ on Γ for some constant $m_1 > 0$.

The Sobolev inequality

Γ_0 and Γ_1 are two disjoint, nonempty open subsets of the boundary Γ,

$$\int_{\Gamma_1} w^2 dx \leq m_2 \int_{\Omega} |\nabla w|^2 dx, \ \forall w \in H^1(\Omega) \tag{2.11}$$

where $m_2 > 0$, $\Gamma = \Gamma_0 \cup \Gamma_1$, and $w = 0$ on Γ_0.

2.2 Damped Strings

For the damped string models, we assume that the string is inextensible and perfectly flexible, the axial tension P is constant, and distributed forcing $f(x,t)$ is applied in the domain $x \in (0, L)$, where the string length is L. First, a string with prescribed boundary displacements and distributed viscous and material damping is considered. Then, we consider a string without damping in the field equation and with a damped boundary condition at $x = L$ and prescribed displacement at $x = 0$.
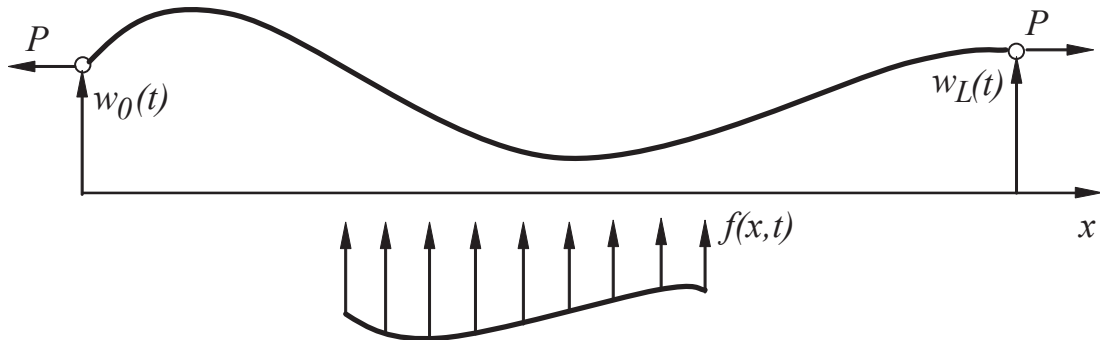
Fig. 2.1. Schematic diagram of a distributed damped string with distributed and boundary disturbances.

2.2.1 Distributed Damped Strings

The equation of motion for the model in Fig. 2.1 is

$$\rho \ddot{w} + b\dot{w} - D\dot{w}_{xx} - Pw_{xx} \;=\; f \;,\; x \in (0, L), \tag{2.12}$$

$$w(0, t) = w_0\,(t) \quad , \quad w(L, t) = w_L\,(t),$$

where ρ is the mass/area, b and D are the viscous and material damping coefficients, and $w_0\,(t)$ and $w_L\,(t)$ are prescribed boundary displacements. We assume that all of the models presented in this chapter are well-posed and possess a unique solution for all initial conditions and bounded inputs.

Theorem 2.1: The response of the damped string governed by (2.12) is bounded, $w(x, t) \in \mathcal{L}_\infty(0, L)$, if f, w_0, $\dot{w}_0$, $\ddot{w}_0$, w_L, $\dot{w}_L$, $\ddot{w}_L \in \mathcal{L}_\infty$ and either b or D is nonzero.

Proof: We transform the model using

$$w^*(x,t) = w(x,t) - (a_0 + a_1 x),$$ (2.13)

where

$$a_0 = w_0(t), \ a_1 = \frac{w_L(t) - w_0(t)}{L},$$

and define $f^* = f - \rho(\ddot{a}_0 + \ddot{a}_1 x) - b(\dot{a}_0 + \dot{a}_1 x)$ with $f^*(x,t) \in \mathcal{L}_\infty$, $\forall x \in (0, L)$ by the theorem assumptions. We drop the $*$ for convenience and the transformed equations are

$$\rho \ddot{w} + b\dot{w} - D\dot{w}_{xx} - Pw_{xx} = f, \ x \in (0, L),$$ (2.14)

$$w(0, t) = 0 \quad , \quad w(L, t) = 0.$$

The energy of the string

$$E = \frac{1}{2} \int_0^L (\rho \dot{w}^2 + Pw_x^2) dx \geq 0$$ (2.15)

has a time rate of change

$$\dot{E} = \int_0^L \dot{w} f dx - b \int_0^L \dot{w}^2 dx + D \int_0^L \dot{w}\dot{w}_{xx} dx + P \int_0^L \dot{w}w_{xx} dx + P \int_0^L w_x \dot{w}_x dx.$$

The power can be upper bounded by

$$
\begin{aligned}
\dot{E} \;\leq\; & \delta_1 \int_0^L \dot{w}^2 dx + \frac{1}{\delta_1}\int_0^L f^2 dx - b\int_0^L \dot{w}^2 dx + D\dot{w}\dot{w}_x\big|_0^L \\
& -D\int_0^L \dot{w}_x^2 dx + P\int_0^L \dot{w}w_{xx}dx + P\dot{w}w_x\big|_0^L - P\int_0^L \dot{w}w_{xx}dx \\
\leq\; & -\left(b + \frac{D}{2L^2} - \delta_1\right)\int_0^L \dot{w}^2 dx + \frac{1}{\delta_1}\int_0^L f^2 dx - \frac{D}{2}\int_0^L \dot{w}_x^2 dx.
\end{aligned}
\tag{2.16}
$$

The first inequality results from the use of the nonlinear damping inequality (2.7) on the first term and integration by parts on the third and fifth terms. Application of inequality (2.9) and the boundary conditions and simplification produces the final result. Note that the positive term resulting from the disturbance, $\delta_1 \int_0^L \dot{w}^2 dx$, can be made negative with either of the damping terms $-\left(b + \frac{D}{2L^2}\right)\int_0^L \dot{w}^2 dx$. The energy cannot be used to establish stability, however, because the strain energy term $\int_0^L w_x^2 dx$ does not appear in $\dot{E}$. We define a new functional by adding the crossing term $C(t)$

$$
V(t) = E(t) + \beta C(t),
\tag{2.17}
$$

where

$$
C(t) = \rho \int_0^L w\dot{w}dx.
\tag{2.18}
$$

The functional $V(t)$ is positive because

$$
|C(t)| \leq \frac{1}{2}\rho \int_0^L \left(\dot{w}^2 + w^2\right) dx \leq \frac{1}{2}\rho \int_0^L \left(\dot{w}^2 + L^2 w_x^2\right) dx
$$

$$\leq \quad \frac{\rho \max\left(1, L^2\right)}{\min\left(\rho, P\right)} \frac{1}{2} \int_0^L \left(\rho \dot{w}^2 + P w_x^2\right) dx$$

$$= \quad \eta E \tag{2.19}$$

using inequality (2.9), where

$$\eta = \frac{\rho \max\left(1, L^2\right)}{\min\left(\rho, P\right)}.$$

This means that

$$0 \leq \lambda_1 E(t) \leq V(t) \leq \lambda_2 E(t), \tag{2.20}$$

where

$$\lambda_1 \quad = \quad 1 - \beta\eta > 0,$$

$$\lambda_2 \quad = \quad 1 + \beta\eta > 1,$$

for sufficiently small β. Differentiation of the crossing term produces

$$\dot{C} \quad = \quad \rho \int_0^L \dot{w}^2 \, dx + \rho \int_0^L w \ddot{w} \, dx$$

$$= \quad \int_0^L \rho \dot{w}^2 \, dx + \int_0^L w \left(f - b\dot{w} + D\dot{w}_{xx} + P w_{xx}\right) dx$$

$$= \quad \rho \int_0^L \dot{w}^2 \, dx + \dot{C}_1 + \dot{C}_2 + \dot{C}_3 + \dot{C}_4. \tag{2.21}$$

The terms in (2.21) simplify as follows

$$\dot{C}_1 = \int_0^L wf\,dx \leq \delta_2 \int_0^L w^2\,dx + \frac{1}{\delta_2} \int_0^L f^2\,dx$$

$$\leq \delta_2 L^2 \int_0^L w_x^2\,dx + \frac{1}{\delta_2} \int_0^L f^2\,dx, \tag{2.22}$$

$$\dot{C}_2 = -\int_0^L bw\dot{w}\,dx \leq b\delta_3 \int_0^L w^2\,dx + \frac{b}{\delta_3} \int_0^L \dot{w}^2\,dx$$

$$\leq b\delta_3 L^2 \int_0^L w_x^2\,dx + \frac{b}{\delta_3} \int_0^L \dot{w}^2\,dx, \tag{2.23}$$

using inequalities (2.7) and (2.9). The third term

$$\dot{C}_3 = D\int_0^L w\dot{w}_{xx}\,dx = Dw\dot{w}_x\big|_0^L - D\int_0^L w_x\dot{w}_x\,dx$$

$$\leq D\left(\delta_4 \int_0^L w_x^2\,dx + \frac{1}{\delta_4} \int_0^L \dot{w}_x\,dx\right), \tag{2.24}$$

using the boundary conditions and inequality (2.7). The fourth term simplifies as follows

$$\dot{C}_4 = P\int_0^L ww_{xx}\,dx = Pww_x\big|_0^L - P\int_0^L w_x^2\,dx = -P\int_0^L w_x^2\,dx, \tag{2.25}$$

using integration by parts and the boundary conditions. Note that this term provides the needed $-\int_0^L w_x^2\,dx$ term that relates $\dot{V}$ to V. Substitution (2.22) – (2.25) into (2.21)

yields

$$
\begin{aligned}
\dot{C} \;\leq\; & -\Big[P - (\delta_2 + b\delta_3)\, L^2 - D\delta_4\Big] \int_\Omega w_x^2\, dx \\
& + \left(\rho + \frac{b}{\delta_3}\right) \int_0^L \dot{w}^2\, dx + \frac{1}{\delta_2} \int_\Omega f^2 dx + \frac{D}{\delta_4} \int_\Omega \dot{w}_x^2 dx.
\end{aligned}
\tag{2.26}
$$

Substitution of the crossing term derivative (2.26) into (2.17) produces

$$
\begin{aligned}
\dot{V} \;\leq\; & -\beta \Big[P - (\delta_2 + b\delta_3)\, L^2 - D\delta_4\Big] \int_0^L w_x^2 dx - D \left(\frac{1}{2} - \frac{\beta}{\delta_4}\right) \int_0^L \dot{w}_x^2 dx \\
& - \left[b + \frac{D}{2L^2} - \delta_1 - \beta \left(\rho + \frac{b}{\delta_3}\right)\right] \int_0^L \dot{w}^2 dx + \left(\frac{1}{\delta_1} + \frac{\beta}{\delta_2}\right) \int_0^L f^2 dx \\
\leq\; & -\lambda_3 E(t) + \varepsilon,
\end{aligned}
\tag{2.27}
$$

where, for sufficiently small β, δ_1, δ_2, δ_3, and δ_4,

$$
\frac{1}{2} \;\geq\; \frac{\beta}{\delta_4},
\tag{2.28}
$$

$$
\varepsilon_1 \;=\; \beta \Big[P - (\delta_2 + b\delta_3)\, L^2 - D\delta_4\Big] > 0,
\tag{2.29}
$$

$$
\varepsilon_2 \;=\; b + \frac{D}{2L^2} - \delta_1 - \beta \left(\rho + \frac{b}{\delta_3}\right) > 0,
\tag{2.30}
$$

$$
\varepsilon \;=\; \left(\frac{1}{\delta_1} + \frac{\beta}{\delta_2}\right) \max_{t\in[0,\infty)} \int_0^L f^2 dx < \infty,
\tag{2.31}
$$

$$
\lambda_3 \;=\; \frac{\min(\varepsilon_1, \varepsilon_2)}{\max(\rho, P)},
\tag{2.32}
$$

Using (2.20), we obtain

$$
\dot{V} \leq \lambda V + \varepsilon,
\tag{2.33}
$$

where $\lambda = \lambda_3/\lambda_2$, with the solution

$$V(t) \leq V(0)e^{-\lambda t} + \frac{\varepsilon}{\lambda} \in \mathcal{L}_\infty. \tag{2.34}$$

Use of (2.8), (2.15), and (2.20) produces

$$\frac{P}{2L}\lambda_1 w^2 \leq \frac{P}{2}\lambda_1 \int_0^L w_x^2 dx \leq \lambda_1 E(t) \leq V(t) \in \mathcal{L}_\infty. \tag{2.35}$$

So

$$w(x,t) \in \mathcal{L}_\infty \quad \forall x \in (0, L).$$

□

2.2.2   Boundary Damped Strings
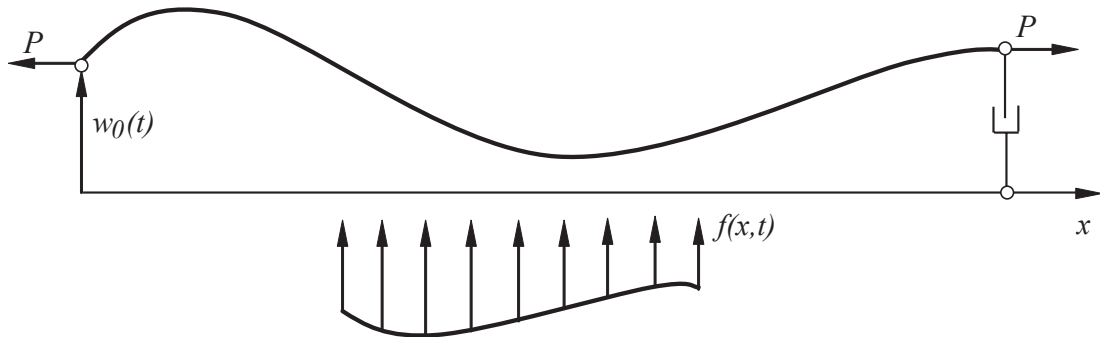
Fig. 2.2.   Schematic diagram of a boundary damped string with distributed and boundary disturbances.

For the boundary damped string in Fig. 2.2, we remove the distributed damping in (2.12) to obtain the one dimensional wave equation

$$\rho\ddot{w} - Pw_{xx} = f, \ x \in (0, L), \tag{2.37}$$

and boundary conditions

$$w(0,t) = w_0(t), \quad w_x(L,t) = -\frac{c_b}{P}\dot{w}(L,t),$$

where c_b is the boundary damping coefficient (See Fig. 2.2).

Theorem 2.2: The response of the boundary damped string governed by (2.37) is bounded, $w(x,t) \in \mathcal{L}_\infty(0,L)$, if f, w_0, $\ddot{w}_0 \in \mathcal{L}_\infty$ and $c_b > 0$.

Proof: First, we transform the boundary conditions using

$$w^*(x,t) = w(x,t) - \frac{(x-L)^2}{L^2}w_0(t) \tag{2.38}$$

and define $f^* = f + \frac{2w_0}{L^2} - \frac{(x-L)^2}{L^2}\ddot{w}_0$. Dropping the $*$ we same obtain the field equation (2.37) and boundary conditions except that $w(0,t) = 0$.

The energy is given in equation (2.15) and time derivative is

$$\dot{E} \leq \delta_1 \int_0^L \dot{w}^2 dx + \frac{1}{\delta_1} \int_0^L f^2 dx - c_b\dot{w}^2(L,t). \tag{2.39}$$

The boundary damper does not match the distributed and boundary inputs providing neither a negative kinetic nor potential energy term. A positive functional is

defined as in (2.17) with a different crossing term

$$C(t) = \rho \int_0^L x w_x \dot{w} \, dx. \tag{2.40}$$

We can bound this crossing term with respect to the system energy as in (2.19) with

$$\eta = \frac{\rho L}{\min(\rho, P)}.$$

The time derivative is calculated to be

$$
\begin{aligned}
\dot{V} \leq\ & -\beta \left(\frac{P}{2} - L\delta_2 \right) \int_0^L w_x^2 dx - \left(\frac{\beta\rho}{2} - \delta_1 \right) \int_0^L \dot{w}^2 dx \\
& + \left(\frac{1}{\delta_1} + \frac{\beta L}{\delta_2} \right) \int_0^L f^2 dx - \left[c_b - \frac{1}{2}\beta L \left(\frac{c_b^2}{P} + \rho \right) \right] \dot{w}^2 (L, t),
\end{aligned} \tag{2.41}
$$

where for sufficiently small β, δ_1, and δ_2,

$$c_b \geq \frac{1}{2}\beta L \left(\frac{c_b^2}{P} + \rho \right),$$

$$\frac{\beta\rho}{2} - \delta_1 > 0,$$

$$\frac{P}{2} - L\delta_2 > 0.$$

The result in (2.41) can be cast in the form of (2.33) with

$$\varepsilon \;=\; \left(\frac{1}{\delta_1} + \frac{\beta L}{\delta_2}\right) \max_{t \in [0,\infty)} \int_0^L f^2 dx, \tag{2.42}$$

$$\lambda_3 \;=\; \frac{\min\left[\frac{\beta \rho}{2} - \delta_1, \beta\left(\frac{P}{2} - L\delta_2\right)\right]}{\max\left(\rho, P\right)}. \tag{2.43}$$

Therefore, (2.34) and (2.35) hold and $w(x,t) \in \mathcal{L}_\infty(0, L)$.

$\square$

2.3 Distributed Beams

In this section, we investigate the b.i.b.o. stability of distributed and boundary damped beams with distributed and boundary excitation. We assume the beams are inextensible and homogeneous with uniform cross-section. The beams have mass/length ρ and bending stiffness EI.

2.3.1 Distributed Damped Beams

Fig. 2.3 shows a schematic diagram of the distributed damped beam model. The system has distributed forcing and prescribed boundary translations and rotations. Distributed viscous and material damping are included. The equation of motion and boundary conditions are

$$\rho \ddot{w} + b\dot{w} + D\dot{w}_{xxxx} + EIw_{xxxx} = f, \;\; x \in (0, L), \tag{2.44}$$
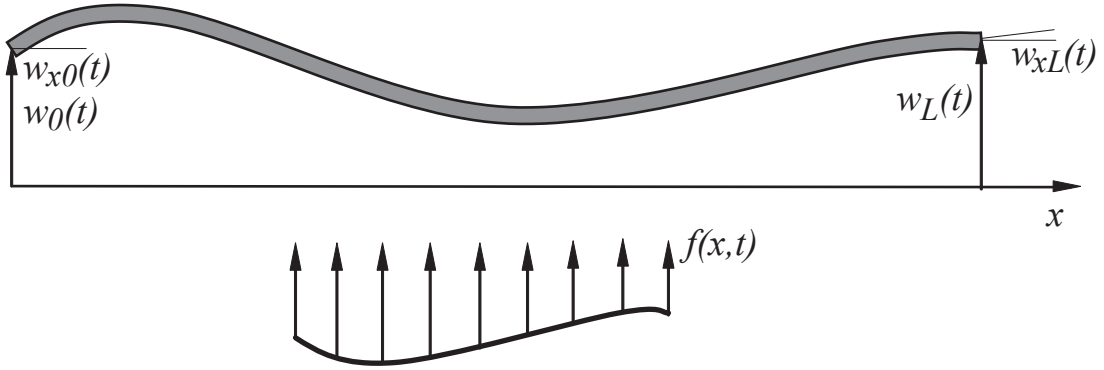
Fig. 2.3.   Schematic diagram of a distributed damped beam with distributed and boundary disturbances.

$$w(0,t) \;\; = \;\; w_0\left(t\right), \;\; w_x(0,t) = w_{x0}\left(t\right),$$

$$w(L,t) \;\; = \;\; w_L\left(t\right), \;\; w_x(L,t) = w_{xL}\left(t\right),$$

where b and D are the viscous and material damping coefficients and $w_0\left(t\right)$, $w_{x0}\left(t\right)$, $w_L\left(t\right)$, and $w_{xL}\left(t\right)$ are prescribed boundary translations and rotations.

Theorem 2.3: The response of the damped beam governed by (2.44) is bounded, $w(x,t) \in \mathcal{L}_\infty(0,L)$, if f, w_0, $\dot{w}_0$, $\ddot{w}_0$, w_{x0}, $\dot{w}_{x0}$, $\ddot{w}_{x0}$, w_L, $\dot{w}_L$, $\ddot{w}_L$, w_{xL}, $\dot{w}_{xL}$, $\ddot{w}_{xL} \in \mathcal{L}_\infty$ and either b or D is nonzero.

Proof: We transform the model using

$$w^*(x,t) = w(x,t) - \left(a_0 + a_1 x + a_3 x^2 + a_4 x^3\right), \tag{2.45}$$

where

$$a_0 = w_0(t), \ a_1 = w_{x0}(t),$$

$$a_2 = \frac{1}{L^2}(3w_L - w_{xL}L - 2w_{x0}L - 3w_0),$$

$$a_3 = \frac{1}{L^3}(3w_{x0}L + w_{xL} + 2w_x - 2w_L),$$

Substitution of (2.45) into (2.44) and dropping the $*$ yields

$$\rho\ddot{w} + b\dot{w} + D\dot{w}_{xxxx} + EIw_{xxxx} = f, \ x \in (0, L), \tag{2.46}$$

$$w(0, t) = 0, \ w_x(0, t) = 0, \ w(L, t) = 0, \ w_x(L, t) = 0,$$

where $f^* = f - \rho\left(\ddot{a}_0 + \ddot{a}_1 x + \ddot{a}_2 x^2 + \ddot{a}_3 x^3\right) - b\left(\dot{a}_0 + \dot{a}_1 x + \dot{a}_2 x^2 + \dot{a}_3 x^3\right)$ is bounded by the theorem assumptions.

The energy of the beam

$$E = \frac{1}{2}\int_0^L (\rho\dot{w}^2 + EIw_{xx}^2)dx \geq 0. \tag{2.47}$$

Differentiation of the energy

$$\dot{E} = -b\int_0^L \dot{w}^2 dx - D\int_0^L \dot{w}\dot{w}_{xxxx}dx + \int_0^L \dot{w}f dx$$

$$-EI\int_0^L \dot{w}w_{xxxx}dx + EI\int_0^L w_{xx}\dot{w}_{xx}dx$$

$$\leq \; -(b - \delta_1) \int_0^L \dot{w}^2 dx + D\dot{w}_x \dot{w}_{xx}\big|_0^L - D \int_0^L \dot{w}_{xx}^2 dx + \frac{1}{\delta_1} \int_0^L f^2 dx$$

$$+ EI\dot{w}_x w_{xx}\big|_0^L - EI \int_0^L w_{xx}\dot{w}_{xx}dx + EI \int_0^L w_{xx}\dot{w}_{xx}dx$$

$$\leq \; -\left(b + \frac{D}{2L^4} - \delta_1\right) \int_0^L \dot{w}^2 dx - \frac{D}{2} \int_0^L \dot{w}_{xx}^2 dx + \frac{1}{\delta_1} \int_0^L f^2 dx, \qquad (2.48)$$

using integration by parts, inequalities (2.7) and (2.8), and the boundary conditions. Both viscous and material damping match the disturbance input, producing a negative kinetic energy term in $\dot{E}$. The energy cannot be used to prove b.i.b.o. stability because the time derivative lacks a $-\int_0^L w_{xx}^2 dx$ term that is found in E. We therefore add the crossing term in (2.18) to form the positive functional as in (2.17). The crossing term can be bounded with respect to the energy as in (2.19) with

$$\eta = \frac{\rho \max\left(1, L^4\right)}{\min\left(\rho, EI\right)}.$$

Differentiation of the crossing term yields an equation in the form of (2.21) with

$$\dot{C}_1 \;=\; \int_0^L wf dx \leq \delta_2 L^4 \int_0^L w_{xx}^2 dx + \frac{1}{\delta_2} \int_0^L f^2 dx, \qquad (2.49)$$

$$\dot{C}_2 \;=\; b \int_0^L w\dot{w}dx \leq bL^4 \delta_3 \int_0^L w_{xx}^2 dx + \frac{b}{\delta_3} \int_0^L \dot{w}^2 dx, \qquad (2.50)$$

where (2.7) and (2.9) are used. Integration by parts simplifies the last two terms to

$$\dot{C}_3 \;=\; -EI \int_0^L w w_{xxxx}dx = -EI \int_0^L w_{xx}^2 dx, \qquad (2.51)$$

$$\dot{C}_4 \;=\; -D \int_0^L w_x \dot{w}_{xxxx}dx \leq D\delta_4 \int_0^L w_{xx}^2 dx + \frac{D}{\delta_4} \int_0^L \dot{w}_{xx}^2 dx. \qquad (2.52)$$

Substitution of (2.49) – (2.52) into (2.21) yields

$$\dot{C} \leq \left(\rho + \frac{b}{\delta_3}\right) \int_0^L \dot{w}^2\,dx + \frac{D}{\delta_2} \int_0^L \dot{w}_{xx}^2\,dx + \frac{1}{\delta_2} \int_0^L f^2 dx$$

$$- \left[EI - (\delta_2 + b\delta_3)\,L^4 - D\delta_4\right] \int_0^L w_{xx}^2\,dx \qquad (2.53)$$

providing the missing negative term in $\dot{E}$. Combination of (2.48) and (2.53) results in

$$\dot{V} \leq -\beta \left[EI - (\delta_2 + b\delta_3)\,L^4 - D\delta_4\right] \int_0^L w_{xx}^2\,dx + \left(\frac{1}{\delta_1} + \frac{\beta}{\delta_2}\right) \int_0^L f^2 dx$$

$$- \left[b + \frac{D}{2L^4} - \delta_1 - \beta\left(\rho + \frac{b}{\delta_3}\right)\right] \int_0^L \dot{w}^2 dx - D\left(\frac{1}{2} - \frac{\beta}{\delta_4}\right) \int_0^L \dot{w}_{xx}^2\,dx$$

$$\leq -\lambda_3 E(t) + \varepsilon, \qquad (2.54)$$

where

$$\varepsilon = \left(\frac{1}{\delta_1} + \frac{\beta}{\delta_2}\right) \max_{t \in [0,\infty)} \int_0^L f^2 dx < \infty,$$

and for sufficiently small β, δ_1, δ_2, δ_3, and δ_4,

$$\frac{1}{2} \geq \frac{\beta}{\delta_4}, \qquad (2.55)$$

$$\varepsilon_1 = \beta\left[EI - (\delta_2 + b\delta_3)\,L^4 - D\delta_4\right] > 0, \qquad (2.56)$$

$$\varepsilon_2 = b + \frac{D}{2L^4} - \delta_1 - \beta\left(\rho + \frac{b}{\delta_3}\right) > 0, \qquad (2.57)$$

$$\lambda_3 = \frac{\min\left(\varepsilon_1, \varepsilon_2\right)}{\max\left(\rho, EI\right)}. \qquad (2.58)$$

Equations (2.20), (2.33), and (2.34) apply so $V(t) < \mathcal{L}_\infty$ and

$$\frac{EI}{L^3}\lambda_1 w^2 \leq \frac{EI}{L^2}\lambda_1 \int_0^L w_x^2 dx \leq \lambda_1 E(t) \leq V(t) \in \mathcal{L}_\infty. \qquad (2.59)$$

□

2.3.2 Boundary Damped Beams
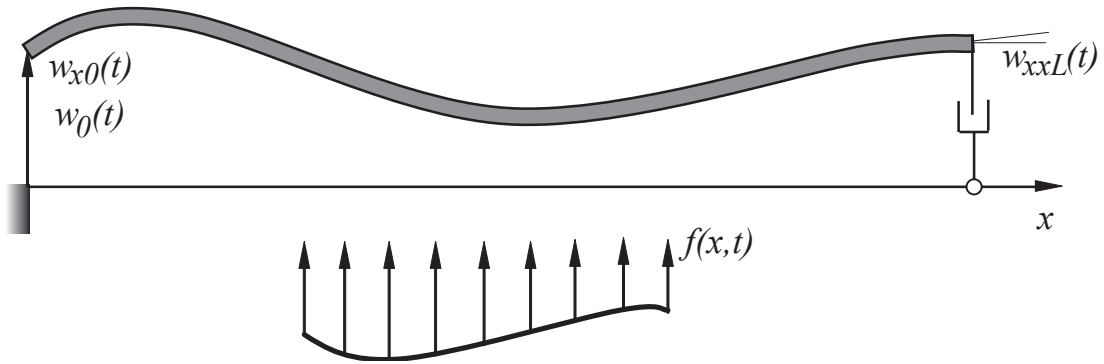
Fig. 2.4. Schematic diagram of a boundary damped beam with distributed and boundary disturbances.

Finally, we consider the boundary damped beam shown in Fig. 2.4. In this case, the viscous and material damping are removed from the field equation and the translational boundary condition at the right end is changed to a damper

$$\rho \ddot{w} + EIw_{xxxx} = f , \; x \in (0, L), \qquad (2.60)$$

$$w(0, t) = w_0(t), \; w_x(0, t) = w_{x0}(t),$$

$$w_{xx}(L, t) = 0, \; EIw_{xxx}(L, t) = c_b \dot{w}(L, t),$$

where c_b is the boundary damping gain.

Theorem 2.4: The response of the damped beam governed by (2.60) is bounded,

$w(x,t) \in \mathcal{L}_\infty(0,L)$, if f, w_0, $\ddot{w}_0$, w_{x0}, $\ddot{w}_{x0} \in \mathcal{L}_\infty$ and $c_b > 0$.

Proof: Using the transformation

$$w^*(x,t) = w(x,t) - \left[a_0 \left(\frac{x-L}{L} \right)^4 + a_1 \left(\frac{x-L}{L} \right)^5 \right], \tag{2.61}$$

where

$$a_0 = 5w_0(t) + w_{x0}(t)L, \ a_1 = 4w_0(t) + w_{x0}(t)L,$$

and $f^* = f - \rho \left[\ddot{a}_0 \left(\frac{x-L}{L} \right)^4 + \ddot{a}_1 \left(\frac{x-L}{L} \right)^5 \right] - \frac{24EI}{L^4} \left[a_0 + \frac{5a_1(x-L)}{L} \right]$.

We drop the $*$ to obtain

$$\rho \ddot{w} + EI w_{xxxx} = f, \ x \in (0,L), \tag{2.62}$$

$$w(0,t) = 0, \ w_x(0,t) = 0,$$

$$w_{xx}(L,t) = 0, \ EI w_{xxx}(L,t) = c_b \dot{w}(L,t).$$

Combination of the energy (2.47) and the crossing term (2.40) produces a positive

functional as in (2.20) with

$$\eta = \frac{\rho L \max(1, L^2)}{\min(\rho, EI)}.$$

The time derivative

$$
\begin{aligned}
\dot{V} &\leq -\left(\frac{\beta\rho}{2} - \delta_1\right)\int_0^L \dot{w}^2 dx - \beta\left[\frac{3}{2}EI - L^3\delta_2 - c_bL^2\delta_3\right]\int_0^L w_{xx}^2 dx \\
&\quad -\left[c_b - \beta L\left(\frac{\rho}{2} + \frac{c_b}{\delta_3}\right)\right]\dot{w}^2(L,t) + \left(\frac{1}{\delta_1} + \frac{\beta L}{\delta_2}\right)\int_0^L f^2 dx \\
&\leq -\lambda_3 E + \varepsilon, \tag{2.63}
\end{aligned}
$$

where, for sufficiently small β, δ_1, δ_2, and δ_3,

$$
c_b \geq \beta L\left(\frac{\rho}{2} + \frac{c_b}{\delta_3}\right), \tag{2.64}
$$

$$
\varepsilon = \left(\frac{1}{\delta_1} + \frac{\beta L}{\delta_2}\right)\max_{t\in[0,\infty)}\int_0^L f^2 dx < \infty, \tag{2.65}
$$

$$
\varepsilon_1 = \beta\left(\frac{3}{2}EI - L^3\delta_2 - c_bL^2\delta_3\right) > 0, \tag{2.66}
$$

$$
\varepsilon_2 = \frac{\beta\rho}{2} - \delta_1 > 0, \tag{2.67}
$$

$$
\lambda_3 = \frac{\min(\varepsilon_1, \varepsilon_2)}{\max(\rho, EI)}. \tag{2.68}
$$

Thus, (2.33), (2.34), and (2.59) apply, so $w(x,t) \in \mathcal{L}_\infty$, $\forall x \in (0,L)$.

$\square$

2.4 Damped Membranes

For the damped membrane model shown in Fig. 2.5, we assume that the membrane is inextensible and perfectly flexible, the in-plane stress P is constant, and bounded distributed forcing $f(\mathbf{x},t)$ is applied in the domain Ω. First, a membrane with distributed viscous and material damping is considered. Then, we consider a membrane without

damping in the field equation and with a damped boundary condition on Γ_1 with the remaining boundary Γ_0 pinned.

2.4.1 Distributed Damped Membranes

The field equation, boundary conditions, and initial conditions of the damped membrane are

$$\rho\ddot{w} + b\dot{w} - D\Delta\dot{w} - P\Delta w \;=\; f \;\; in \; \Omega \times R_+, \tag{2.69}$$

$$w(\mathbf{x}, t) \;=\; 0 \;\; on \; \Gamma \times R_+, \tag{2.70}$$

$$w(\mathbf{x}, 0) \;=\; w_0 \; on \; \Omega, \tag{2.71}$$

$$\dot{w}(\mathbf{x}, 0) \;=\; \dot{w}_0 \; on \; \Omega, \tag{2.72}$$

where dots indicate time differentiation, ρ is the mass/area, b is viscous damping, D is Kelvin-Voigt damping, Γ is the boundary, Ω is the open, bounded, connected, Lipschitz, 2D domain, and $\mathbf{n}$ is the unit-normal vector to Γ pointing toward the exterior of Ω.

Theorem 2.5: The response of the damped membrane governed by (2.69) – (2.72) is weakly bounded if either b or D is nonzero and $f(\mathbf{x}, t)$ is bounded $\forall \mathbf{x} \in \Omega$ and $t > 0$ ($f \in \mathcal{L}_\infty(\Omega)$).

Proof: The energy of the membrane

$$E = \frac{1}{2} \int_\Omega (\rho\dot{w}^2 + P\,|\nabla w|^2) dx \geq 0 \tag{2.73}$$
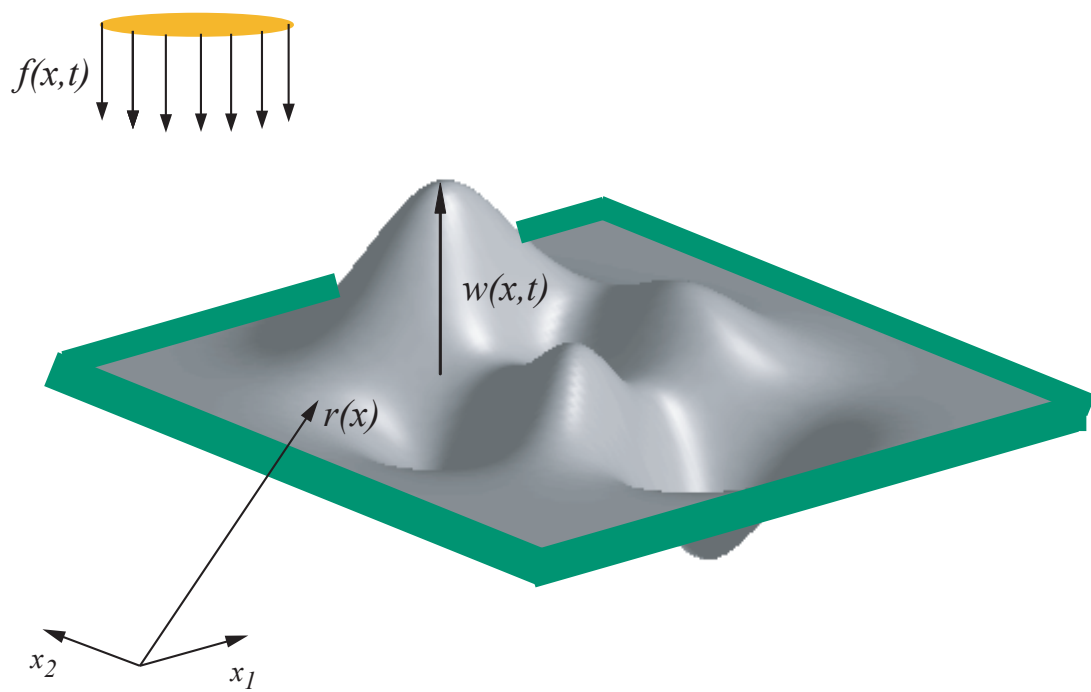
Fig. 2.5. Schematic diagram of a distributed damped membrane with distributed disturbances.

has a time rate of change which can be upper bounded by

$$
\begin{aligned}
\dot{E} &= \int_{\Omega} \left[\dot{w} \left(f - b\dot{w} + D\Delta\dot{w} + P\Delta w \right) + P\nabla w \cdot \nabla\dot{w} \right] dx \\
&\leq \delta_1 \int_{\Omega} \dot{w}^2 dx - b \int_{\Omega} \dot{w}^2 dx + D \int_{\Gamma} \frac{\partial \dot{w}}{\partial n} \dot{w} d\Gamma + P \int_{\Omega} \left(\nabla w \cdot \nabla\dot{w} \right) dx \\
&\quad - D \int_{\Omega} |\nabla\dot{w}|^2 dx + P \int_{\Gamma} \frac{\partial w}{\partial n} \dot{w} d\Gamma - P \int_{\Omega} \left(\nabla w \cdot \nabla\dot{w} \right) dx + \frac{1}{\delta_1} \int_{\Omega} f^2 dx \\
&\leq - \left(b + \frac{D}{2m_1} - \delta_1 \right) \int_{\Omega} \dot{w}^2 dx - \frac{D}{2} \int_{\Omega} |\nabla\dot{w}|^2 dx + \frac{1}{\delta_1} \int_{\Omega} f^2 dx, \qquad (2.74)
\end{aligned}
$$

where (2.3), (2.7), and (2.10) are used. Inequality (2.74) lacks the $\int_{\Omega} |\nabla w|^2$ term that appears in E. We therefore define a functional as (2.17) by adding the crossing term $C(t)$, where

$$
C(t) = \rho \int_{\Omega} \dot{w} w dx. \qquad (2.75)
$$

The functional $V(t)$ is positive because

$$
\begin{aligned}
|C(t)| &\leq \frac{1}{2}\rho \int_{\Omega} \left(\dot{w}^2 + w^2 \right) dx \leq \frac{1}{2}\rho \int_{\Omega} \left(\dot{w}^2 + m_1 |\nabla w|^2 \right) dx \\
&\leq \frac{\rho \max \left(1, m_1 \right)}{\min \left(\rho, P \right)} \frac{1}{2} \int_{\Omega} \left(\rho\dot{w}^2 + P |\nabla w|^2 \right) dx \\
&= \eta E, \qquad (2.76)
\end{aligned}
$$

using inequalities (2.7) and (2.10), where

$$
\eta = \frac{\rho \max \left(1, m_1 \right)}{\min \left(\rho, P \right)}. \qquad (2.77)
$$

This means that

$$0 \leq \lambda_1 E(t) \leq V(t) \leq \lambda_2 E(t), \tag{2.78}$$

where

$$\lambda_1 \;=\; 1 - \beta\eta > 0,$$

$$\lambda_2 \;=\; 1 + \beta\eta > 1,$$

for sufficiently small β. Differentiation of the crossing term produces

$$
\begin{aligned}
\dot{C} \;&=\; \int_\Omega \rho \ddot{w}\, w dx + \int_\Omega \rho \dot{w}^2\, dx \\
&=\; \int_\Omega (f - b\dot{w} + D\Delta\dot{w} + P\Delta w)\, w dx + \rho \int_\Omega \dot{w}^2\, dx \\
&=\; \rho \int_\Omega \dot{w}^2\, dx + \dot{C}_1 + \dot{C}_2 + \dot{C}_3 + \dot{C}_4.
\end{aligned}
\tag{2.79}
$$

The terms in (2.79) simplify as follows

$$
\begin{aligned}
\dot{C}_1 \;&=\; \int_\Omega f w dx \leq \delta_2 \int_\Omega w^2 dx + \frac{1}{\delta_2} \int_\Omega f^2 dx \\
&\leq\; \delta_2 m_1 \int_\Omega |\nabla w|^2\, dx + \frac{1}{\delta_2} \int_\Omega f^2 dx,
\end{aligned}
\tag{2.80}
$$

$$
\begin{aligned}
\dot{C}_2 \;&=\; -\int_\Omega b\dot{w} w dx \leq b\delta_3 \int_\Omega w^2 dx + \frac{b}{\delta_3} \int_\Omega \dot{w}^2 dx \\
&\leq\; b m_1 \delta_3 \int_\Omega |\nabla w|^2\, dx + \frac{b}{\delta_3} \int_\Omega \dot{w}^2 dx,
\end{aligned}
\tag{2.81}
$$

$$\dot{C}_3 \;=\; \int_\Omega Dw\Delta\dot{w}dx = D\int_\Gamma \frac{\partial\dot{w}}{\partial n}wd\Gamma - D\int_\Omega \left(\nabla w\cdot\nabla\dot{w}\right)dx$$

$$\leq\; D\delta_4\int_\Omega |\nabla w|^2\,dx + \frac{D}{\delta_4}\int_\Omega |\nabla\dot{w}|^2\,dx, \tag{2.82}$$

$$\dot{C}_4 \;=\; \int_\Omega Pw\Delta wdx = \int_\Gamma P\frac{\partial w}{\partial n}wd\Gamma - P\int_\Omega |\nabla w|^2\,dx$$

$$=\; -P\int_\Omega |\nabla w|^2\,dx, \tag{2.83}$$

using the boundary condition (2.70) and (2.3), (2.7), and (2.10). Substitution of (2.80) – (2.83) into (2.79) yields

$$\dot{C} \;\leq\; \left(\rho+\frac{b}{\delta_3}\right)\int_\Omega \dot{w}^2\,dx + \frac{D}{\delta_4}\int_\Omega |\nabla\dot{w}|^2\,dx + \frac{1}{\delta_2}\int_\Omega f^2 dx$$

$$-\left[P - \left(\delta_2+b\delta_3\right)m_1 - D\delta_4\right]\int_\Omega |\nabla w|^2\,dx. \tag{2.84}$$

Substitution of the derivative of crossing term (2.84) into (2.17) produces

$$\dot{V} \;\leq\; -\left[b + \frac{D}{2m_1} - \delta_1 - \beta\left(\rho+\frac{b}{\delta_3}\right)\right]\int_\Omega \dot{w}^2 dx + \left(\frac{1}{\delta_1}+\frac{\beta}{\delta_2}\right)\int_\Omega f^2 dx$$

$$-\beta\left[P - \left(\delta_2+b\delta_3\right)m_1 - D\delta_4\right]\int_\Omega |\nabla w|^2\,dx - D\left(\frac{1}{2}-\frac{\beta}{\delta_4}\right)\int_\Omega |\nabla\dot{w}|^2\,dx$$

$$\leq\; -\lambda_3 E + \varepsilon, \tag{2.85}$$

where, for sufficiently small β, δ_1, δ_2, δ_3, and δ_4,

$$\frac{1}{2} \geq \frac{\beta}{\delta_4}, \tag{2.86}$$

$$\varepsilon_1 = b + \frac{D}{2m_1} - \delta_1 - \beta\left(\rho + \frac{b}{\delta_3}\right) > 0, \tag{2.87}$$

$$\varepsilon_2 = \beta\left[P - (\delta_2 + b\delta_3)m_1 - D\delta_4\right] > 0, \tag{2.88}$$

$$\varepsilon = \left(\frac{1}{\delta_1} + \frac{\beta}{\delta_2}\right)\max_{t\in[0,\infty)}\int_\Omega f^2 dx < \infty, \tag{2.89}$$

$$\lambda_3 = \frac{\min\left(\varepsilon_1, \varepsilon_2\right)}{\max\left(\rho, P\right)} > 0 \tag{2.90}$$

for bounded f. Using (2.78), we obtain

$$\dot{V} \leq -\lambda V + \varepsilon, \tag{2.91}$$

where $\lambda = \lambda_3/\lambda_2$, with the solution

$$V(t) \leq V(0)e^{-\lambda t} + \frac{\varepsilon}{\lambda} \in \mathcal{L}_\infty \tag{2.92}$$

and

$$E(t) \leq \frac{1}{\lambda_1}V(t) \in \mathcal{L}_\infty. \tag{2.93}$$

$\square$

Thus, the system is weakly stable with respect to the energy norm.

2.4.2   Boundary Damped Membranes

We remove the distributed damping in (2.69) to obtain the two dimensional wave equation with partially damped boundary conditions shown in Fig. 2.6. The governing equations are

$$\rho \ddot{w} - P\Delta w \;=\; f \;\; in \; \Omega \times R_+, \tag{2.94}$$

$$w \;=\; 0 \;\; on \; \Gamma_0 \times R_+, \tag{2.95}$$

$$P\frac{\partial w}{\partial n} + c\dot{w} \;=\; 0 \;\; on \; \Gamma_1 \times R_+, \tag{2.96}$$

where $\Gamma = \Gamma_0 \cup \Gamma_1$, c is boundary damping coefficient, and the initial conditions are given in (2.71) and (2.72). We assume the boundary normals satisfy

$$\mathbf{r} \cdot \mathbf{n} \;\leq\; 0 \;\; on \; \Gamma_0, \tag{2.97}$$

$$\mathbf{r} \cdot \mathbf{n} \;>\; 0 \;\; on \; \Gamma_1, \tag{2.98}$$

where $\mathbf{r} = \mathbf{x} - \mathbf{x}_0$ and $x_0 \in \mathbb{R}^2$ [38, 40].

Theorem 2.6: The response of the boundary damped membrane governed by (2.94) – (2.96) is weakly bounded if $c > 0$, $f \in \mathcal{L}_\infty(\Omega)$, and the boundary normal conditions (2.97) and (2.98) are satisfied.

Proof: The energy given in (2.73) has a time derivative

$$\begin{aligned}
\dot{E} \;&=\; \int_\Omega (\dot{w}f + P\dot{w}\Delta w + P\nabla w \cdot \nabla \dot{w})dx \\
&\leq\; -c\int_{\Gamma_1} \dot{w}^2 d\Gamma + \delta_1 \int_\Omega \dot{w}^2 dx + \frac{1}{\delta_1}\int_\Omega f^2 dx,
\end{aligned} \tag{2.99}$$
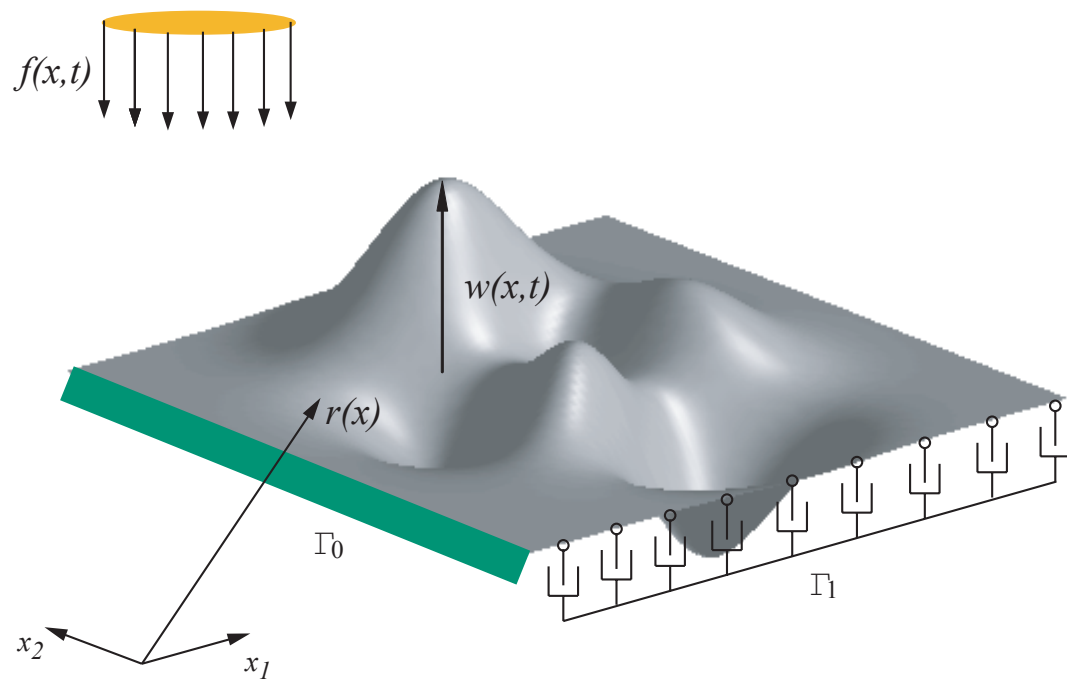
Fig. 2.6. Schematic diagram of a boundary damped membrane with distributed disturbances.

using (2.3), (2.7), and (2.96).

The boundary damper does not match the distributed input, providing neither a negative kinetic nor potential energy domain integral. A positive functional is defined as in (2.17) with a different crossing term

$$C(t) = C_1 + C_2, \qquad (2.100)$$

where $C_1 = 2 \int_\Omega \rho \dot{w} \, (\mathbf{r} \cdot \nabla w) \, dx$ and $C_2 = \int_\Omega \rho \dot{w} \, w dx$.

We bound the crossing term (2.100) with respect to the system energy as follows:

$$
\begin{aligned}
|C(t)| &\leq 2\rho R \int_\Omega |\dot{w}| \, |\nabla w| \, dx + \frac{1}{2}\rho \int_\Omega \left(\dot{w}^2 + w^2 \right) dx \\
&\leq \frac{2\rho R}{2} \int_\Omega \left(\dot{w}^2 + |\nabla w|^2 \right) dx + \frac{1}{2}\rho \int_\Omega \left(\dot{w}^2 + m_1 \, |\nabla w|^2 \right) dx \\
&\leq \eta E, \qquad (2.101)
\end{aligned}
$$

using (2.7) and (2.10), where

$$
\begin{aligned}
R &= \sup_{\Gamma_1} \|\mathbf{r}(\mathbf{x})\| , \qquad (2.102) \\
\eta &= \frac{\rho \max \left[(2R+1), \ (2R+m_1) \right]}{\min (\rho, P)}. \qquad (2.103)
\end{aligned}
$$

The time derivative of the crossing term (2.100) depends on

$$\dot{C}_1 = 2 \int_\Omega (f + P\Delta w) \, (\mathbf{r} \cdot \nabla w) \, dx + 2\rho \int_\Omega \dot{w} \, (\mathbf{r} \cdot \nabla \dot{w}) \, dx$$

$$\leq \quad 2R \int_{\Omega} |f| \, |\nabla w| \, dx + 2P \int_{\Omega} \Delta w \, (\mathbf{r} \cdot \nabla w) \, dx + 2\rho \int_{\Omega} \dot{w} \, (\mathbf{r} \cdot \nabla \dot{w}) \, dx$$

$$\leq \quad 2R\delta_2 \int_{\Omega} |\nabla w|^2 \, dx + \frac{2R}{\delta_2} \int_{\Omega} f^2 dx + \dot{C}_3 + \dot{C}_4, \tag{2.104}$$

where inequality (2.7) is used.

The third term in (2.104) simplifies as follows

$$\dot{C}_3 \quad = \quad 2P \int_{\Omega} \Delta w \, (\mathbf{r} \cdot \nabla w) \, dx$$

$$= \quad 2P \int_{\Gamma} (\mathbf{r} \cdot \mathbf{n}) \, |\nabla w|^2 \, d\Gamma - 2P \int_{\Omega} |\nabla w|^2 \, dx - P \int_{\Omega} \mathbf{r} \cdot \nabla \left(|\nabla w|^2 \right) dx$$

$$\leq \quad \frac{Rc^2}{P} \int_{\Gamma_1} \dot{w}^2 d\Gamma, \tag{2.105}$$

using the boundary conditions (2.95) and (2.96), (2.2) – (2.4), and (2.7). Based on (2.2) and the boundary condition (2.97), $2P \int_{\Gamma_0} (\mathbf{r} \cdot \mathbf{n}) \, |\nabla w|^2 \, d\Gamma \leq 0$ is dropped from (2.105). The forth term in Eq. (2.104),

$$\dot{C}_4 \quad = \quad 2\rho \int_{\Omega} \dot{w} \, (\mathbf{r} \cdot \nabla \dot{w}) \, dx$$

$$\leq \quad 2\rho R \int_{\Gamma_1} \dot{w}^2 d\Gamma - 4\rho \int_{\Omega} \dot{w}^2 dx - \dot{C}_4, \tag{2.106}$$

using the boundary conditions, (2.2), and (2.7). Solving (2.106),

$$\dot{C}_4 \leq \rho R \int_{\Gamma_1} \dot{w}^2 d\Gamma - 2\rho \int_{\Omega} \dot{w}^2 dx. \tag{2.107}$$

The time derivative of crossing term C_2

$$
\begin{aligned}
\dot{C_2} &= \int_\Omega (f + P\Delta w)\, w\, dx + \rho \int_\Omega \dot{w}^2 dx \\
&\leq -\left[P - \delta_3 m_1 - \frac{1}{2} c m_2 \right] \int_\Omega |\nabla w|^2\, dx + \rho \int_\Omega \dot{w}^2 dx \\
&\quad + \frac{1}{\delta_3} \int_\Omega f^2 dx + \frac{1}{2} c \int_{\Gamma_1} \dot{w}^2 d\Gamma,
\end{aligned}
\tag{2.108}
$$

using (2.3), (2.7), (2.10), and (2.11).   Substitution of (2.100), (2.104), (2.105), and (2.107) into (2.17) yields

$$
\begin{aligned}
\dot{V} &\leq -\beta \left[P - 2R\delta_2 - \delta_3 m_1 - \frac{1}{2} c m_2 \right] \int_\Omega |\nabla w|^2\, dx - (\beta\rho - \delta_1) \int_\Omega \dot{w}^2 dx \\
&\quad + \left[\frac{1}{\delta_1} + \beta \left(\frac{2R}{\delta_2} + \frac{1}{\delta_3} \right) \right] \int_\Omega f^2 dx \\
&\quad - \left\{ c - \beta \left[R \left(\frac{c^2}{P} + \rho \right) + \frac{1}{2} c \right] \right\} \int_{\Gamma_1} \dot{w}^2 d\Gamma,
\end{aligned}
\tag{2.109}
$$

where for sufficiently small β, δ_1, δ_2, and δ_3,

$$
c \geq \beta \left[R \left(\frac{c^2}{P} + \rho \right) + \frac{1}{2} c \right],
\tag{2.110}
$$

$$
\varepsilon_1 = \beta\rho - \delta_1 > 0,
\tag{2.111}
$$

$$
\varepsilon_2 = \beta \left[P - 2R\delta_2 - \delta_3 m_1 - \frac{1}{2} c m_2 \right] > 0,
\tag{2.112}
$$

$$
\varepsilon = \left(\frac{1}{\delta_1} + \frac{2\beta R}{\delta_2} + \frac{\beta}{\delta_3} \right) \max_{t \in [0,\infty)} \int_\Omega f^2 dx,
\tag{2.113}
$$

$$
\lambda_3 = \frac{\min \left(\varepsilon_1, \varepsilon_2 \right)}{\max \left(\rho, P \right)} > 0.
\tag{2.114}
$$

Therefore, (2.93) holds and the response is weakly bounded.
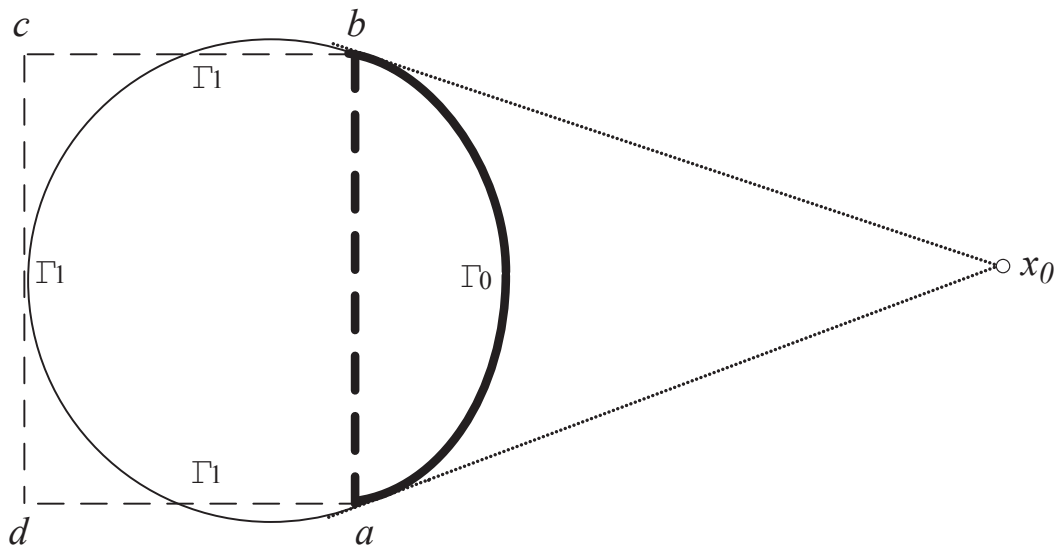
Fig. 2.7. Circular (solid) and rectangular (dashed) domain showing damped (thin) and undamped (thick) boundaries.

The partially damped boundary normal conditions (2.97) and (2.98) require damp-

ing on part of the boundary ($\Gamma_1 \neq \varnothing$). We are free to choose $\mathbf{x}_0$ to determine the

minimal Γ_1 for stability. If $\mathbf{x}_0$ is located at the center of a star shaped domain, then

the entire boundary has $\mathbf{r} \cdot \mathbf{n} > 0$ so $\Gamma_1 = \Gamma$ and the entire boundary must be damped.

Locating $\mathbf{x}_0$ outside Ω, however leads to $\Gamma_0 \neq \varnothing$ and part of the boundary need not be

damped. Fig. 2.7 shows example circular (solid) and rectangular (dashed) domains with

$\mathbf{x}_0 \notin \Omega$. In both cases, damping is not required on $\overline{ab}$. In the limit as $\mathbf{x}_0 \to \infty$, half

of the circular domain is damped. For the rectangular domain as $\mathbf{x}_0 \to \infty$, $\mathbf{r} \cdot \mathbf{n} < 0$ on

$\overline{ab}$ and $\mathbf{r} \cdot \mathbf{n} = \mathbf{0}$ on $\overline{bc}$ and $\overline{da}$, so $\mathbf{r} \cdot \mathbf{n} \leq 0$ on $\overline{da} \cup \overline{ab} \cup \overline{bc}$. Thus, only one side $\overline{cd} = \Gamma_1$

requires damping.

2.5 Distributed Plates

In this section, we investigate the stability of distributed and boundary damped

Kirchhoff plates with distributed excitation. We assume the plates are inextensible and

homogeneous with uniform cross-section.

2.5.1 Distributed Damped Plates

The field equation of the distributed damped plate includes distributed viscous

and material damping and forcing:

$$\rho \ddot{w} + b \dot{w} + D \Delta^2 \dot{w} + D_E \Delta^2 w = f \quad in \ \Omega \times R_+, \tag{2.115}$$

with boundary condition

$$w = 0 \ on \ \Gamma \times R_+, \qquad (2.116)$$

$$\frac{\partial w}{\partial n} = 0 \ on \ \Gamma \times R_+, \qquad (2.117)$$

where D_E is the plate flexural rigidity. The initial conditions are given in (2.71) and (2.72).

Theorem 2.7: The response of the damped plate governed by (2.115) – (2.117) is weakly bounded if either b or D is nonzero and $f \in \mathcal{L}_\infty$.

Proof: The energy of the plate is

$$E = \frac{1}{2} \int_\Omega \left\{ 2 \left(1 - \mu \right) \left[\left(\frac{\partial^2 w}{\partial x_1 \partial x_2} \right)^2 - \frac{\partial^2 w}{\partial x_1^2} \frac{\partial^2 w}{\partial x_2^2} \right] + \rho \dot{w}^2 + D_E \left(\Delta w \right)^2 \right\} dx, \quad (2.118)$$

where μ is Poisson's ratio. The Gaussian curvature $2 \left(1 - \mu \right) \left[\left(\frac{\partial^2 w}{\partial x_1 \partial x_2} \right)^2 - \frac{\partial^2 w}{\partial x_1^2} \frac{\partial^2 w}{\partial x_2^2} \right]$ complicates the energy. For a clamped plate with either a rectangular domain or a smooth boundary, however, the Gaussian curvature integral is zero [60].

Elimination of the Gaussian curvature integral and differentiation of (2.118) produces

$$\dot{E} = \int_\Omega \left[\dot{w} \left(f - b\dot{w} - D\Delta^2 \dot{w} - D_E \Delta^2 w \right) + D_E \Delta w \Delta \dot{w} \right] dx$$

$$\leq - \left(b + \frac{D}{2m_1^2} - \delta_1 \right) \int_\Omega \dot{w}^2 dx - \frac{D}{2} \int_\Omega \left(\Delta \dot{w} \right)^2 dx + \frac{1}{\delta_1} \int_\Omega f^2 dx, \quad (2.119)$$

where (2.2), (2.3), (2.7), and (2.10) are used.

Both viscous and material damping match the disturbance input, producing a negative kinetic energy term in $\dot{E}$. The energy cannot be used to prove stability, however, because the time derivative lacks the $-\int_\Omega (\Delta w)^2 \, dx$ term that is found in E. We therefore add the crossing term in (2.75) to form positive functional (2.17). The crossing term can be bounded by (2.76), where

$$\eta = \frac{\rho \max \left(1, m_1^2\right)}{\min \left(\rho, D_E\right)}. \tag{2.120}$$

The time derivative of the crossing term (2.75) has the form of (2.84) with

$$\dot{C}_3 \leq D\delta_4 \int_\Omega (\Delta w)^2 \, dx + \frac{D}{\delta_4} \int_\Omega (\Delta \dot{w})^2 \, dx \tag{2.121}$$

and

$$\dot{C}_4 = -D_E \int_\Omega (\Delta w)^2 \, dx. \tag{2.122}$$

Substitution of (2.80), (2.81), (2.121), and (2.122) into (2.84) produces

$$
\begin{aligned}
\dot{V} \leq \; & -\left[b + \frac{D}{2m_1^2} - \delta_1 - \beta\left(\rho + \frac{b}{\delta_3}\right)\right] \int_\Omega \dot{w}^2 dx - D\left(\frac{1}{2} - \frac{\beta}{\delta_4}\right) \int_\Omega (\Delta \dot{w})^2 \, dx \\
& -\beta\left[D_E - (\delta_2 + b\delta_3)\, m_1^2 - D\delta_4\right] \int_\Omega (\Delta w)^2 \, dx + \left(\frac{1}{\delta_1} + \frac{\beta}{\delta_2}\right) \int_\Omega f^2 dx \\
\leq \; & -\lambda_3 E + \varepsilon, \tag{2.123}
\end{aligned}
$$

where, for sufficiently small β, δ_1, δ_2, δ_3, and δ_4,

$$\frac{1}{2} \geq \frac{\beta}{\delta_4}, \tag{2.124}$$

$$\varepsilon_1 = b + \frac{D}{2m_1^2} - \delta_1 - \beta\left(\rho + \frac{b}{\delta_3}\right) > 0, \tag{2.125}$$

$$\varepsilon_2 = \beta\left[D_E - (\delta_2 + b\delta_3)\, m_1^2 - D\delta_4\right] > 0, \tag{2.126}$$

$$\varepsilon = \left(\frac{1}{\delta_1} + \frac{\beta}{\delta_2}\right) \max_{t\in[0,\infty)} \int_\Omega f^2 dx < \infty, \tag{2.127}$$

$$\lambda_3 = \frac{\min(\varepsilon_1, \varepsilon_2)}{\max(\rho, D_E)} > 0. \tag{2.128}$$

Therefore, (2.93) holds and the system is weakly stable.

□

2.5.2 Boundary Damped Plates

For the boundary clamped plate model, the viscous and material damping are removed from the field equation and clamped boundary condition is changed to a damper on Γ_1. The field equation and boundary conditions are

$$\rho\ddot{w} + D_E\Delta^2 w = f \ in \ \Omega \times R_+, \tag{2.129}$$

$$w = 0 \ on \ \Gamma_0 \times R_+, \tag{2.130}$$

$$\frac{\partial}{\partial n}w = 0 \ on \ \Gamma_0 \times R_+, \tag{2.131}$$

$$\Delta w = 0 \ on \ \Gamma_1 \times R_+, \tag{2.132}$$

$$D_E\frac{\partial}{\partial n}\Delta w - c\dot{w} = 0 \ on \ \Gamma_1 \times R_+, \tag{2.133}$$

and the initial conditions are given in (2.71) and (2.72)

Theorem 2.8: The response of the boundary damped plate governed by (2.129) – (2.133) is bounded if $c > 0$, $f \in \mathcal{L}_\infty(\Omega)$, and the normal boundary conditions (2.97) and (2.98) are satisfied.

Proof: The time derivative of the energy

$$\dot{E} \leq -c \int_{\Gamma_1} \dot{w}^2 d\Gamma + \delta_1 \int_\Omega \dot{w}^2 dx + \frac{1}{\delta_1} \int_\Omega f^2 dx, \tag{2.134}$$

using boundary conditions and (2.7).

The boundary damper does not match the distributed input, providing neither a negative kinetic nor potential energy domain integral term. A positive functional is defined as in (2.17) with a different crossing term

$$C(t) = \int_\Omega \rho \dot{w} \, (\mathbf{r} \cdot \nabla w) \, dx. \tag{2.135}$$

We can bound this crossing term with respect to the system energy as in (2.101) using (2.7), (2.10), and (2.11), where

$$\eta = \frac{\rho R \max(1, m_1)}{\min(\rho, D_E)}. \tag{2.136}$$

The time derivative of the crossing term

$$
\begin{aligned}
\dot{C} &= \int_\Omega \left(f - D_E \Delta^2 w \right) (\mathbf{r} \cdot \nabla w) \, dx + \int_\Omega \rho \dot{w} \, (\mathbf{r} \cdot \nabla \dot{w}) \, dx \\
&\leq Rm_1 \delta_2 \int_\Omega (\Delta w)^2 \, dx + \frac{R}{\delta_2} \int_\Omega f^2 dx + \dot{C}_3 + \dot{C}_4,
\end{aligned}
\tag{2.137}
$$

using (2.2), (2.4), (2.7), and (2.10).

The third term in (2.137) simplifies as follows

$$
\begin{aligned}
\dot{C}_3 &= -\int_{\Omega} D_E \Delta^2 w \left(\mathbf{r} \cdot \nabla w \right) dx \\
&= -D_E \int_{\Gamma} \frac{\partial \Delta w}{\partial n} \left(\mathbf{r} \cdot \nabla w \right) d\Gamma + D_E \int_{\Gamma} \Delta w \frac{\partial}{\partial n} \left(\mathbf{r} \cdot \nabla w \right) d\Gamma \\
&\quad - D_E \int_{\Omega} \Delta \left(\mathbf{r} \cdot \nabla w \right) \Delta w dx \\
&= -D_E \int_{\Gamma} \frac{\partial \Delta w}{\partial n} \left(\mathbf{r} \cdot \nabla w \right) d\Gamma - \frac{1}{2} D_E \int_{\Omega} \mathbf{r} \cdot \nabla \left(\Delta w \right)^2 dx \\
&\quad + D_E \int_{\Gamma} \Delta w \left[\nabla \left(\mathbf{r} \cdot \nabla w \right) \cdot \mathbf{n} \right] d\Gamma - 2 D_E \int_{\Omega} \left(\Delta w \right)^2 dx \\
&\leq \frac{Rc}{\delta_3} \int_{\Gamma_1} \dot{w}^2 d\Gamma + Rc\delta_3 \int_{\Gamma_1} |\nabla w|^2 d\Gamma - D_E \int_{\Omega} \left(\Delta w \right)^2 dx \\
&\quad + \frac{1}{2} D_E \int_{\Gamma_0} \left(\mathbf{r} \cdot \mathbf{n} \right) \left(\Delta w \right)^2 d\Gamma \\
&\leq -\left(D_E - Rcm_2\delta_3 \right) \int_{\Omega} \left(\Delta w \right)^2 dx + \frac{Rc}{\delta_3} \int_{\Gamma_1} \dot{w}^2 d\Gamma, \quad\quad (2.138)
\end{aligned}
$$

using the boundary conditions and (2.2) – (2.7), and (2.10). Based on the boundary conditions (2.97), $\frac{1}{2} D_E \int_{\Gamma_0} \left(\mathbf{r} \cdot \mathbf{n} \right) \left(\Delta w \right)^2 d\Gamma \leq 0$ can be dropped. The fourth term in (2.137),

$$
\dot{C}_4 = \int_{\Omega} \rho \dot{w} \left(\mathbf{r} \cdot \nabla \dot{w} \right) dx \leq \frac{\rho R}{2} \int_{\Gamma_1} \dot{w}^2 d\Gamma - \rho \int_{\Omega} \dot{w}^2 dx, \quad\quad (2.139)
$$

using boundary conditions and (2.2), (2.4), and (2.102).

Substitution of (2.134), (2.137) – (2.139) into (2.17) produces

$$
\begin{aligned}
\dot{V} \;\leq\; & -\left[c - \beta R\left(\frac{\rho}{2} + \frac{c}{\delta_3}\right)\right] \int_{\Gamma_1} \dot{w}^2 d\Gamma - (\beta\rho - \delta_1) \int_\Omega \dot{w}^2 dx \\
& -\beta\left[D_E - R\left(m_1\delta_2 - cm_2\delta_3\right)\right] \int_\Omega (\Delta w)^2 \, dx + \left(\frac{1}{\delta_1} + \frac{\beta R}{\delta_2}\right) \int_\Omega f^2 dx \\
\leq\; & -\lambda_3 E + \varepsilon,
\end{aligned}
\tag{2.140}
$$

where, for sufficiently small β, δ_1, δ_2, and δ_3,

$$
c \;\geq\; \beta R\left(\frac{\rho}{2} + \frac{c}{\delta_3}\right),
\tag{2.141}
$$

$$
\varepsilon_1 \;=\; \beta\rho - \delta_1 > 0,
\tag{2.142}
$$

$$
\varepsilon_2 \;=\; \beta\left(D_E - Rm_1\delta_2 - Rcm_2\delta_3\right) > 0,
\tag{2.143}
$$

$$
\varepsilon \;=\; \left(\frac{1}{\delta_1} + \frac{\beta R}{\delta_2}\right) \max_{t\in[0,\infty)} \int_\Omega f^2 dx < \infty,
\tag{2.144}
$$

$$
\lambda_3 \;=\; \frac{\min\left(\varepsilon_1, \varepsilon_2\right)}{\max\left(\rho, D_E\right)} > 0.
\tag{2.145}
$$

Therefore, (2.93) holds and the response is weakly stable.

□

Chapter 3

Iterative Learning Velocity and Tension Control
for Axially Moving Materials

In this chapter, we apply the ILC approach in [55] to a single span axially moving material system with bounded periodic velocity perturbations at one boundary roller and a control torque applied to the other boundary roller. First, we prove boundedness of the distributed response under PD control [66]. Then we prove boundedness of the ILC controlled system and compare the simulated response of open loop, PD, and ILC control.

3.1 System Model

Figure 3.1 shows a schematic diagram of the axially moving material model. The axial motion $u(x,t)$ depends on position x and time t. The right end $(x = L)$ undergoes prescribed periodic motion with $\dot{u}_L(t) = \dot{u}_L(t + T)$. The left end $(x = 0)$ is controlled by the torque input $\tau_0(t)$ applied to a pulley with radius r_0, rotary inertia J_0, and applied upstream tension P_B. The material has uniform axial stiffness EA and mass/length ρ. The linear field equation is

$$\rho\ddot{u} - EA\,u_{xx} = 0 \ \ \forall\, x \in (0, L), \tag{3.1}$$
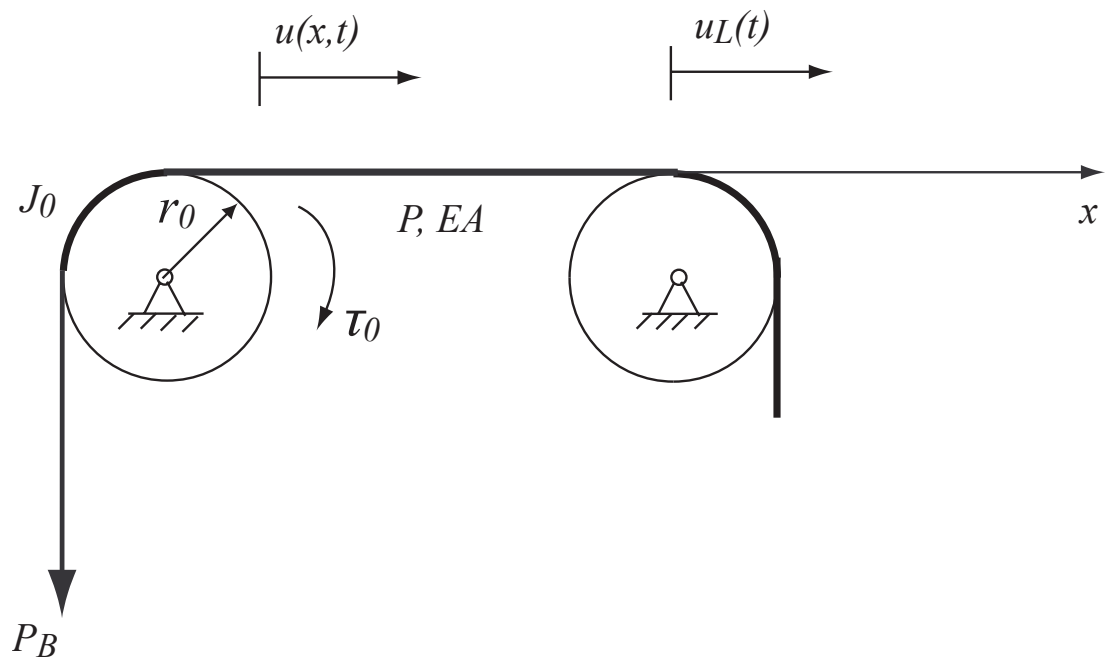
Fig. 3.1.   Schematic diagram of an axially moving material system.

where $(\dot{\ })$ and subscript x indicate time and spatial differentiation, respectively. The boundary conditions are

$$m\ddot{u}\left(0,t\right) - EA\,u_x\left(0,t\right) \;=\; f_0\left(t\right), \tag{3.2}$$

$$u\left(L,t\right) \;=\; u_L\left(t\right), \tag{3.3}$$

where $m = \dfrac{J_0}{r_0^2}$ and $f_0\left(t\right) = \dfrac{\tau_0(t)}{r_0} - P_B$. The string tension

$$P\left(x,t\right) = EAu_x\left(x,t\right). \tag{3.4}$$

We transform the displacement field

$$v\left(x,t\right) = u_L\left(t\right) - u\left(x,t\right) + \frac{P_D}{EA}\left(x - L\right), \tag{3.5}$$

where P_D is the constant desired material tension. The transformed Eq. (3.1)

$$\rho\ddot{v}\left(x,t\right) - EA\,v_{xx}\left(x,t\right) = \rho\ddot{u}_L\left(t\right) \quad \forall\; x \in \left(0,L\right), \tag{3.6}$$

and boundary conditions

$$m\ddot{v}\left(0,t\right) - EA\,v_x\left(0,t\right) + P_D \;=\; m\ddot{u}_L\left(t\right) - f_0\left(t\right), \tag{3.7}$$

$$v\left(L,t\right) \;=\; 0. \tag{3.8}$$

We assume the model described by Eqs. (3.7) and (3.8) is well posed and has an unique solution for all $f_0(t)$, $\dot{u}_L(t)$, and $\ddot{u}_L(t) \in \mathcal{L}_\infty$.

If we design $f_0(t)$ to ensure $v(x,t) = 0$, then $u(x,t) = u_L(t) + \frac{P_D}{EA}(x-L)$ and $P(x,t) = P_D$. The material translates under constant tension, P_D. In addition, $u(0,t) = u_L(t) - \frac{P_D L}{EA}$. So the left end follows the right end displacement offset by the constant material stretch. In practice, $u_L(t)$ may be unknown, so the result $v(x,t) = 0$ may not be achieved. If $v(x,t)$ can be shown to be bounded, however, then the tension and displacement will be weakly and pointwise bounded, respectively.

3.2 Control Formulation

We define the combined velocity/tension setpoint error

$$\eta(t) = \dot{v}(0,t) - \kappa v_x(0,t) = \dot{u}_L(t) - \eta_m(t), \qquad (3.9)$$

using Eqs. (3.4) and (3.5), where κ is a positive scalar control gain and $\eta_m(t) = \dot{u}(0,t) + \frac{\kappa}{EA}[P_D - P(0,t)]$ is the measurable part of $\eta(t)$. In Theorem 3.1 we show that PD tension plus D velocity feedback can ensure exponential transient $v(x,t)$ decay and bounded $v(x,t)$ in the presence of bounded disturbance $\dot{u}_L$, $\ddot{u}_L \in \mathcal{L}_\infty$.

Theorem 3.1: In the absence of a disturbance ($\ddot{u}_L(t) \equiv 0$), the response $v(x,t)$ of the system governed by Eqs. (3.6) – (3.8) decays exponentially for a control law of the form

$$f_0(t) = \frac{m\kappa}{EA}\dot{P}(0,t) - P(0,t) - k_s \eta_m(t). \qquad (3.10)$$

With a bounded disturbance ($\dot{u}_L(t)$, $\ddot{u}_L(t) \in \mathcal{L}_\infty$), $v(x,t)$ is bounded.

Proof: We define a Lyapunov functional

$$V(t) = E_s(t) + E_c(t) + \frac{1}{2}m\eta^2, \tag{3.11}$$

where the energy related term

$$E_s(t) = \frac{1}{2}\beta_s \int_0^L (\rho\dot{v}^2 + EA\, v_x^2)dx \geq 0 \tag{3.12}$$

includes kinetic and potential energy and the crossing term

$$E_c(t) = 2\beta_c\rho \int_0^L (x - L)\,\dot{v}v_x dx. \tag{3.13}$$

where β_s and β_c are constants. $E_c(t)$ can be bounded by

$$|E_c(t)| \leq \beta_c\rho L \int_0^L \left(\dot{v}^2 + v_x^2\right)dx = \xi E_s(t) \tag{3.14}$$

using inequality (2.7), where

$$\xi = \frac{2\beta_c\rho L}{\beta_s \min(\rho, EA)}.$$

This means that

$$0 \leq (1 - \xi)E_s \leq E_s + E_c \leq (1 + \xi)E_s.$$

Therefore, we can obtain the upper and lower bounds,

$$0 \leq \lambda_1\left(E_s + \eta^2\right) \leq V \leq \lambda_2\left(E_s + \eta^2\right), \tag{3.15}$$

where

$$\lambda_1 \;=\; \min\left(\xi_1, \frac{m}{2}\right) > 0,$$

$$\lambda_2 \;=\; \max\left(\xi_2, \frac{m}{2}\right) > 1.$$

The time derivative of Eq. (3.12)

$$
\begin{aligned}
\dot{E}_s \;=\;& \beta_s \rho \int_0^L \ddot{u}_L \dot{v}\,dx + \beta_s EA \int_0^L v_{xx}\dot{v}\,dx + \beta_s EA \int_0^L v_x \dot{v}_x\,dx \\[2mm]
=\;& \beta_s \rho \int_0^L \ddot{u}_L \dot{v}\,dx - \beta_s EA v_x\left(0,t\right)\dot{v}\left(0,t\right) \\[2mm]
=\;& \beta_s \rho \int_0^L \ddot{u}_L \dot{v}\,dx - \frac{\beta_s EA}{2\kappa}\dot{v}^2\left(0,t\right) + \frac{\beta_s EA}{2\kappa}\eta^2 - \frac{\beta_s \kappa EA}{2}v_x^2\left(0,t\right) \quad (3.16)
\end{aligned}
$$

using Eq. (3.9).

The time derivative of Eq. (3.13) simplifies to

$$
\begin{aligned}
\dot{E}_c \;=\;& 2\beta_c \rho \int_0^L \left(x - L\right)\ddot{u}_L v_x\,dx + 2\beta_c \rho \int_0^L \left(x - L\right)\dot{v}\dot{v}_x\,dx \\[2mm]
& +2\beta_c EA \int_0^L \left(x - L\right)v_{xx}v_x\,dx \\[2mm]
=\;& 2\beta_c \left[\rho \int_0^L \left(x - L\right)\ddot{u}_L v_x\,dx - EA \int_0^L v_x^2\,dx \right. \\[2mm]
& -\rho \int_0^L \dot{v}^2\,dx - EA \int_0^L \left(x - L\right)v_{xx}v_x\,dx \\[2mm]
& \rho\left(x - L\right)\dot{v}^2\big|_0^L + EA\left(x - L\right)v_x^2\big|_0^L - \rho \int_0^L \left(x - L\right)\dot{v}\dot{v}_x\,dx \\[2mm]
=\;& \beta_c \left[2\rho \int_0^L \left(x - L\right)\ddot{u}_L v_x\,dx + EALv_x^2\left(0,t\right) \right. \\[2mm]
& \left. +\rho L\dot{v}^2\left(0,t\right) - EA \int_0^L v_x^2\,dx - \rho \int_0^L \dot{v}^2\,dx \right], \quad (3.17)
\end{aligned}
$$

using the boundary conditions (3.7) and (3.8).

The time derivative of the final term in Eq. (3.11)

$$
\begin{aligned}
\frac{d}{dt}\left(\frac{1}{2}m\eta^2\right) &= \eta\left[m\ddot{v}\left(0,t\right) - m\kappa\dot{v}_x\left(0,t\right)\right] \\
&= \eta\left[m\ddot{u}_L + EAv_x\left(0,t\right) - f_0 - P_D - m\kappa\dot{v}_x\left(0,t\right)\right] \\
&= \eta\left\{m\ddot{u}_L - P\left(0,t\right) + \frac{m\kappa}{EA}\dot{P}\left(0,t\right) - \frac{m\kappa}{EA}\dot{P}\left(0,t\right)\right. \\
&\qquad \left. +P\left(0,t\right) + k_s\left\{\dot{u}\left(0,t\right) + \frac{\kappa}{EA}\left[P_D - P\left(0,t\right)\right]\right\}\right\} \\
&= \eta\left[-k_s\eta + m\ddot{u}_L + k_s\dot{u}_L\right] \\
&= -k_s\eta^2 + \eta q(t), \tag{3.18}
\end{aligned}
$$

using Eqs. (3.4), (3.5), (3.7), (3.9), and (3.22), where

$$
q\left(t\right) = m\ddot{u}_L + k_s\dot{u}_L. \tag{3.19}
$$

Substitution of Eqs. (3.16) – (3.18) into Eq. (3.11) produces

$$
\begin{aligned}
\dot{V} &= -\left(k_s - \frac{\beta_s EA}{2\kappa}\right)\eta^2 - \left(\frac{\beta_s \kappa EA}{2} - \beta_c EAL\right)v_x^2\left(0,t\right) \\
&\quad +\eta q - \beta_c\rho\int_0^L \dot{v}^2 dx - \beta_c EA\int_0^L v_x^2 dx + \beta_s\rho\int_0^L \ddot{u}_L\dot{v}dx \\
&\quad -\left(\frac{\beta_s EA}{2\kappa} - \beta_c\rho L\right)\dot{v}^2\left(0,t\right) + 2\beta_c\rho\int_0^L \left(x-L\right)\ddot{u}_L v_x dx \\
&\leq -\left(k_s - \frac{\beta_s EA}{2\kappa} - \delta_3\right)\eta^2 - \rho\left(\beta_c - \beta_s\delta_1\right)\int_0^L \dot{v}^2 dx \\
&\quad -\beta_c\left(EA - 2\rho L\delta_2\right)\int_0^L v_x^2 dx + \varepsilon \\
&\leq -\lambda V + \varepsilon, \tag{3.20}
\end{aligned}
$$

where

$$\varepsilon_1 = \rho\left(\beta_c - \beta_s\delta_1\right) > 0,$$

$$\varepsilon_2 = \beta_c\left(EA - 2\rho L\delta_2\right) > 0,$$

$$\varepsilon_3 = k_s - \frac{\beta_s EA}{2\kappa} - \delta_3 > 0,$$

for sufficiently small β_s, δ_1, δ_2, and δ_3,

$$\varepsilon = \rho L\left(\frac{\beta_s}{\delta_1} + \frac{2\beta_c L}{\delta_2}\right)\max_{t\in[0,\infty)}\left(\ddot{u}_L^2\right) + \frac{1}{\delta_3}\max_{t\in[0,\infty)}\left(m\ddot{u}_L + k_s\dot{u}_L\right)^2 \in \mathcal{L}_\infty,$$

and

$$\lambda_3 = \frac{2\min\left(\varepsilon_1, \varepsilon_2\right)}{\beta_s\max\left(\rho, EA\right)},$$

$$\lambda = \frac{\min\left(\lambda_3, \varepsilon_3\right)}{\max\left(\lambda_3, \frac{m}{2}\right)}.$$

In the absence of a disturbance ($u_L = 0$), we have $\varepsilon = 0$ and υ and V decay exponentially. Using Eqs. (2.8), (3.12), and (3.15), we can show

$$\frac{\beta_s EA}{2L}\upsilon^2\left(x, t\right) \leq \frac{\beta_s EA}{2}\int_0^L \upsilon_x^2\left(x, t\right)dx \leq E_s \leq V \qquad (3.21)$$

So $u\left(x, t\right) \to \frac{P_D}{EA}\left(x - L\right)$ exponentially using Eq. (3.5). With disturbance, $V \in \mathcal{L}_\infty$ and using inequality (3.21), $\upsilon\left(x, t\right)$ and $u\left(x, t\right) \in \mathcal{L}_\infty$. We cannot show pointwise boundedness of $P\left(x, t\right)$ but inequality (3.21) implies weak boundedness.

□

Theorem 3.1 shows that bounded inputs produce bounded response for the control law (3.10). In Theorem 3.2 we prove that the control law can be augmented with an iterative feedforward term if $\dot{u}_L(t) = \dot{u}_L(t+T)$. The iterative control law

$$f_0(t) = f_{0,j}(\tau) = \frac{m\kappa}{EA}\dot{P}(0,t) - P(0,t) + \Delta_j(\tau) - k_s\eta_m(t) \qquad (3.22)$$

where $\tau = t - jT \in [0,T]$ and j indicates the trial number that relates to the local time τ during each trial to time t. The learning term Δ_j is designed to compensate the unknown time function while maintaining stability. It is updated from trial to trial by the following learning law: for $\tau \in [0,\ T]$ and $j \geq 0$,

$$\gamma\dot{\Delta}_j + (1+\beta)\Delta_j = (1-\gamma)\Delta_{j-1} - \eta_m, \qquad (3.23)$$

where $\beta \geq 0$ and $0 < \gamma < 1$ are control gains. The conditions for the ILC are

$$\Delta_{-1} = 0, \qquad (3.24)$$

$$\Delta_j(0) = \Delta_{j-1}(T). \qquad (3.25)$$

Theorem 3.2: The control law (3.22) – (3.25) ensures that the response of the system (3.6) and (3.8) $\upsilon(x,t) \in \mathcal{L}_\infty$ for any $u_L(t) = u_L(t+T)$ with $\dot{u}_L(t)$, $\ddot{u}_L(t)$, and $\dddot{u}_L(t) \in \mathcal{L}_\infty$.

Proof: We define the Lyapunov functional $V(t)$, the energy related term $E_s(t)$ and the crossing term $E_c(t)$ as in (3.11) – (3.13). The time derivative of the boundary

term

$$
\begin{aligned}
\frac{d}{dt}\left(\frac{1}{2}m\eta^2\right) &= \eta\left\{m\ddot{u}_L - P(0,t) + \frac{m\kappa}{EA}\dot{P}(0,t) - \frac{m\kappa}{EA}\dot{P}(0,t) + P(0,t)\right.\\
&\qquad\left. -\Delta_j(\tau) + k_s\left\{\dot{u}(0,t) + \frac{\kappa}{EA}\left[P_D - P(0,t)\right]\right\}\right\}\\
&= -k_s\eta^2 + \eta\left[q(t) - \Delta_j(\tau)\right],
\end{aligned}
\tag{3.26}
$$

using Eqs. (3.4), (3.5), (3.7), (3.9), and (3.22).

Substitution of Eqs. (3.16), (3.17), and (3.26) into (3.11) produces

$$
\begin{aligned}
\dot{V} &\leq -\left(k_s - \frac{\beta_s EA}{2\kappa}\right)\eta^2 - \rho\left(\beta_c - \beta_s\delta_1\right)\int_0^L \dot{v}^2 dx\\
&\qquad -\beta_c\left(EA - 2\rho L\delta_2\right)\int_0^L v_x^2 dx + \eta\left[q - \Delta_j(\tau)\right] + \varepsilon\\
&\leq -\lambda V + \varepsilon + \eta\left[q - \Delta_j(\tau)\right],
\end{aligned}
\tag{3.27}
$$

where

$$
\begin{aligned}
\frac{\beta_s EA}{2\kappa} &\geq \beta_c\rho L,\\
\frac{\beta_s\kappa}{2} &\geq \beta_c L,\\
\varepsilon_1 &= \rho\left(\beta_c - \beta_s\delta_1\right) > 0,\\
\varepsilon_2 &= \beta_c\left(EA - 2\rho L\delta_2\right) > 0,\\
\varepsilon_3 &= k_s - \frac{\beta_s EA}{2\kappa} > 0,
\end{aligned}
$$

for sufficiently small δ_1, δ_2, and β_s. The constant

$$\varepsilon = \rho L \left(\frac{\beta_s}{\delta_1} + \frac{2\beta_c L}{\delta_2} \right) \max_{t \in [0,\infty)} \left(\ddot{u}_L^2 \right) \in \mathcal{L}_\infty,$$

and the exponent

$$\lambda = \frac{\min \left(\lambda_3, \varepsilon_3 \right)}{\max \left(\lambda_3, \frac{m}{2} \right)}.$$

where $\lambda_3 = \frac{2 \min(\varepsilon_1, \varepsilon_2)}{\beta_s \max(\rho, EA)}$. Eq. (3.27) can be rewritten as

$$\dot{V} \le -\lambda V + \varepsilon + (\dot{u}_L - \eta_m) \left[q - \Delta_j \left(\tau \right) \right]. \tag{3.28}$$

Now we define a positive function for the learning algorithm

$$L_j = \frac{1}{2} \left(1 - \gamma \right) \int_0^T \left[q \left(\tau \right) - \Delta_j \left(\tau \right) \right]^2 d\tau + \frac{1}{2} \gamma \left[q \left(T \right) - \Delta_j \left(T \right) \right]^2. \tag{3.29}$$

The incremental change of L_j from trial $j - 1$ to j is

$$
\begin{aligned}
\delta L_j \;=\;& L_j - L_{j-1} \\
=\;& \frac{1}{2} \gamma \left\{ \left[q \left(T \right) - \Delta_j \left(T \right) \right]^2 - \left[q \left(T \right) - \Delta_{j-1} \left(T \right) \right]^2 \right\} \\
& + \frac{1}{2} \left(1 - \gamma \right) \int_0^T \left[\left(q - \Delta_j \right)^2 - \left(q - \Delta_{j-1} \right)^2 \right] d\tau \\
=\;& \frac{1}{2} \left(1 - \gamma \right) \int_0^T \left[\left(q - \Delta_j \right)^2 - \left(q - \Delta_{j-1} \right)^2 \right] d\tau \\
& + \frac{1}{2} \gamma \left\{ \left[q \left(T \right) - \Delta_j \left(T \right) \right]^2 - \left[q \left(0 \right) - \Delta_j \left(0 \right) \right]^2 \right\},
\end{aligned}
$$

using (3.25) and $q\left(T\right)=q\left(0\right)$. Further simplification produces

$$
\begin{aligned}
\delta L_j &= \frac{1}{2}\left(1-\gamma\right)\int_0^T\left[\left(q-\Delta_j\right)^2-\left(q-\Delta_{j-1}\right)^2\right]d\tau \\
&\quad +\frac{1}{2}\gamma\int_0^T\frac{d}{dt}\left[\left(q-\Delta_j\right)^2\right]d\tau \\
&= \frac{1}{2}\left(1-\gamma\right)\int_0^T\left[\left(q-\Delta_j\right)^2-\left(q-\Delta_{j-1}\right)^2\right]d\tau \\
&\quad +\gamma\int_0^T\left(q-\Delta_j\right)\left(\dot{q}-\dot{\Delta}_j\right)d\tau \\
&= \int_0^T\left\{-\left(q-\Delta_j\right)\left(\dot{u}_L-\eta_m\right)-\beta\left(q-\Delta_j\right)^2\right.\\
&\quad -\frac{1}{2}\left(1-\gamma\right)\left(\Delta_{j-1}-\Delta_j\right)^2 \\
&\quad -\left\{\frac{1}{2\sqrt{\gamma}}\left[\gamma\dot{q}+\left(\beta-\gamma\right)q+\dot{u}_L\right]+\sqrt{\gamma}\Delta_j\right\}^2 \\
&\quad \left.+\frac{1}{4\gamma}\left[\gamma\dot{q}+\left(\beta+\gamma\right)q+\dot{u}_L\right]^2\right\}d\tau
\end{aligned}\tag{3.30}
$$

using Eq. (3.23). Finally, discarding the negative third and fourth terms in Eq. (3.30)

$$
\delta L_j\le\int_0^T\left[d-\beta\left(q-\Delta_j\right)^2-\left(q-\Delta_j\right)\left(\dot{u}_L-\eta_m\right)\right]d\tau,\tag{3.31}
$$

where

$$
d\left(t\right)=\frac{1}{4\gamma}\left[\gamma\dot{q}+\left(\beta+\gamma\right)q+\dot{u}_L\right]^2\in\mathcal{L}_\infty\tag{3.32}
$$

by the Theorem assumptions.

Now we combine Eqs. (3.11) and (3.29) to produce

$$
V_T\left(t\right)=V\left(t\right)+V_L\left(t\right)>0,\tag{3.33}
$$

with

$$V_L = \frac{1}{2}(1-\gamma)\int_{t-T}^{t}(q-\Delta)^2\,d\tau + \frac{1}{2}\gamma(q-\Delta)^2, \tag{3.34}$$

where for all $j \geq 0$

$$\Delta(\tau) = \Delta_j(t-jT) \quad \tau \in [jT,\ (j+1)T]. \tag{3.35}$$

The learning law (3.23) can be rewritten as

$$\gamma\dot{\Delta}(t) + (1+\beta)\Delta(t) = (1-\gamma)\Delta(t-T) - \eta_m. \tag{3.36}$$

Substituting Eq. (3.36) into the time derivative of Eq. (3.34) yields

$$\dot{V}_L \leq d - \beta[q(t)-\Delta(t)]^2 - [q(t)-\Delta(t)](\dot{u}_L - \eta_m). \tag{3.37}$$

Substitution of Eq. (3.37) into the time derivative of (3.33) produces

$$\begin{aligned}\dot{V}_T \;\leq\; & -\lambda V + \varepsilon + (\dot{u}_L - \eta_m)\Big[q - \Delta_j(\tau)\Big] + d \\ & - [q(t)-\Delta(t)](\dot{u}_L - \eta_m) - \beta[q(t)-\Delta(t)]^2 \end{aligned} \tag{3.38}$$

using Eq. (3.37). The right hand side of inequality (3.38) contains all the terms in Eq. (3.33) with negative coefficients except $\int_{t-T}^{t}(q-\Delta)^2\,d\tau$ term in V_L. Boundedness of the integrand, however, implies boundedness of the finite integral because $\int_{t-T}^{t}(q-\Delta)^2\,d\tau \leq T\max_{t\in(t-T,t)}(q-\Delta)^2$. Thus, for sufficiently large V_T, $\dot{V}_T < 0$ so

$V_T \in \mathcal{L}_\infty$ [54] and

$$\frac{\beta_s EA}{2L} v^2(x,t) \leq \frac{\beta_s EA}{2} \int_0^L v_x^2(x,t)\, dx \leq E_s \leq V \leq V_T \in \mathcal{L}_\infty,$$

using (2.8), (3.12), (3.15), and (3.33).

☐

3.3   Simulation

In this section, numerical simulation verifies the stability and performance of the open loop system and PD and ILC closed loop systems.   Eq. (3.1) can be rewritten in the form

$$\ddot{\boldsymbol{v}} + \boldsymbol{A}\boldsymbol{v} = \boldsymbol{B}\boldsymbol{f},$$

where $\boldsymbol{v}(x,t) = [v(x,t)\ \ v(0,t)]^T \in H$ denotes the composite displacement vector that contains all dynamic distributed and lumped displacement, $\boldsymbol{A}$ is the stiffness matrix operator with $\boldsymbol{A}\boldsymbol{v} = -EA\left[v_{xx}(x)\quad v_{xx}(0)\right]^T$, $\boldsymbol{B}$ is the control input operator, and $\boldsymbol{f}$ $\in \mathbb{R}^m$ is the control input vector with $\boldsymbol{B}\boldsymbol{f} = \left[\rho\ddot{u}_L(t)\quad m\ddot{u}_L(t) - f_0(t)\right]^T$.

The system is discretized using a four admissible function expansion

$$\boldsymbol{v}(x,t) = \sum_{j=1}^{4} q_j(t)\, \Phi_j(x),$$

with

$$\Phi_j(x) = \left[\Phi_j(x)\quad \Phi_j(0)\right]^T$$

and free-pinned string eigenfunctions for $\Phi_j(x)$. Application of Galerkin's method produces the discretized equations.

These equations and Eq. (3.36) are numerically integrated using Matlab with the parameters in Table 3.1.

Table 3.1.   Simulation Parameters

Parameters	Values
Equivalent mass m	0.5 $[kg]$
Span length L	1.5 $[m]$
Material linear density ρ	0.01 $[kg/m]$
Material Young's modulus EA	1000 $[N]$
Desired tension P_D	50 $[N]$

Figure 3.2 shows the stop-start $\dot{u}_L(t)$ used in simulation. Figures 3.2(a)-(b) show the right end starts with constant acceleration at 24 m/s^2 and then switches to -24 m/s^2. The material dwells at zero velocity to produce an overall $T = 0.042$ s, near the first natural frequency of the open loop system (12 Hz). The speed trajectory corresponds to forward indexing of the material and does not satisfy the bounded jerk assumption of Theorem 3.2. Figure 3.2 (c) shows the open loop velocity error $\dot{v}(0,t) = \dot{u}_L(t) - \dot{u}(0,t)$ from Eq. (3.5) is almost ten times the input velocity. Figure 3.2(d) shows almost 100% tension error.

Figure 3.3 shows velocity error, learning term Δ, tension error, and control force at the left transport under PD and ILC control using control gains in the Table 3.2.
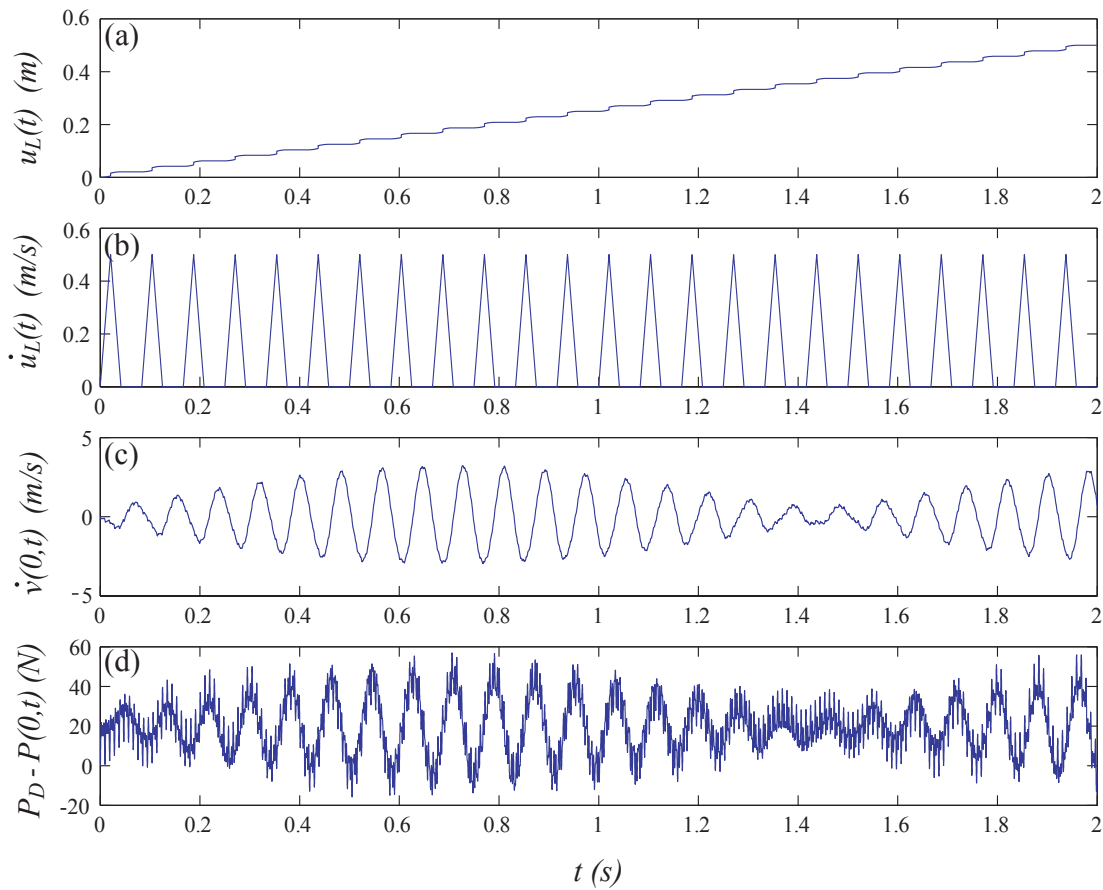
Fig. 3.2. Open loop response of the system: (a) Disturbance position, $u_L(t)$, (b) Disturbance velocity, $\dot{u}_L(t)$, (c) Velocity error, $\dot{v}(0,t)$, and (d) Tension error, $P_D - P(0,t)$.

Table 3.2.   Control Gains

Parameters	Values
κ	100
k_s	10
β	0.01
γ	0.0001

The PD controller reduces the velocity and tension errors by an order of magnitude to less than 0.3 m/s and 3 N, respectively.   The iterative term in Fig. 3.3(b) slowly increases as the controller learns the periodic disturbance.   The velocity and tension errors decrease to less than 0.15 m/s and 1 N by the end of the simulation ($t = 3$ s). The ILC controller uses almost the same control effort amplitude to achieve this performance improvement.

3.4   Robustness

The ILC control law (3.22) and (3.23) depends on $P(0, t)$ and $\dot{u}(0, t)$ which are measured tension and velocity at controlled roller, $\dot{P}(0, t)$ which can be calculated by time derivative of measured tension, and the desired tension P_D. The control law also requires exact knowledge of the parameters m and EA. EA appears in two places in Eq. (3.22) in the form m/EA. Thus, changes in EA scale the control gain κ and may lead to changes in performance but not stability. Changes in m, however, directly affect a feedforward term in (3.22) so instability is possible.

To investigate the stability and performance robustness of the ILC controller, we simulate the following cases: (i) $m = 0.067$ kg, $EA = 667$ N; (ii) $m = 0.067$ kg,
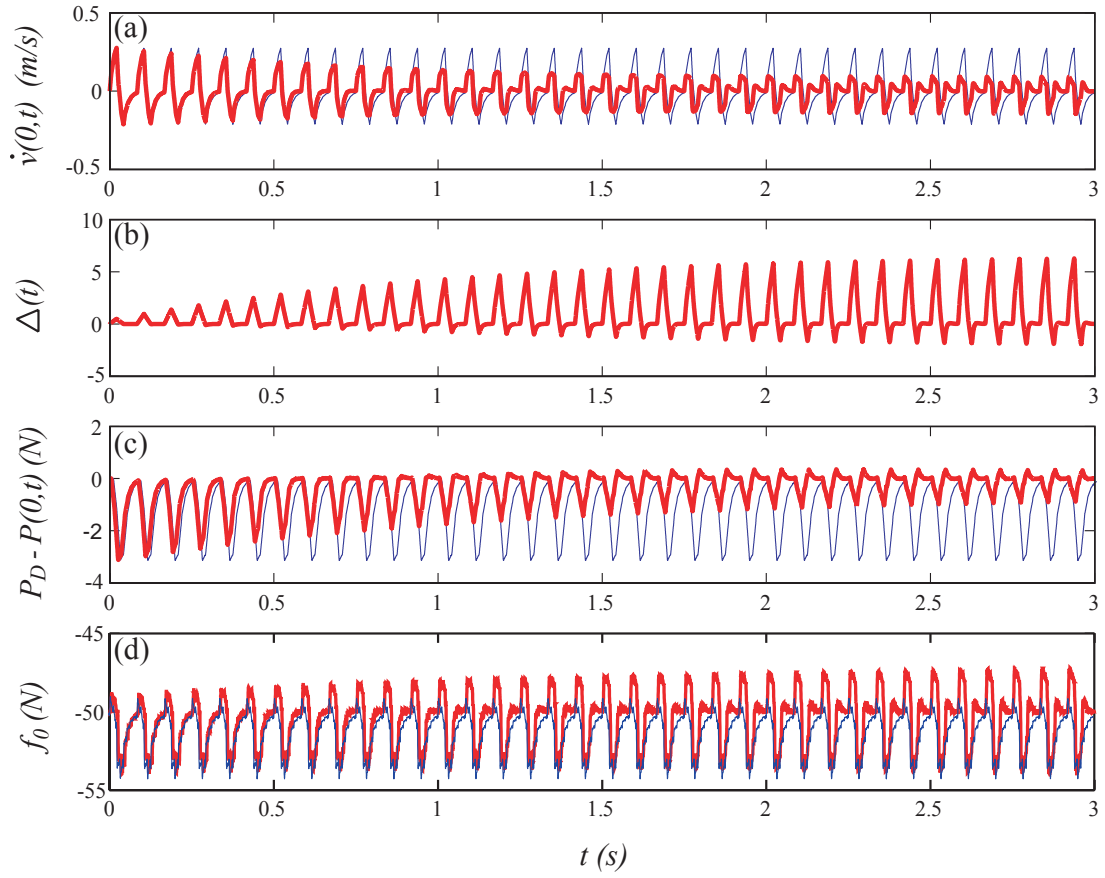
Fig. 3.3. Closed loop response of the system under PD (thin) and ILC (thick) control: (a) Velocity error, $\dot{v}(0,t)$, (b) Learning term, $\Delta(t)$, (c) Tension error, $P_D - P(0,t)$, and (d) Control effort, $f_0(t)$.

$EA = 1500$ N; (iii) $m = 0.15$ kg, $EA = 667$ N; and (iv) $m = 0.15$ kg, $EA = 1500$ N with

the same control gains in Table 3.2. These cases correspond to ± 3 dB changes in m and

EA. The simulation results (see Appendix A shows stable and improved performance

response.

Chapter 4

Repetitive Control of an Electrostatic
Microbridge Actuator

In this chapter, we apply the RLC approach in [23] to an electrostatic micro-bridge actuator with a bounded periodic desired trajectory, a distributed electrostatic force actuator, and distributed displacement sensing. Offline processing that updates a waveform generator's parameters based on measured response reduces errors between the desired and actual output. First, we prove boundedness of the distributed response under distributed damping using the energy multiplier method [56, 66]. Then, we prove boundedness of the repetitive controlled system and compare the simulated response under open loop and RLC. The contributions of this chapter include (i) a novel, feedforward control strategy for MEMS actuators, (ii) the first repetitive controller with proven stability characteristics designed for a distributed flexible system, and (iii) simulated response showing significant performance improvement under RLC.

4.1 System Model

Figure 4.1 shows a schematic diagram of the electrostatic microbridge model. It includes a partial differential equation for transverse displacement $w(x, t)$ as a function of a distributed electrostatic applied force $f(t)$. It is assumed that the transverse stiffness of the microbridge is due mainly to the residual tensile stress associated with device

fabrication and that bending stiffness can be neglected. Thus, a string model is used with uniform distributed forcing over the domain.
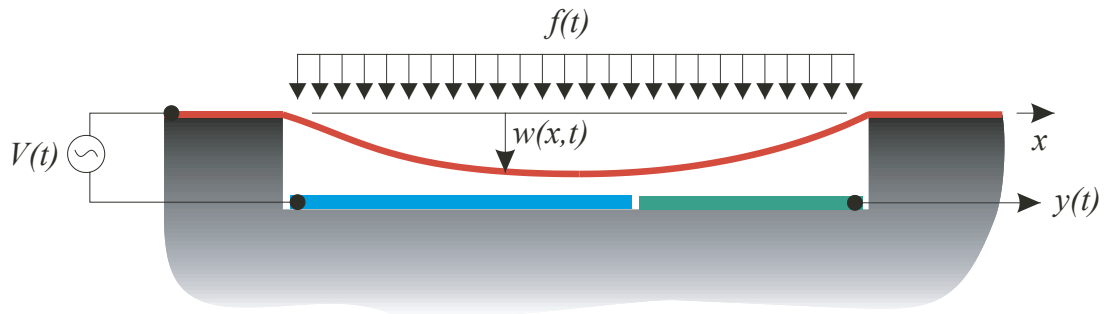
Fig. 4.1.   Schematic diagram of the electrostatic microbridge model.

The field equation and boundary conditions are

$$\rho \ddot{w} + c\dot{w} - Pw_{xx} = f, \ \forall \ x \in (0, L), \tag{4.1}$$

$$w(0, t) = w(L, t) = 0, \tag{4.2}$$

where ρ is the mass/length, P is the residual tension, L is the length, c is squeeze film damping coefficient, and $f(t)$ is uniformly distributed electrostatic force.   We assume that the microbridge operates around a nonzero voltage equilibrium and the force variation $f(t)$ in Eq. (4.1) is proportional to the applied voltage variation.

The control objective for the microbridge is to force the displacement $w(x, t)$ to track a desired shape and time trajectory $v(x, t)$. The desired trajectory is assumed to be bounded, periodic, and satisfying boundary conditions $v(0, t) = v(L, t) = 0$.   We

define the distributed response error $e(x, t) = v(x, t) - w(x, t)$ and the transformed

equations are

$$\rho \ddot{e} + c \dot{e} - P e_{xx} = q - f, \ \forall \ x \in (0, L), \tag{4.3}$$

$$e(0, t) = e(L, t) = 0, \tag{4.4}$$

where $q(x, t) = \rho \ddot{v} + c \dot{v} - P v_{xx}$ is periodic but unknown due to the unknown parameters

ρ, c, and P.

We assume that system is designed such that the device capacitance can be mea-

sured in real-time. Capacitance depends on the average gap between microbridge and

electrode so the output $y(t) = \int_0^L w \, dx$ is therefore available via high-speed data acqui-

sition.

4.2 Control Architecture

The control objective is to design the control input $V(t)$ to force the bridge to

follow a periodic desired spatial and time trajectory $v(x, t)$ based on the measured out-

put $y(t)$. Figure 4.2 shows the proposed control architecture to achieve this objective.

The actuation voltage is produced by a waveform generator that is periodically triggered

with a sample period of T. The structure reacts to the forcing and produces the mea-

sured time response $y(t)$. Several periods of the output are buffered in the high speed

Analog to Digital Converter (ADC). A block of N samples of the ADC data (sampled at

T/N) is loaded into the control microprocessor every T_R seconds. The repetitive algorithm is implemented on this microprocessor and used to update the waveform generator trajectory.
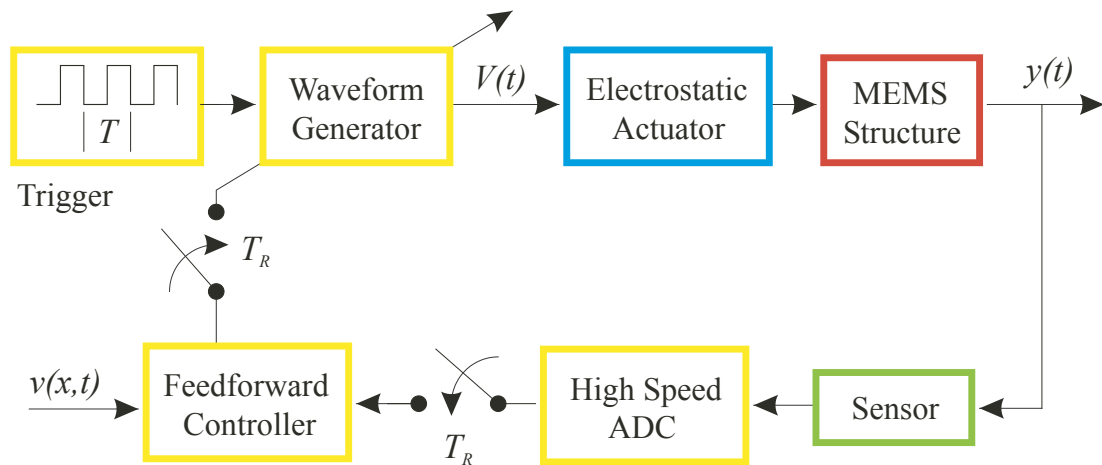
Fig. 4.2.   Repetitive control block diagram.

4.3   Control Formulation

The current method for setpoint regulation in microbridge actuators uses square wave inputs that move the structure quickly but produce excessive residual vibration. Between waveform generator updates in the proposed control approach (*e.g.* $0 < t < T_R$), the actuator is also forced with a bounded and periodic $f(t)$.   In both case, therefore, it is important to determine that damping ensures bounded response.

In Theorem 4.1 we show that distributed squeeze film damping can ensure bounded $w\left(x,t\right)$ under bounded uniformly distributed electrostatic force $f\left(t\right)$ for all $x \in \left(0, L\right)$ $\left(f\left(t\right) \in \mathcal{L}_{\infty}\right)$.

Theorem 4.1: Under uniformly distributed electrostatic force, the response $w\left(x,t\right)$ of the system governed by Eqs. (4.1) and (4.2) is bounded under distributed squeeze film damping with bounded input $f\left(t\right) \in \mathcal{L}_{\infty}$.

Proof: We define a Lyapunov functional

$$V\left(t\right) = E_{s}\left(t\right) + E_{c}\left(t\right), \tag{4.5}$$

where the energy related term $E_{s}\left(t\right)$ and the crossing term $E_{c}\left(t\right)$ for the microbridge are

$$E_{s}\left(t\right) \;=\; \frac{1}{2}\beta_{s}\int_{0}^{L}(\rho\dot{w}^{2} + Pw_{x}^{2})dx \geq 0, \tag{4.6}$$

$$E_{c}\left(t\right) \;=\; \beta_{c}\rho\int_{0}^{L}\dot{w}wdx, \tag{4.7}$$

where β_{s} and β_{c} are positive constants. $E_{c}\left(t\right)$ can be bounded by

$$\begin{aligned}
\left|E_{c}\left(t\right)\right| \;&\leq\; \frac{\beta_{c}\rho}{2}\int_{0}^{L}\left(\dot{w}^{2} + w^{2}\right)dx \\
&\leq\; \frac{\beta_{c}\max\left(1, L^{2}\right)}{\beta_{s}\min\left(\rho, P\right)}\frac{1}{2}\beta_{s}\int_{0}^{L}\left(\rho\dot{w}^{2} + Pw_{x}^{2}\right)dx \\
&=\; \xi E_{s}\left(t\right)
\end{aligned} \tag{4.8}$$

using the inequality (2.7), where

$$\xi = \frac{\beta_c \max\left(1, L^2\right)}{\beta_s \min\left(\rho, P\right)}.$$

This means that

$$0 \leq \xi_1 E_s \leq E_s + E_c \leq \xi_2 E_s,$$

where

$$\xi_1 = 1 - \xi > 0,$$

$$\xi_2 = 1 + \xi > 1.$$

Time derivative of the energy related term (4.6)

$$\dot{E}_s = \beta_s P \int_0^L \dot{w} w_{xx} dx - \beta_s c \int_0^L \dot{w}^2 dx + \beta_s \int_0^L f\dot{w} dx + \beta_s P \int_0^L w_x \dot{w}_x dx$$

$$\leq -\left(\beta_s c - \beta_s \delta_1\right) \int_0^L \dot{w}^2 dx + \frac{\beta_s}{\delta_1} \int_0^L f^2 dx. \tag{4.9}$$

using integration by parts and Ineq. (2.7).

Time derivative of the crossing term (4.7)

$$\dot{E}_c = \beta_c \rho \int_0^L \dot{w}^2 dx - \beta_c c \int_0^L w\dot{w} dx + \beta_c P \int_0^L w w_{xx} dx + \beta_c \int_0^L fw dx$$

$$\leq \beta_c \rho \int_0^L \dot{w}^2 dx + \beta_c \delta_2 L^2 \int_0^L w_x^2 dx + \frac{\beta_c}{\delta_2} \int_0^L f^2 dx + \dot{C}_1 + \dot{C}_2, \tag{4.10}$$

using (2.9), where $\dot{C}_1 = -\beta_c c \int_0^L w \dot{w} dx$ and $\dot{C}_2 = \beta_c P \int_0^L w w_{xx} dx$. Using (2.7)

$$
\begin{aligned}
\dot{C}_1 &\leq \frac{\beta_c c}{\delta_3} \int_0^L \dot{w}^2 dx + \beta_c \delta_3 c \int_0^L w^2 dx \\
&\leq \frac{\beta_c c}{\delta_3} \int_0^L \dot{w}^2 dx + \beta_c \delta_3 c L^2 \int_0^L w_x^2 dx.
\end{aligned}
\tag{4.11}
$$

Integration by parts produces

$$
\dot{C}_2 = -\beta_c P \int_0^L w_x^2 dx.
\tag{4.12}
$$

Use of $(4.9) - (4.12)$ produces

$$
\begin{aligned}
\dot{V} \leq &-\left[\beta_s \left(c - \delta_1\right) - \beta_c \left(\rho + \frac{c}{\delta_3}\right)\right] \int_0^L \dot{w}^2 dx \\
&-\beta_c \left[P - \left(\delta_2 + \delta_3 c\right) L^2\right] \int_0^L w_x^2 dx + \varepsilon,
\end{aligned}
$$

where, for sufficiently small δ_1, δ_2, δ_3, and β_c,

$$
\beta_s \left(c - \delta_1\right) - \beta_c \left(\rho + \frac{c}{\delta_3}\right) > 0,
\tag{4.13}
$$

$$
\beta_c \left[P - \left(\delta_2 + \delta_3 c\right) L^2\right] > 0,
\tag{4.14}
$$

$$
\varepsilon = \max_{t \in [0,\infty)} \left(\frac{\beta_s}{\delta_1} + \frac{\beta_c}{\delta_2}\right) \int_0^L f^2 dx \in \mathcal{L}_\infty.
\tag{4.15}
$$

Thus, $\dot{V} \leq -\lambda V + \varepsilon$ and $V(t) \leq \varepsilon/\lambda$. Using (4.6), (4.8), and inequality (2.9) we can show

$$\frac{\beta_s EA}{2L} w^2(x,t) \leq \frac{\beta_s EA}{2} \int_0^L w_x^2(x,t)\, dx \leq E_s \leq V \in \mathcal{L}_\infty. \tag{4.16}$$

□

Theorem 4.1 shows that bounded inputs produce bounded response for the string model under distributed squeeze film damping. In Theorem 4.2 we prove that the control law can be augmented with a repetitive feedforward term if $v(t) = v(t+T)$. We divide the control input into a square wave $f_0(t)$ plus the learning term $\Delta(t)$. The learning law updates $\Delta(t)$ based on the previous $\Delta(t-T)$ and "error" $q_e(t)$ as follows:

$$\Delta(t) = \text{sat}_\sigma [\Delta(t-T)] + q_e(t-T) \quad \text{for } t \in [0,\ T] \tag{4.17}$$

where

$$\text{sat}_\sigma(\zeta) = \begin{cases} \zeta, & \text{for } |\zeta| \leq \sigma \\ \text{sgn}(\zeta)\,\sigma, & \text{for } |\zeta| > \sigma \end{cases} \tag{4.18}$$

and

$$q_e(t) = \int_0^L \left(\beta_s \dot{e} + \beta_c e \right) dx. \tag{4.19}$$

The second term in Eq. (4.19) is measured using the capacitance $y(t)$. The first term, however, is measured by differentiation of the capacitance signal. This is not real-time differentiation but offline processing of periodic data for $t \in [0,\ T]$. Thus, central difference and data smoothing filters can be applied to reduce noise. The desired space/time trajectory is chosen and combined with the measured integrated

displacement and integrals in Eq. (4.19). For each period T (known), $\Delta(t)$ is updated using the previous period $q_e(t)$. In practice, many periods of data could be collected and averaged before the waveform generator is updated. Finally, the ILC control law does not require knowledge of the systems parameters. The control gains β_s and β_c must satisfy inequalities based on the system parameters but these can be conservative, worst case estimates.

Theorem 4.2: Without exact knowledge of the parameters ρ, c, and P, the control law (4.17) – (4.19) ensures that the error response of the system governed by Eqs. (4.3) and (4.4), $e(x,t) \in \mathcal{L}_\infty$ for any $v(x,t) = v(x, t+T)$ with $f_0(t)$, $v(x,t)$, $\dot{v}(x,t)$, and $\ddot{v}(x,t) \in \mathcal{L}_\infty$ if $\dfrac{\beta_s}{\beta_c} > \dfrac{\rho + \frac{L^2 c^2}{P}}{c}$.

Proof: We define the Lyapunov functional $V(t)$, the energy related term $E_s(t)$ and the crossing term $E_c(t)$ as in (4.5) – (4.7) except with $w(x,t)$ replaced by $e(x,t)$.

Substitution of time derivatives of Eqs. (4.6) and (4.7) into the derivative of Eq. (4.5) considering electrostatic force produces

$$
\begin{aligned}
\dot{V} \;\leq\; & -\left(\beta_s c - \beta_c \rho - \frac{\beta_c c}{\delta_3} \right) \int_0^L \dot{e}^2 \, dx - \beta_c \left(P - \delta_3 c L^2 \right) \int_0^L e_x^2 \, dx \\
& + \int_0^L \left(q - f_0 - \Delta \right) \left(\beta_s \dot{e} + \beta_c e \right) dx.
\end{aligned}
$$

The third term can be written as

$$\int_0^L \left(q - f_0 - \Delta \right) \left(\beta_s \dot{e} + \beta_c e \right) dx$$

$$\leq \beta_s \delta_1 \int_0^L \dot{e}^2 dx + \beta_c \delta_2 L^2 \int_0^L e_x^2 dx - \Delta \int_0^L \left(\beta_s \dot{e} + \beta_c e \right) dx$$

$$+ \left(\frac{\beta_s}{\delta_1} + \frac{\beta_c}{\delta_2} \right) \int_0^L \left(q - f_0 \right)^2 dx.$$

So

$$\dot{V} \leq -\left[\beta_s \left(c - \delta_1 \right) - \beta_c \left(\rho + \frac{c}{\delta_3} \right) \right] \int_0^L \dot{e}^2 dx$$

$$- \beta_c \left[P - \left(\delta_2 + \delta_3 c \right) L^2 \right] \int_0^L e_x^2 dx + \varepsilon - \Delta(t) q_e(t) \qquad (4.20)$$

using Ineqs. (2.7) and (2.9) and Eq. (4.19). For sufficiently small δ_1, δ_2, δ_3, and β_c, Ineqs. (4.13), (4.14), and

$$\varepsilon = \left(\frac{\beta_s}{\delta_1} + \frac{\beta_c}{\delta_2} \right) \int_0^L \left(q - f_0 \right)^2 dx \qquad (4.21)$$

hold true. Ineq. (4.13) limits the gain ratio $\frac{\beta_s}{\beta_c} > \frac{\rho + \frac{c}{\delta_3}}{c - \delta_1}$ where $\delta_3 < \frac{\frac{P}{L^2} - \delta_2}{c}$ from Ineq. (4.13). If we choose $\delta_2 \ll \frac{P}{L^2}$ and $\delta_1 \ll c$, then $\delta_3 \approx \frac{P}{L^2 c}$ and $\frac{\beta_s}{\beta_c} > \frac{\rho + \frac{L^2 c^2}{P}}{c}$.

Inequality (4.20) can be rewritten as

$$\dot{V} \leq -\lambda V + \varepsilon - \Delta(t) q_e(t). \qquad (4.22)$$

Now we form the total Lyapunov functional

$$V_T(t) = V(t) + V_L(t) > 0, \tag{4.23}$$

with the learning function

$$V_L = \frac{1}{2} \int_{t-T}^{t} \left\{ \text{sat}_\sigma \left[\Delta(\tau) \right] \right\}^2 d\tau > 0.$$

The time derivative of (4.23)

$$
\begin{aligned}
\dot{V}_T \;\leq\;\; & -\lambda V + \varepsilon - \Delta q_e + \frac{1}{2} \left\{ \text{sat}_\sigma \left[\Delta(t) \right] \right\}^2 - \frac{1}{2} \left\{ \text{sat}_\sigma \left[\Delta \left(t - T_b \right) \right] \right\}^2 \\
\leq\;\; & -\lambda V + \varepsilon - \frac{1}{2} \left\{ \Delta^2 - \left[\text{sat}_\sigma (\Delta) \right]^2 \right\} \\
\leq\;\; & -\lambda V + \varepsilon.
\end{aligned}
$$

Therefore,

$$\frac{\beta_s EA}{2L} e_x^2(x,t) \leq \frac{\beta_s EA}{2} \int_0^L e_x^2(x,t)\, dx \leq E_s \leq V \leq V_T \in \mathcal{L}_\infty,$$

using (2.9), (4.6), (4.8), and (4.23).

□

This result indicates that RLC can be applied to distributed MEMS actuators and provide stable response. This means that none of the infinite modes will be destabilized by the control. The control law is also implementable using capacitive sensing and a programmable waveform generator.

4.4 Simulation

In this section, numerical simulation verifies the stability and performance of the open loop system and the repetitively controlled closed loop system.

The system is discretized using a five mode expansion,

$$e(x,t) = \sum_{j=1}^{5} p_j(t)\,\Phi_j(x)$$

with pinned-pinned string eigenfunctions for $\Phi_j(x)$. Application of Galerkin's method produces the discretized equations. These equations and Eq. (4.17) are numerically integrated using Matlab with the typical microbridge parameters in Table 4.1 [59]. The desired spatial and time trajectory for the string $v(x,t) = \phi_d(x)\,P_d(t)$ is shown in Figure 4.3.

<div align="center">

Table 4.1. Microbridge Simulation Parameters

Parameters	Values
Length, L	$100 \times 10^{-6}\ [m]$
Mass/length, ρ	$9.32 \times 10^{-9}\ [kg/m]$
Low damping coefficient, c	$2.66 \times 10^{-13}\ [Ns/m]$
High damping coefficient, c	$7 \times 10^{-5}\ [Ns/m]$
Tension, P	$10^{-7}\ [N]$

</div>

Table 4.2 shows the control gains used for the actual (low damping) case and a high damping case. Note that $\dfrac{\beta_s}{\beta_c} > 3.5 \times 10^4$ and 1.1×10^{-3} for the low and high
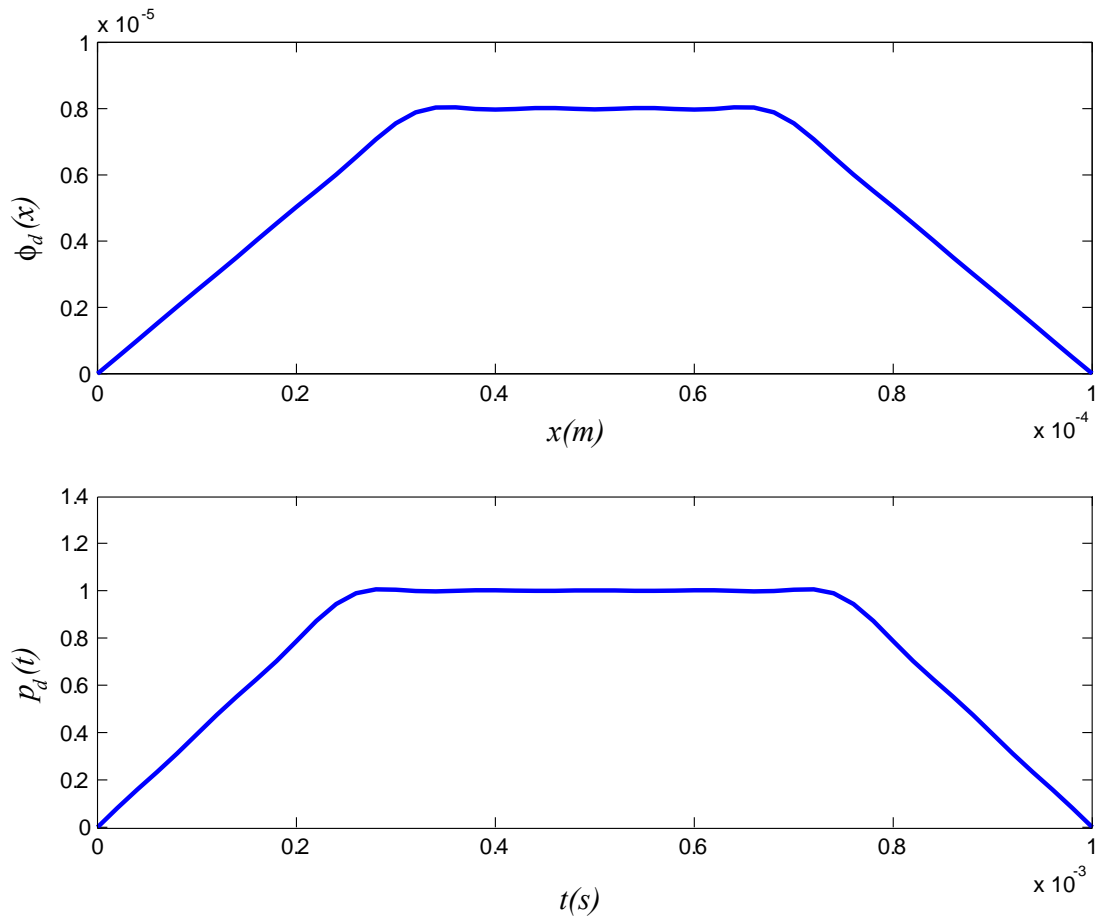
Fig. 4.3.   Desired trajectory $v(x,t)$: (a) Spatial distribution scale, $\phi_d(x)$, (b) One time period, $p_d(t)$, $t \in [0, T]$.

damping case, respectively. Table 4.2 shows that the "best" gains (based on trial and error) have $\beta_s = \beta_c$, violating the proof conditions for the low damping case. For the high damping case, however, these conditions are satisfied.

Table 4.2. Control Gains

Gains	Low Damping	High Damping
β_s	1	50
β_c	1	50
σ	7×10^{-4}	0.05

Figure 4.4 shows the simulation results for RLC of the microbridge under low damping with $v(x,t)$ given in Figure 4.3. The spatial variation of the desired trajectory $\phi_d(x)$ is designed to provide a large spatial range (35 μm $< x <$ 65 μm) with constant displacement. The desired time trajectory $p_d(t)$ provides fast response with short transitions (< 0.3 ms) from one state to another.

Figure 4.4 shows the open and closed loop response of the microbridge to the square wave (thin) and repetitive (thick) input in Figure 4.4(a). The midpoint response shows significant vibration in response to the inputs due to the small squeeze film damping. The measured error signal is fed to the repetitive algorithm with $T_R = T$ to show fast convergence. The repetitive controller, due to the low gains, does not change the control effort much but has a significant affect on the response, reducing q_e from 1.2×10^{-3} to 0.32×10^{-3}. The midpoint displacement error also reduces by half.

Fig. 4.4. Open loop (thin) and closed loop (thick) response with low damping: (a) Control effort $f_0(t)$, (b) Learning error integral, $q_e(t)$, (c) Midpoint displacement $w(L/2, t)$.
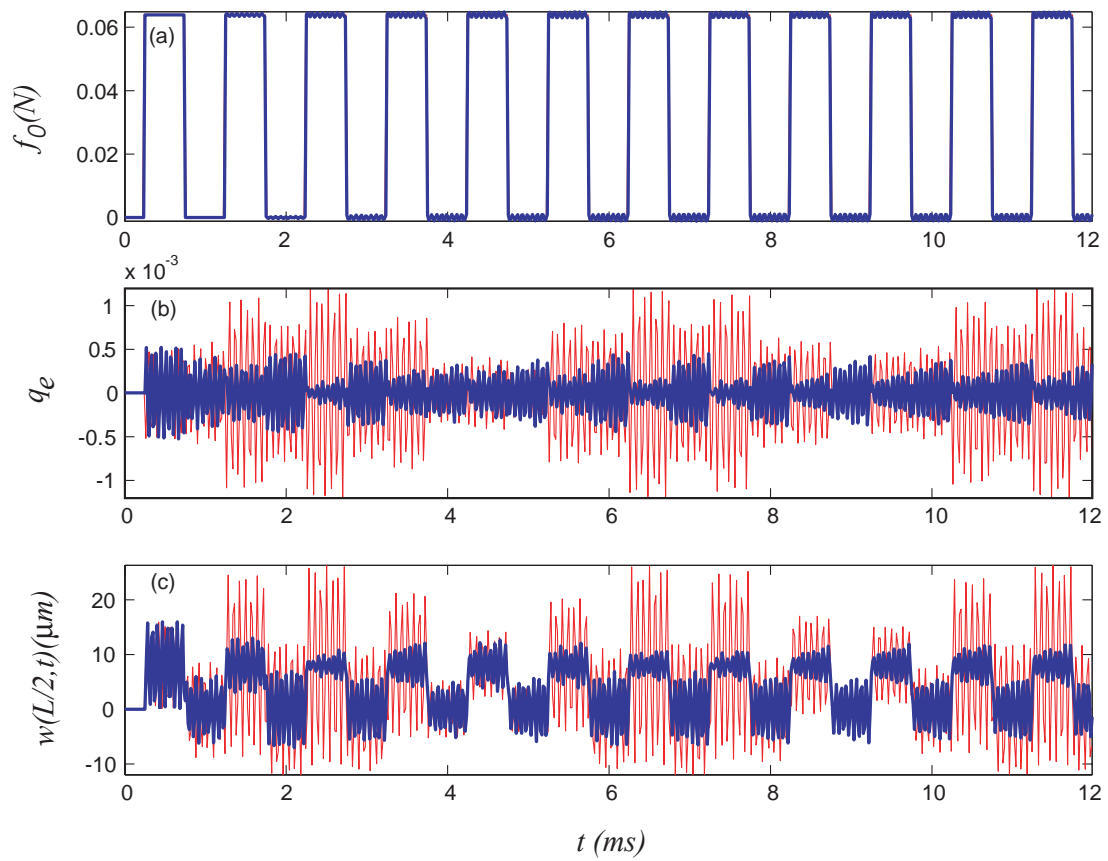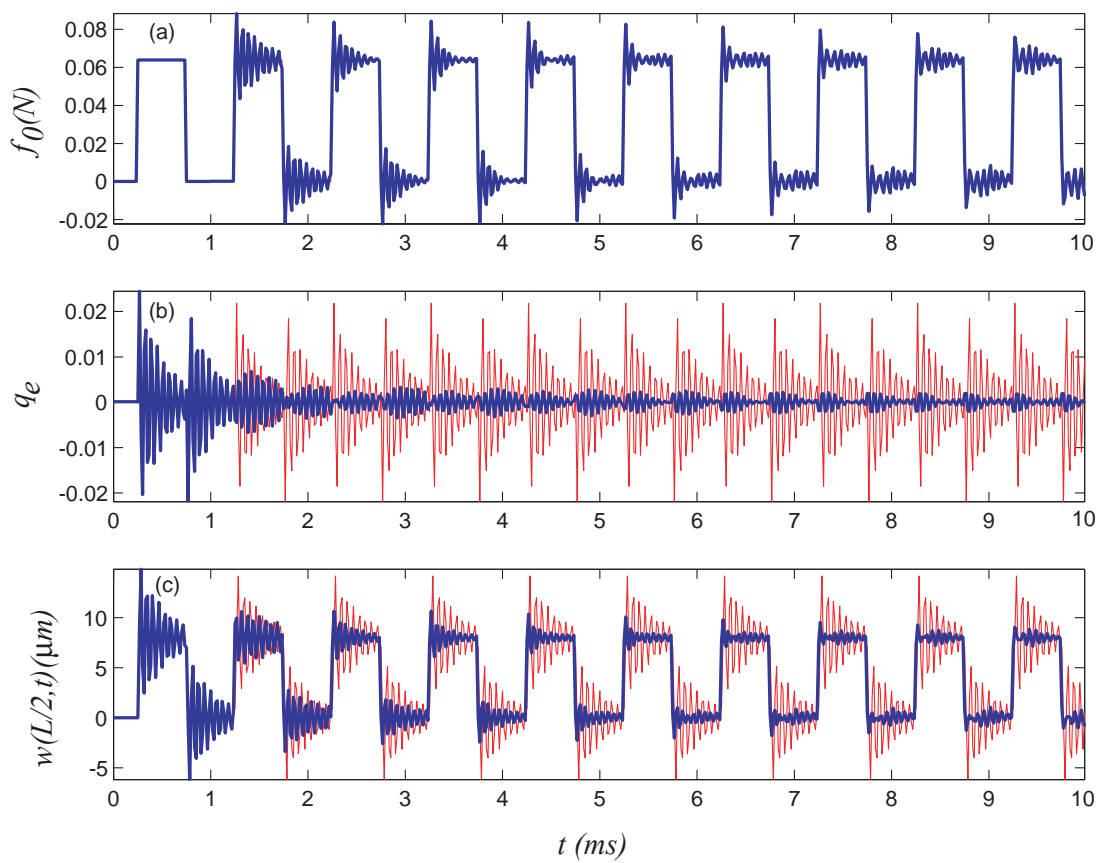
Fig. 4.5. Open loop (thin) and closed loop (thick) response with low damping : (a) Control effort $f_0(t)$, (b) Learning error integral, $q_e(t)$, (c) Midpoint displacement $w(L/2, t)$.

Figure 4.5 shows much improved performance with higher damping. The error converges within 3 cycles to less than 7×10^{-4}. The midpoint displacement improves by an order of magnitude from open loop to closed loop, providing a maximum midspan displacement overshoot of 36%.

Figure 4.6 shows the desired spatial distribution of the bridge deflection $\phi_d(x)$ (solid) and the actual displacement $w\left(x, \frac{2N-1}{2}T\right)$ under RLC during the first ($N = 1$, dashed) and last ($N = 10$, dash-dotted) iterations. The plotted actual displacement distributions are fixed time snapshots in the middle of the constant amplitude, dwell region of the periodic desired time trajectory $\left(\frac{T}{2}\right)$. The RLC algorithm is based on the spatial integral of error between the desired and actual distributions or the average error over the domain. The figure shows that, after 10 periods of RLC, the error reduces significantly. The bridge maintains constant amplitude during the dwell period so the resulting shape is a half-sine, corresponding to steady-state bridge response under uniform loading. This physical limitation on the achievable displacement profile could be used in the desired spatial distribution design. The theory predicts only bounded response, so any desired spatial distribution can be specified. The repetitive controller reduces the average error between the desired and actual distributions. One would expect, therefore, that the midpoint error could be further reduced by using a physically motivated, half-sine desired spatial distribution.
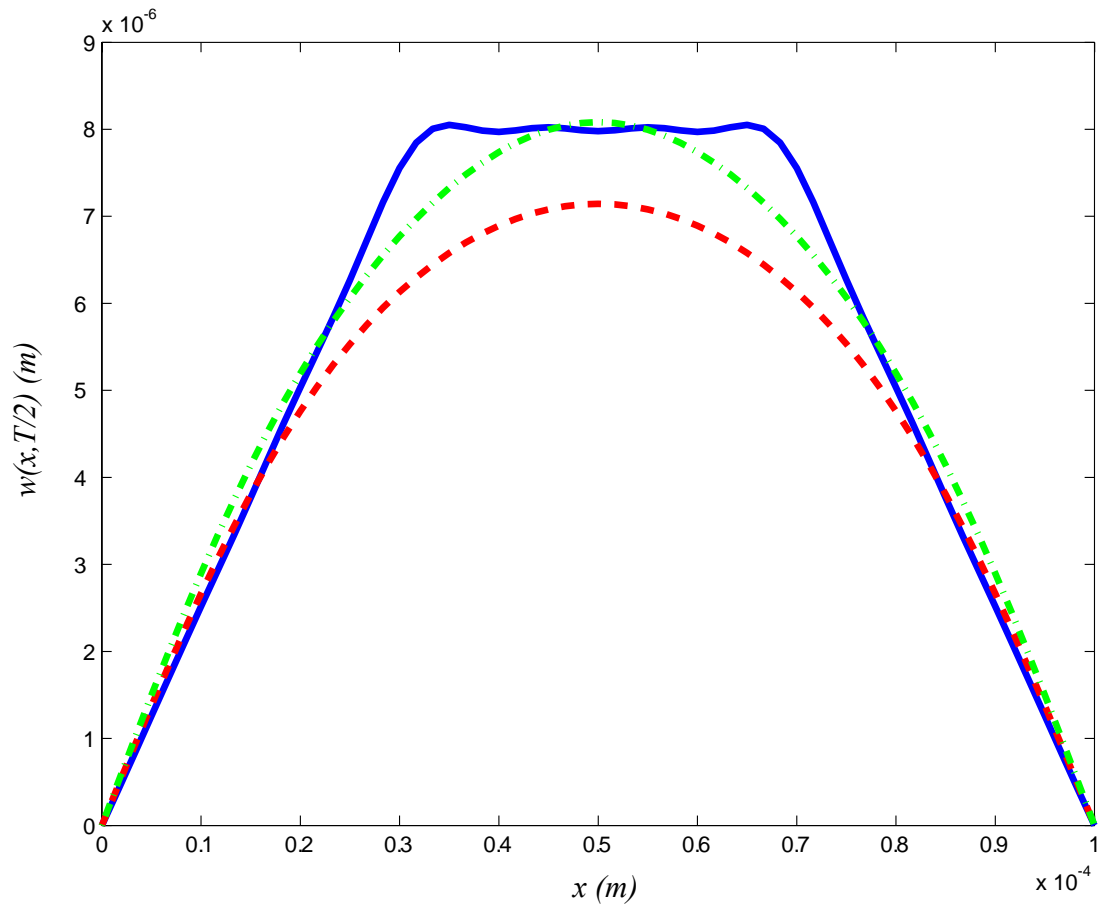
Fig. 4.6. Spatial distribution: Desired $\phi_d(x)$ (solid line) and actual shape for the first period ($w\left(x, \frac{T}{2}\right)$ - dashed line), and 10th period ($w\left(x, 9T + \frac{T}{2}\right)$ - dash-dotted line).

Chapter 5

Repetitive Contact Imaging

In this chapter, we apply the RLC approach in [23, 67] to 3D contact imaging. This is the first time that this control approach has been applied to a distributed parameter beam system. Distributed model-based control has the advantages of generating implementable, physically motivated controllers while eliminating spillover instabilities [5] associated with discretized (*e.g.* FEM, modal, and finite difference) model-based controllers. The repetitive controller moves the whisker back and forth across the object while regulating the vertical contact force using hub moment and encoder feedback. First, we prove boundedness of the distributed response under distributed damping using the energy multiplier method [56, 66]. Then, we prove boundedness of the repetitive controlled system. Finally, we experimentally implement the controller and compare the response under PD and RLC.

5.1 System Model

Figure 5.1 shows the 3D contact imager [19]. A flexible whisker is mounted to a pitch-yaw gimballed platform through a load cell. The yaw axis is PID controlled to provide a prescribed yaw trajectory that sweeps back and forth across the object. RLC is implemented on the pitch axis to regulated the contact force between the whisker and the object.
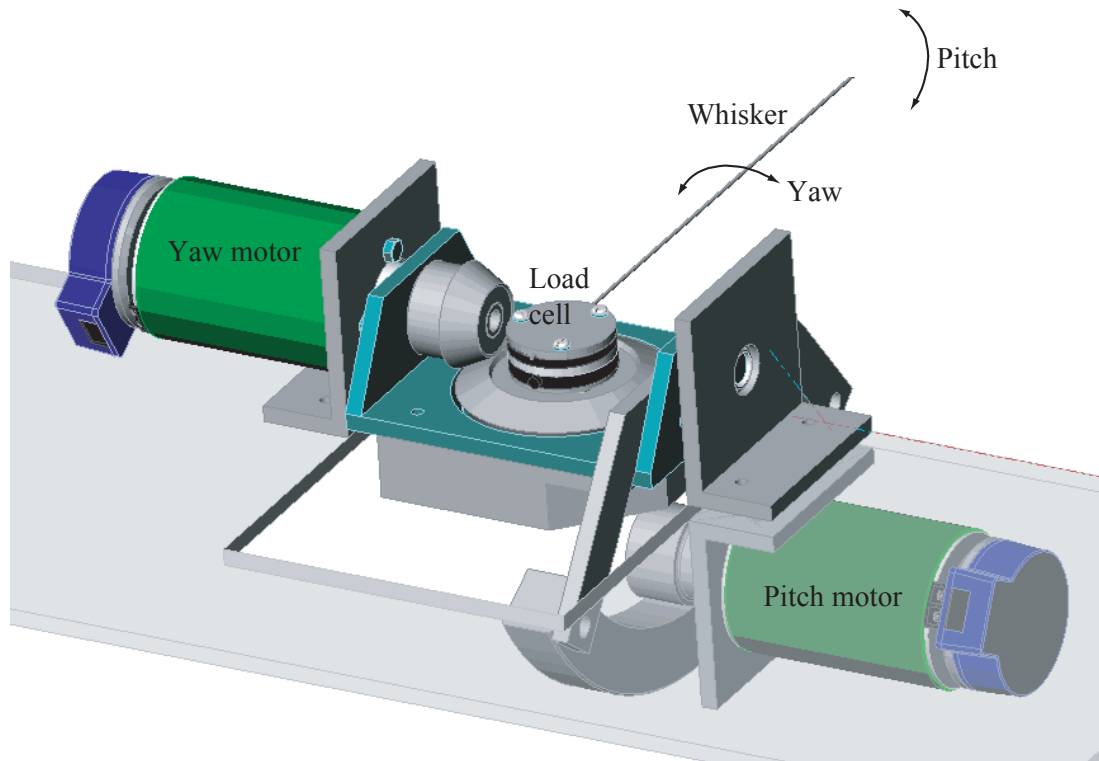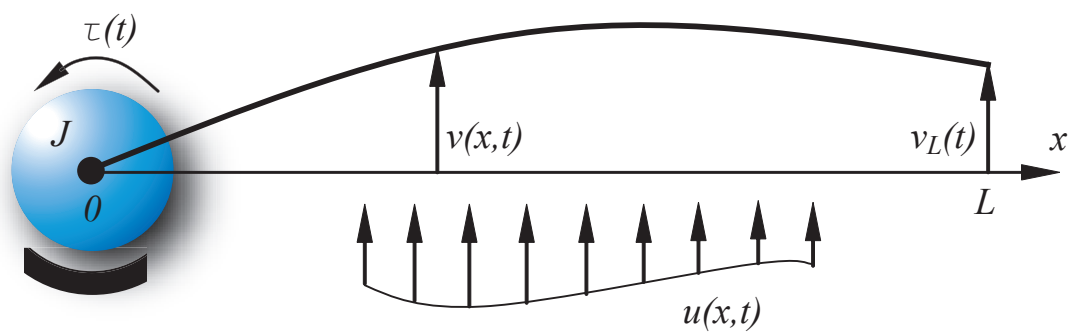
Fig. 5.1. 3D contact imager.

Fig. 5.2. Schematic diagram of the pitch axis model.

Figure 5.2 shows a schematic diagram of the pitch axis model. The distributed transverse displacement $v(x,t)$ depends on position x and time t. The right end $(x = L)$ undergoes prescribed motion $v_L(t)$ associated with the whisker sweeping over the contacted object. The left end $(x = 0)$ is controlled by the motor torque input $\tau(t)$ applied to an effective rotary inertia J. The whisker has uniform stiffness EI and mass/length ρ. The linear field equation is

$$\rho\ddot{v} + b\dot{v} + EIv_{xxxx} = u \ , \ x \in (0, L), \tag{5.1}$$

with boundary conditions

$$v(0,t) = 0, \ J\ddot{v}_x(0,t) - EIv_{xx}(0,t) = \tau(t), \tag{5.2}$$

$$v(L,t) = v_L(t), \ v_{xx}(L,t) = 0, \tag{5.3}$$

where b is damping coefficient and $u(x,t)$ is a bounded disturbance force [56]. We transform the displacement field

$$\omega(x,t) = v(x,t) - \frac{x}{L}v_L(t), \tag{5.4}$$

to move all disturbances to the transformed field equation

$$\rho\ddot{\omega} + b\dot{\omega} + EI\omega_{xxxx} = f \ , \ x \in (0, L), \tag{5.5}$$

and obtain transformed boundary conditions

$$\omega(0,t) = 0, \quad J\ddot{\omega}_x(0,t) - EI\omega_{xx}(0,t) = \tau(t) - \frac{J}{L}\ddot{v}_L(t),$$ (5.6)

$$\omega(L,t) = \omega_{xx}(L,t) = 0,$$ (5.7)

where $f = u - \frac{\rho x}{L}\ddot{v}_L - \frac{bx}{L}\dot{v}_L$. This produces the pinned boundary condition (5.7) at $x = L$.

We assume the model given by Eqs. (5.5) – (5.7) is well posed and has an unique solution for all $f(x,t) \in \mathcal{L}_\infty(0,L)$ and $\ddot{v}_L(t) \in \mathcal{L}_\infty$.

The control objective for the pitch axis is to maintain contact between the whisker and the contacted object. We can approach this control objective by regulating the hub bending moment $EIw_{xx}(0,t)$ at a specified value M_0. This maintains the whisker in a bent configuration pressing into the object.

5.2   Control Formulation

We define the combined moment setpoint error

$$\eta(t) = \dot{\omega}_x(0,t) - \kappa\left[\omega_{xx}(0,t) - \frac{M_0}{EI}\right]$$

$$= \eta_m(t) - \frac{1}{L}\dot{v}_L(t),$$ (5.8)

using Eq. (5.4), where κ is a positive scalar control gain and $\eta_m(t) = \dot{v}_x(0,t) - \kappa\left[v_{xx}(0,t) - \frac{M_0}{EI}\right]$ is the measurable part of $\eta(t)$. In Theorem 5.1, we show that

PD plus moment setpoint regulation (PDM) feedback control with distributed damping

can ensure bounded $\omega(x, t)$ in the presence of bounded disturbances f, $\dot{v}_L$, and $\ddot{v}_L$.

Theorem 5.1: With the PDM control law

$$\tau(t) = -k_s \eta_m - EI v_{xx}(0, t) + J \kappa \dot{v}_{xx}(0, t), \tag{5.9}$$

where k_s and κ are positive control gains, the response $v(x, t)$ of Eqs. (5.5) − (5.7) is

strongly bounded $(v(x, t) \in \mathcal{L}_\infty)$ if $f \in \mathcal{L}_\infty(0, L)$ and $\dot{v}_L$ and $\ddot{v}_L(t) \in \mathcal{L}_\infty$.

Proof: We define a Lyapunov functional

$$V(t) = E_s(t) + E_c(t) + \frac{1}{2} J \eta^2(t), \tag{5.10}$$

where β_s and β_c are positive constants and the energy related term

$$E_s = \frac{1}{2} \beta_s \int_0^L (\rho \dot{\omega}^2 + EI \omega_{xx}^2) dx \geq 0 \tag{5.11}$$

includes kinetic and potential energy. The crossing term

$$E_c(t) = \beta_c \rho \int_0^L \omega \dot{\omega} dx \tag{5.12}$$

can be bounded by

$$\left| E_c(t) \right| \leq \frac{1}{2} \beta_c \rho \int_0^L \left(\dot{\omega}^2 + \omega^2 \right) dx = \xi E_s(t) \tag{5.13}$$

using inequalities (2.7) and (2.9), where

$$\xi = \frac{\beta_c \rho \max\left(1, L^4\right)}{\beta_s \min\left(\rho, EI\right)}.$$

This means that

$$0 \le \xi_1 E_s \le E_s + E_c \le \xi_2 E_s,$$

where

$$\xi_1 = 1 - \xi,$$

$$\xi_2 = 1 + \xi.$$

Therefore, we can obtain the upper and lower bounds, where

$$0 \le \lambda_1 \left(E_s + \eta^2\right) \le V \le \lambda_2 \left(E_s + \eta^2\right), \tag{5.14}$$

$$\lambda_1 = \min\left(\xi_1, \frac{J}{2}\right) > 0,$$

$$\lambda_2 = \max\left(\xi_2, \frac{J}{2}\right) > 1.$$

The time derivative of Eq. (5.10) is

$$\dot{V} \le -\lambda V + \varepsilon \tag{5.15}$$

where $\lambda, \varepsilon > 0$ (see Lemma 1 in Appendix B).

Using Eqs. (2.8), (5.9), (5.11), and (5.14), we can show

$$\frac{\beta_s EI}{2L^3} \omega^2 (x,t) \leq \frac{\beta_s EI}{2} \int_0^L \omega_{xx}^2 (x,t)\, dx \leq E_s$$

$$\leq V \leq V(0)\, e^{-\lambda t} + \frac{\varepsilon}{\lambda}. \tag{5.16}$$

Thus, $V \in \mathcal{L}_\infty$ and $\omega(x,t)$ and $v(x,t) \in \mathcal{L}_\infty (0,L)$. We cannot show pointwise boundedness of $EI\omega_{xx}(0,t)$, but inequality (5.16) implies weak boundedness.

□

Theorem 5.1 shows that bounded inputs produce bounded response with distributed damping and the control law (5.9). In Theorem 5.2 we prove that the control law can be augmented with a repetitive feedforward term if $v_L(t) = v_L(t+T)$. The repetitive learning (RL) control law

$$\tau(t) = -k_s \left\{ \dot{\omega}_x (0,t) - \kappa \left[\omega_{xx}(0,t) - \frac{M_0}{EI} \right] \right\} - EI\omega_{xx}(0,t)$$

$$+ J\kappa \dot{\omega}_{xx}(0,t) - \frac{k_s}{L} \dot{v}_L(t) + \Delta(t)$$

$$= -k_s \eta_m - EI\omega_{xx}(0,t) + J\kappa \dot{\omega}_{xx}(0,t) - \frac{k_s}{L} \dot{v}_L(t) + \Delta(t) \tag{5.17}$$

includes the term Δ that is designed to learn the unknown boundary motion while ensuring stability. It is updated from trial to trial by the learning law:

$$\Delta(t) = \mathrm{sat}_\sigma \left[\Delta(t-T) \right] - \eta_m(t) \quad \text{for } t \in [0,\ T], \tag{5.18}$$

where

$$\text{sat}_\sigma(\zeta) = \begin{cases} \zeta, & \text{for } |\zeta| \le \sigma \\ \\ \text{sgn}(\zeta)\,\sigma, & \text{for } |\zeta| > \sigma. \end{cases} \tag{5.19}$$

Theorem 5.2: The RLC law (5.17) – (5.19) ensures that the response of the system (5.5) – (5.7) $v(x,t) \in \mathcal{L}_\infty(0,L)$ for any $v_L(t) = v_L(t+T)$ with $\dot{v}_L(t)$, $\ddot{v}_L(t) \in \mathcal{L}_\infty$ and $f \in \mathcal{L}_\infty(0,L)$.

Proof: We define the Lyapunov functional $V(t)$, the energy related term $E_s(t)$, and the crossing term $E_c(t)$ as in Eqs. (5.10) – (5.12), so the Ineq. (5.14) holds. Lemma 2 in the Appendix B shows that $\dot{V} \le -\lambda V + \varepsilon + \eta\,[\Delta(t) - q(t)]$ and $q(t) = \frac{1}{L}\left[k_s\dot{v}_L(t) + J\ddot{v}_L(t)\right]$.

Now we add a learning term $V_L(t)$ to the positive functional in Eq. (5.10) as follows

$$V_T(t) = V(t) + V_L(t) > 0, \tag{5.20}$$

where

$$V_L = \frac{1}{2}\int_{t-T}^{t}\left[\text{sat}_\sigma(\Delta) - \text{sat}_\sigma(q)\right]^2 d\tau,$$

where for all $j \ge 0$

$$\Delta(\tau) = \Delta_j(t - jT), \quad \tau \in [jT,\ (j+1)\,T]. \tag{5.21}$$

We define an estimation error term $\tilde{q}(t) = \Delta(t) - q(t) = \text{sat}_\sigma[\Delta(t-T)] - \text{sat}_\sigma[q(t)] - \eta(t) - \frac{1}{L}\dot{v}_L(t)$.

The time derivative of (5.20)

$$
\begin{aligned}
\dot{V}_T &\leq -\lambda V + \varepsilon + \eta \left[\Delta\left(t\right) - q\left(t\right) \right] + \frac{1}{2} \left\{ \mathrm{sat}_\sigma \left[\Delta\left(t\right) \right] - \mathrm{sat}_\sigma \left[q\left(t\right) \right] \right\}^2 \\
&\quad - \frac{1}{2} \left[\Delta\left(t\right) - q\left(t\right) + \eta\left(t\right) + \frac{1}{L}\dot{v}_L\left(t\right) \right]^2 \\
&= -\lambda V + \varepsilon - \frac{1}{2} \left\{ \left[\Delta\left(t\right) - q\left(t\right) \right]^2 - \left\{ \mathrm{sat}_\sigma \left[\Delta\left(t\right) \right] - \mathrm{sat}_\sigma \left[q\left(t\right) \right] \right\}^2 \right\} \\
&\quad - \left\{ \mathrm{sat}_\sigma \left[\Delta\left(t-T\right) \right] - \mathrm{sat}_\sigma \left[q\left(t\right) \right] - \frac{1}{2L}\dot{v}_L(t) \right\} \frac{1}{L}\dot{v}_L\left(t\right) - \frac{1}{2}\eta^2\left(t\right) \\
&\leq -\lambda V + \varepsilon_T, && (5.22)
\end{aligned}
$$

using (5.8) and (5.18), where $\varepsilon_T = \varepsilon + 4\sigma^2 + \frac{1}{L^2}\max\limits_{t\in(0,\infty)} \dot{v}_L^2 \in \mathcal{L}_\infty$. Therefore $V_T \in \mathcal{L}_\infty$ and [55],

$$
\frac{\beta_s EI}{2L^3}\omega^2\left(x,t\right) \leq \frac{\beta_s EI}{2} \int_0^L \omega_{xx}^2\left(x,t\right) dx \leq E_s \leq V \leq V_T \in \mathcal{L}_\infty
$$

using (2.8), (5.11), (5.14), and (5.20). Thus, $v\left(x,t\right) \in \mathcal{L}_\infty\left(0,L\right)$.

□

5.3   Experiment

Figure 5.3 shows the repetitive imaging experimental hardware [19].   The test stand consists of a whisker mounted on a two degree-of-freedom robot through a load cell. A 1.19 mm diameter steel whisker of length 45.5 cm attaches to the top of an ATI Mini 40 six-axis force/torque sensor. Two Maxon brushed-DC motors torque gear trains that control pitch and yaw motions. Encoders (4000 count/rev with quadrature) attach to the motor shafts and provide rotational feedback. Forces and moments are fed into

the control PC. The RLC algorithm is implemented in QNX using the real-time Qmotor software. The contacted object is covered with a 1 mm thick Teflon sheet to minimize sharp edges and high friction surfaces that may snag the whisker.

The yaw motor sweeps sinusoidally back and forth across the object under PID control at 0.1 Hz. The pitch axis is controlled using either the PDM control algorithm (5.9) or the RLC algorithm (5.17) – (5.19) with the control gains in Table 5.1. The desired hub moment $M_0 = 0.05$ Nm.

Table 5.1.   Control Gains

Parameters	Values
k_s	0.001
κ	200000
σ	1300

Figure 5.4 shows the experimental results. The whisker starts above the object surface, moves down into contact, and slides back and forth across the object. The yaw angle (Fig. 5.4(a)) sweeps sinusoidally between 0 and 40 degrees. During the first 20 seconds, PDM control is applied. The maximum moment error (Fig. 5.4(c)) is 0.012 Nm and the pitch axis (Fig. 5.4(b)) does not move to accurately track the object shape. After $t = 20$ s, the RL controller is applied. The learning term $\Delta(t)$ for the period $20\text{s} \leq t \leq 30$ s uses error data from the previous period. The learning term converges after a few cycles, the control voltage adjusts accordingly, and the moment error reduces to 0.003 Nm. The object profile can be discerned from the pitch trajectory. Further
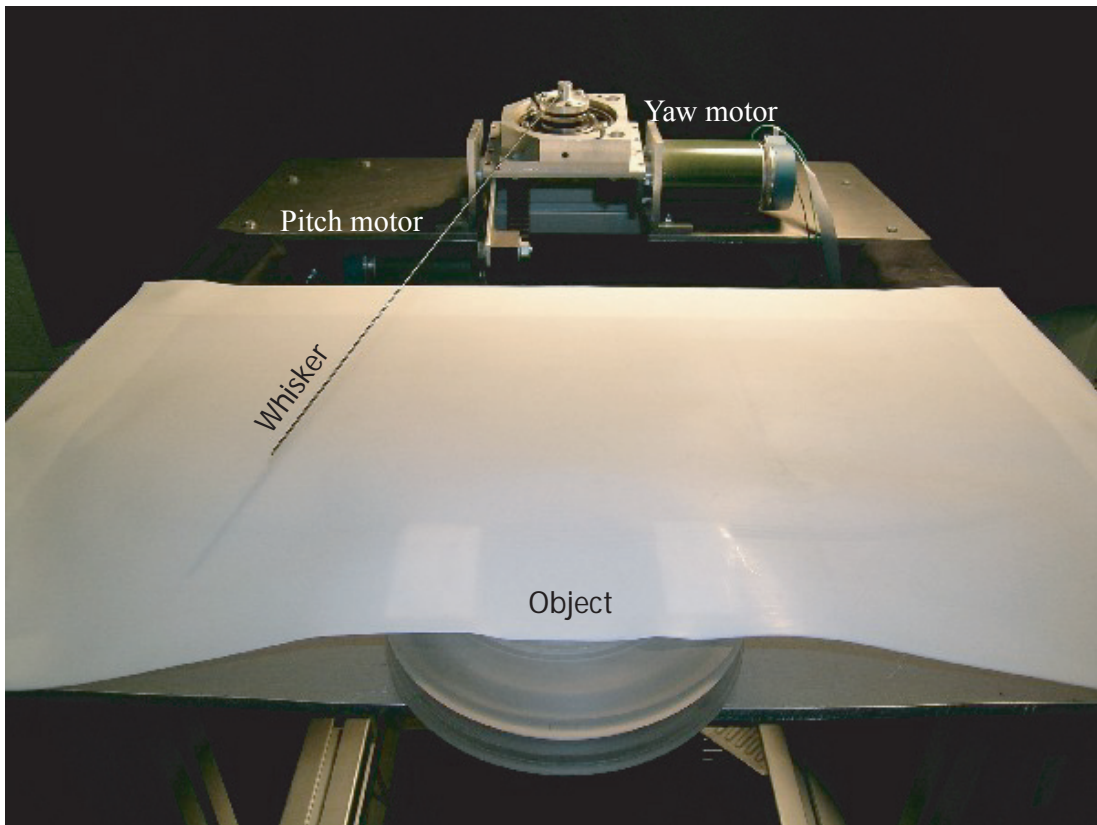
Fig. 5.3.   Repetitive contact imaging experiment.

processing of the load cell and encoder data using the elastica algorithm [19, 58] can produce a 3D contact point trajectory.

The performance of the repetitive contact imager is limited by the modeling assumptions. The linear, decoupled pitch-yaw model means that surface normals must be close to vertical or the whisker becomes stuck. A combination of the RLC algorithm presented in this chapter and the nonlinear algorithm in [19, 58] would provide the best performance. The endpoint contact assumptions, however, does not affect performance in the objects tested. The object in Fig. 5.3, for example, had contact at the endpoint and in the domain $x \in (0, L)$ at different points in the trajectory. The stability and convergence of the response is unaffected by contact point location in these cases (see the Appendix C).

5.4 Robustness

The RLC law (5.17) and (5.18) can be rewritten as

$$\tau\left(t\right) = -k_s \dot{v}_x\left(0,t\right) + \frac{k_s \kappa}{EI}\left[EIv_{xx}\left(0,t\right) - M_0\right] - EIv_{xx}\left(0,t\right) + \frac{J\kappa}{EI}EI\dot{v}_{xx}\left(0,t\right), \quad (5.23)$$

$$\triangle\left(t\right) = \mathrm{sat}_\sigma\left[\triangle\left(t-T\right)\right] - \dot{v}_x\left(0,t\right) + \frac{\kappa}{EI}\left[EIv_{xx}\left(0,t\right) - M_0\right] \quad \text{for } t \in \left[0,\ T\right], \quad (5.24)$$

where $EIv_{xx}\left(0,t\right)$ and $\dot{v}_x\left(0,t\right)$ are the measured moment and angle velocity at the load cell, $EI\dot{v}_{xx}\left(0,t\right)$ can be calcuated by time derivative of measured moment, and M_0 is desired moment.

The RL controller also requires knowledge of the system parameters EI and J. The parameter EI appears as $\frac{\kappa}{EI}$ in Eqs. (5.23) and (5.24) so it acts to scale the control
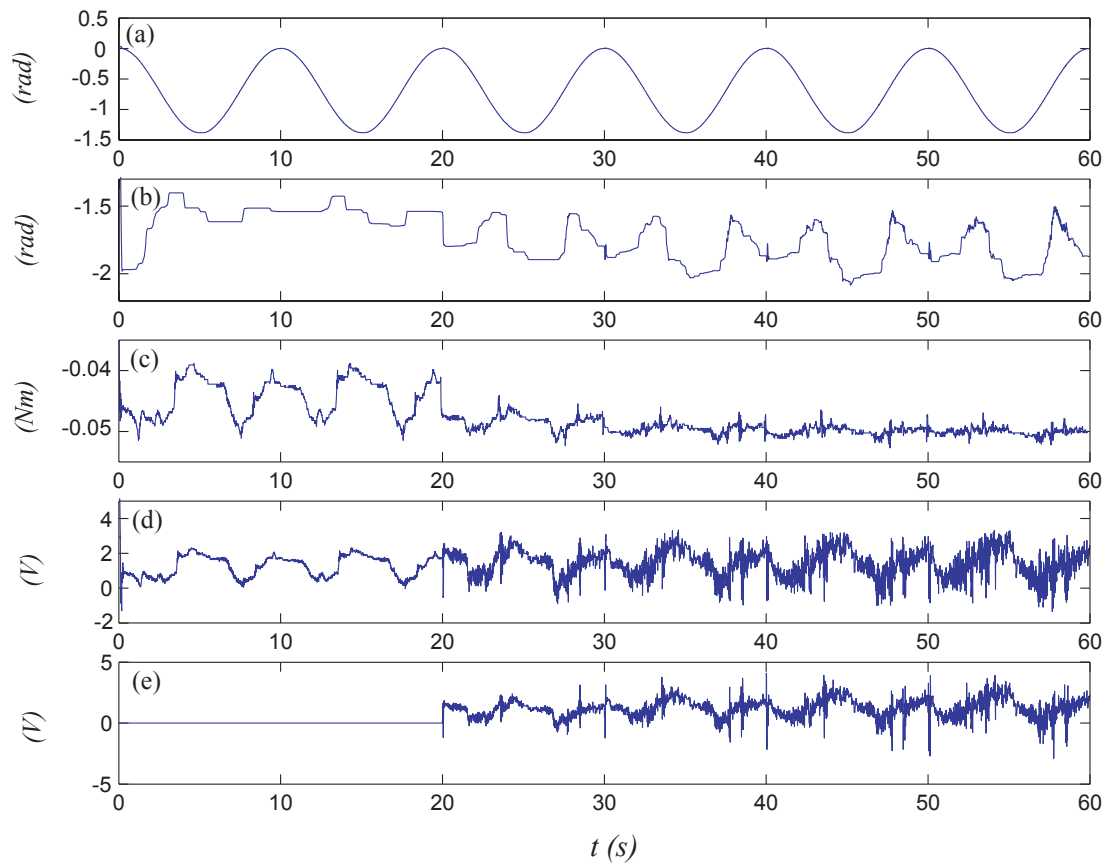
Fig. 5.4.   Experiment results: (a) Yaw angle, (b) Pitch angle, (c) Hub bending moment $EIw_{xx}(0,t)$, (d) Control voltage, and (e) Learning term Δ.

gain κ. The system is proven stable for all $\kappa > 0$ so changes in EI change performance but not stability. The parameter J, however, appears as a feedforward term in Eq. (5.23) and, if not perfectly known, may cause instability. This term was not implemented in the experimental control with no ill effects.

Chapter 6

Conclusions, Contributions, and Future Work

6.1 Conclusions

The purpose of this dissertation is two-fold. First, we prove b.i.b.o. stability for one and two dimensional distributed parameter systems under distributed and boundary disturbance based on energy multiplier method. Second, we theoretically prove, simulate, and experimentally implement feedforward DPS model-based controllers for several flexible distributed parameter systems.

6.1.1 BIBO Stability of Distributed Flexible Systems

Chapter 2 shows that distributed and boundary damping can ensure bounded response for strings and beams under boundary and distributed excitation and for pinned membranes and clamped plates under distributed excitation. Either external, viscous damping or internal, material damping ensures boundedness for strings and beams and weak stability with respect to the energy norm for membranes and plates. The distributed input can include spatial and time variations provided it is $\mathcal{L}_2$ spatially and $\mathcal{L}_\infty$ temporally bounded, respectively. Thus, time-bounded point forces are allowed because they have a bounded $\mathcal{L}_2$ spatial norm.

For string systems, the boundary displacement can be arbitrary but bounded on both boundaries under distributed damping or on one boundary when the other

boundary has a damper. For damped beam systems, prescribed boundary rotations and translations combined with distributed forcing result in bounded response if the inputs are bounded. For two dimensional DPSs, boundary damping must satisfy the normal boundary conditions (2.97) and (2.98) to ensure stability. Circular and rectangular domains satisfy these conditions with damping on half and one side, respectively.

For each of the cases studied, $\varepsilon = 0$ if $f = 0$ so without inputs these systems are strongly exponentially stable.

6.1.2   Iterative Learning Velocity and Tension Control for Axially Moving Materials

In Chapter 3 we prove that the PD tension/speed controller (3.10) ensures strong and weak boundedness of the axially moving material displacement and tension, respectively, in response to bounded speed disturbances. Addition of the ILC compensation in Eqs. (3.22) – (3.25) produces the same theoretical result, provided the disturbance has a known period. Simulations demonstrate, however, that the ILC controller outperforms PD control with half the speed error and 30% of the tension error using the same control effort.

6.1.3   Repetitive Control of an Electrostatic Microbridge Actuator

In Chapter 4 we prove that distributed squeeze film damping ensures boundedness of the transverse displacement of a microbridge in response to bounded force inputs. RLC is proven to provide bounded error for a bounded desired trajectory. Simulations demonstrate that the repetitive controller outperforms distributed damping alone with

70% less q_e and 50% less $e\left(\frac{L}{2}, t\right)$ under low damping and 97% less q_e and 36% less $e\left(\frac{L}{2}, t\right)$ under high damping.

6.1.4 Repetitive Contact Imaging

In Chapter 5, we prove that the PDM controller (5.9) ensures boundedness of force/moment in response to a bounded periodic input. Addition of RLC compensation in Eqs. (5.17) – (5.19) produces the same theoretical result, provided the disturbance has a known period. Experiments demonstrate that RL outperforms PDM with 75% reduction in the moment error using only 50% increase of control effort.

6.2 Contributions

This dissertation provides the following contributions:

- Extended energy multiplier method to study the b.i.b.o. stability of flexible DPSs.

- Proved the b.i.b.o. stability of domain and boundary damped string, beam, membrane, and plate DPS models under bounded inputs.

- Developed, proved stability, and simulated the first DPS model-based ILC controller for axially moving systems.

- Developed, proved stability, and simulated the first DPS model-based repetitive controller for second order flexible systems.

- Developed, proved stability, and experimentally implemented the first DPS model-based repetitive controller for fourth order flexible systems.

6.3 Future Work

This dissertation proves b.i.b.o. stability for one and two dimensional distributed parameter systems and provides several learning control applications with design, simulation, and experiments. Future work can also be divided into these two categories.
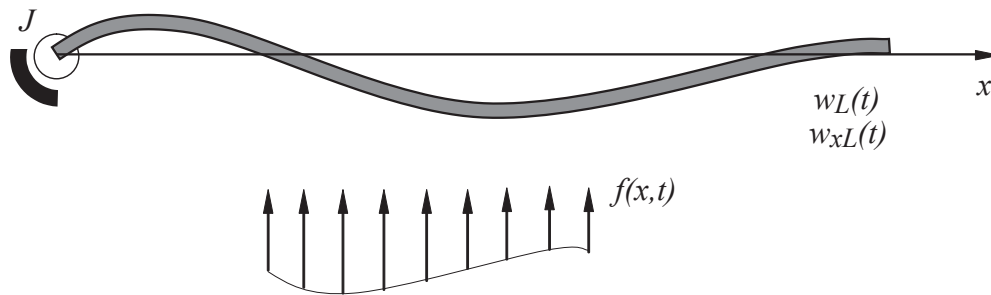
6.3.1 BIBO Stability

Fig. 6.1. Schematic diagram of a boundary rotary damped beam with distributed and boundary disturbances.

The b.i.b.o. stability proofs in Chapter 2 provide the fundamental theorems for the following chapters in the dissertation. Many cases which are not mentioned in Chapter 2 can be analyzed as future work. For example, consider the boundary rotary damped beam shown in Figure 6.1. In this case, the field equation and boundary

conditions are

$$\rho\ddot{w} + EIw_{xxxx} = f \, , \, x \in (0, L), \tag{6.1}$$

$$J\ddot{w}_x(0, t) - EIw_{xx}(0, t) = -c_b\dot{w}_{x0}(t) \, , \, w_{xxx}(0, t) = 0,$$

$$w(L, t) = w_L(t) \, , \, w_x(L, t) = w_{xL}(t)$$

where c_b is the boundary rotary damping gain. We have been unable to prove that the response of the damped beam governed by (6.1) is bounded, $w(x, t) \in \mathcal{L}_\infty(0, L)$, if f, w_L, $w_{xL} \in \mathcal{L}_\infty$ and $c_b > 0$.

6.3.2 Additional Applications of ILC/Repetitive Control

The proposed research has broader impacts beyond three applications discussed in Chapters 3 - 5. The control theory developed can be applied to noise control, cable vibration control, flexible robot manipulator control, and process control. Thus, the research impacts a wide range of applications including HVAC systems, underwater vehicles, civil engineering structures, aerospace systems, and manufacturing. Future work can be to extend the approaches used in this dissertation to other systems.

Based on the string model for the electrostatic microbridge in Chapter 4, for example, we can extend the model to one dimensional, fourth order differential equation with four boundary conditions if bending stiffness is considered (see Figure 6.2). A piezoelectrically actuated microcantilever has a similar model with the distributed forcing replaced by a boundary control moment on the free end.
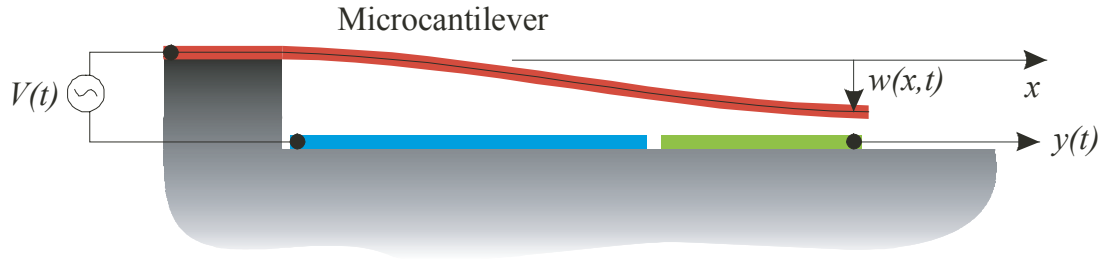
Microcantilever

Fig. 6.2.   Schematic diagram of microcantilever model.

The control approach can also be applied to the elimination of vibration in macroscale civil, mechanical, and aerospace structures where setpoint regulation and/or periodic disturbances or reference trajectories are required. The most typical application would be periodic disturbances resulting from rotating unbalance mass. Piezoelectric actuators on an aircraft wing could reduce the periodic vibration induced by engine rotation, for example. As illustrated in [4, 33], the feedforward vibration control has the potential to impact cable control technology where cable deformations caused by cross flows and/or high frequency strumming vibrations severely degrade the overall performance.

Finally, learning control algorithms have yet to be applied to 2D DPSs such as web sheets, flexible space mirrors, or aircraft fuselages. Sensing and actuation are much more complicated because the boundary is distributed. Feedforward learning techniques such as ILC and RLC have tremendous potential to improve the performance of 2D systems.

Appendix A

Robustness Discussion for Iterative Learning Velocity and Tension Control for Axially Moving Materials

Case 1: m = 0.067 kg, EA = 667 N

Figure A.1(c) shows the open loop velocity error $\dot{v}(0,t) = \dot{u}_L(t) - \dot{u}(0,t)$ is almost ten times the input velocity. Figure A.1(d) shows almost 75% tension error. The PD controller reduces the velocity and tension errors by an order of magnitude to less than 0.3 m/s and 2 N, respectively. The iterative term in Fig. A.2(b) slowly increases as the controller learns the periodic disturbance. The velocity and tension errors decrease to less than 0.15 m/s and 0.05 N by the end of the simulation ($t = 3$ s). The ILC controller uses almost the same control effort amplitude to achieve this performance improvement.

Case 2: m = 0.067 kg, EA = 1500 N

Figure A.3(c) shows the open loop velocity error $\dot{v}(0,t) = \dot{u}_L(t) - \dot{u}(0,t)$ is almost ten times the input velocity. Figure A.3(d) shows almost 75% tension error. The PD controller reduces the velocity and tension errors by an order of magnitude to less than 0.35 m/s and 3.3 N, respectively. The iterative term in Fig. A.4(b) slowly increases as the controller learns the periodic disturbance. The velocity and tension errors decrease to less than 0.1 m/s and 1 N by the end of the simulation ($t = 3$ s). The ILC controller uses almost the same control effort amplitude to achieve this performance improvement.

Case 3: m = 0.15 kg, EA = 667 N

Figure A.5(c) shows the open loop velocity error $\dot{v}(0,t) = \dot{u}_L(t) - \dot{u}(0,t)$ is almost ten times the input velocity. Figure A.5(d) shows almost 150% tension error. The PD controller reduces the velocity and tension errors by an order of magnitude to less than 0.15 m/s and 3 N, respectively. The iterative term in Fig. A.6(b) slowly increases as the controller learns the periodic disturbance. The velocity error is almost same, but the tension errors decreases to less than 1 N by the end of the simulation ($t = 3$ s). The ILC controller uses almost the same control effort amplitude to achieve this performance improvement.

Case 4: m = 0.15 kg, EA = 1500 N

Figure A.7(c) shows the open loop velocity error $\dot{v}(0,t) = \dot{u}_L(t) - \dot{u}(0,t)$ is almost ten times the input velocity. Figure A.7(d) shows almost 150% tension error. The PD controller reduces the velocity and tension errors by an order of magnitude to less than 0.2 m/s and 4 N, respectively. The iterative term in Fig. A.8(b) slowly increases as the controller learns the periodic disturbance. The velocity and tension errors decrease to less than 0.15 m/s and 1.5 N by the end of the simulation ($t = 3$ s). The ILC controller uses almost the same control effort amplitude to achieve this performance improvement.
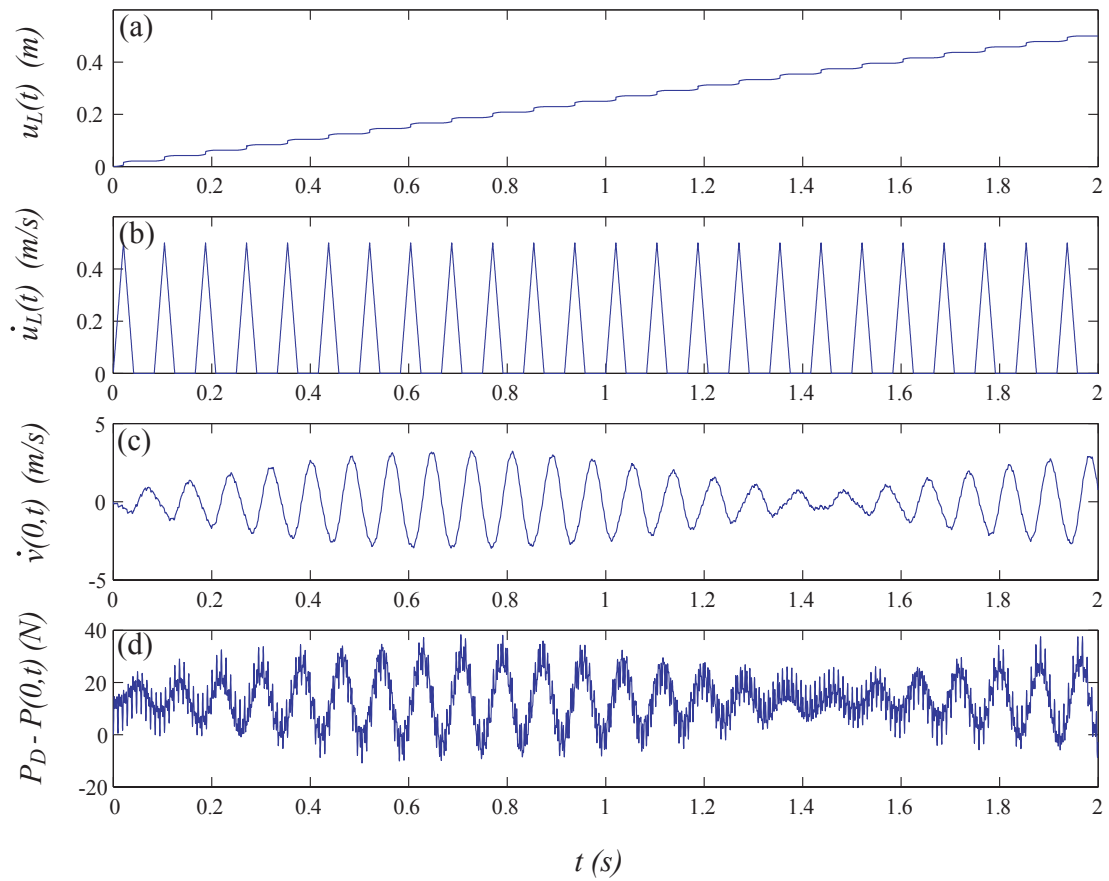
Fig. A.1.   Open loop response of the system for case 1: (a) Disturbance position, $u_L(t)$, (b) Disturbance velocity, $\dot{u}_L(t)$, (c) Velocity error, $\dot{v}(0,t)$, and (d) Tension error, $P_D - P(0,t)$.
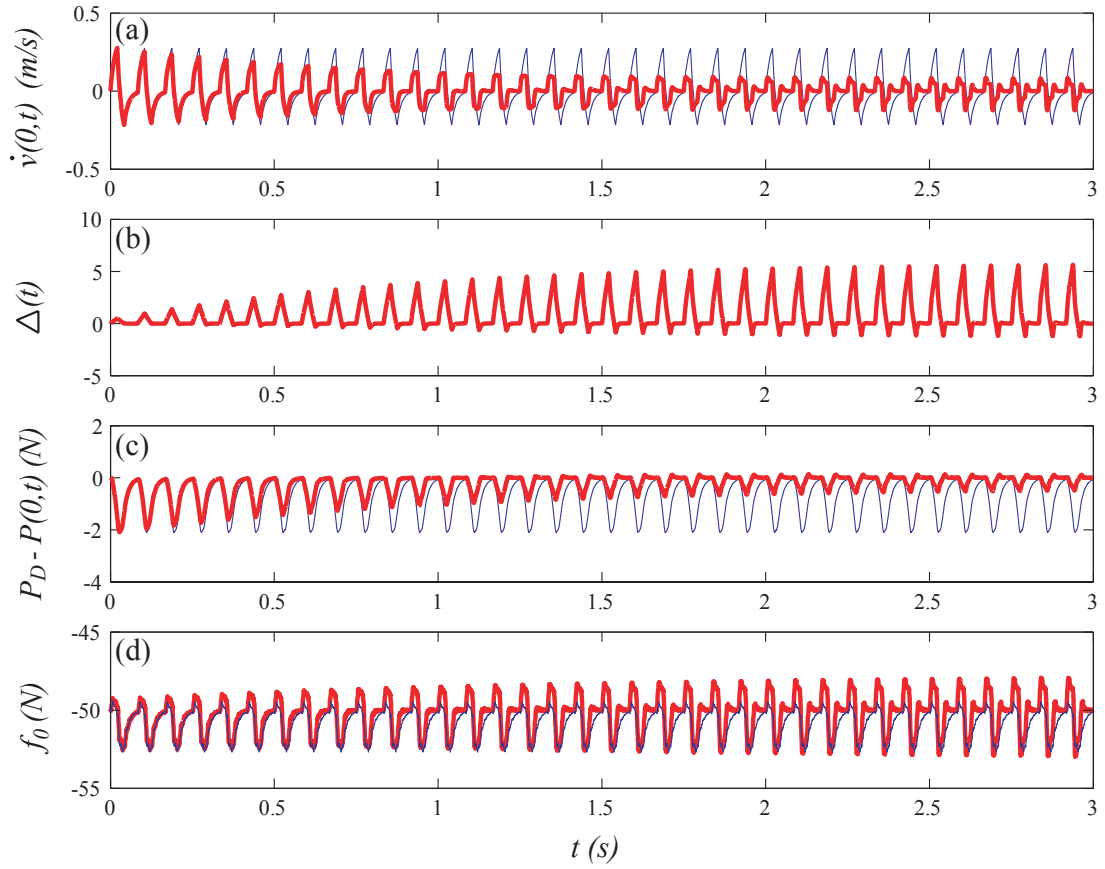
Fig. A.2. Closed loop response of the system for case 1 under PD (thin) and ILC (thick) control: (a) Velocity error, $\dot{v}(0,t)$, (b) Learning term, $\Delta(t)$, (c) Tension error, $P_D - P(0,t)$, and (d) Control effort, $f_0(t)$.

Fig. A.3. Open loop response of the system for case 2: (a) Disturbance position, $u_L(t)$, (b) Disturbance velocity, $\dot{u}_L(t)$, (c) Velocity error, $\dot{v}(0,t)$, and (d) Tension error, $P_D - P(0,t)$.

Fig. A.4. Closed loop response of the system for case 2 under PD (thin) and ILC (thick) control: (a) Velocity error, $\dot{v}(0,t)$, (b) Learning term, $\Delta(t)$, (c) Tension error, $P_D - P(0,t)$, and (d) Control effort, $f_0(t)$.
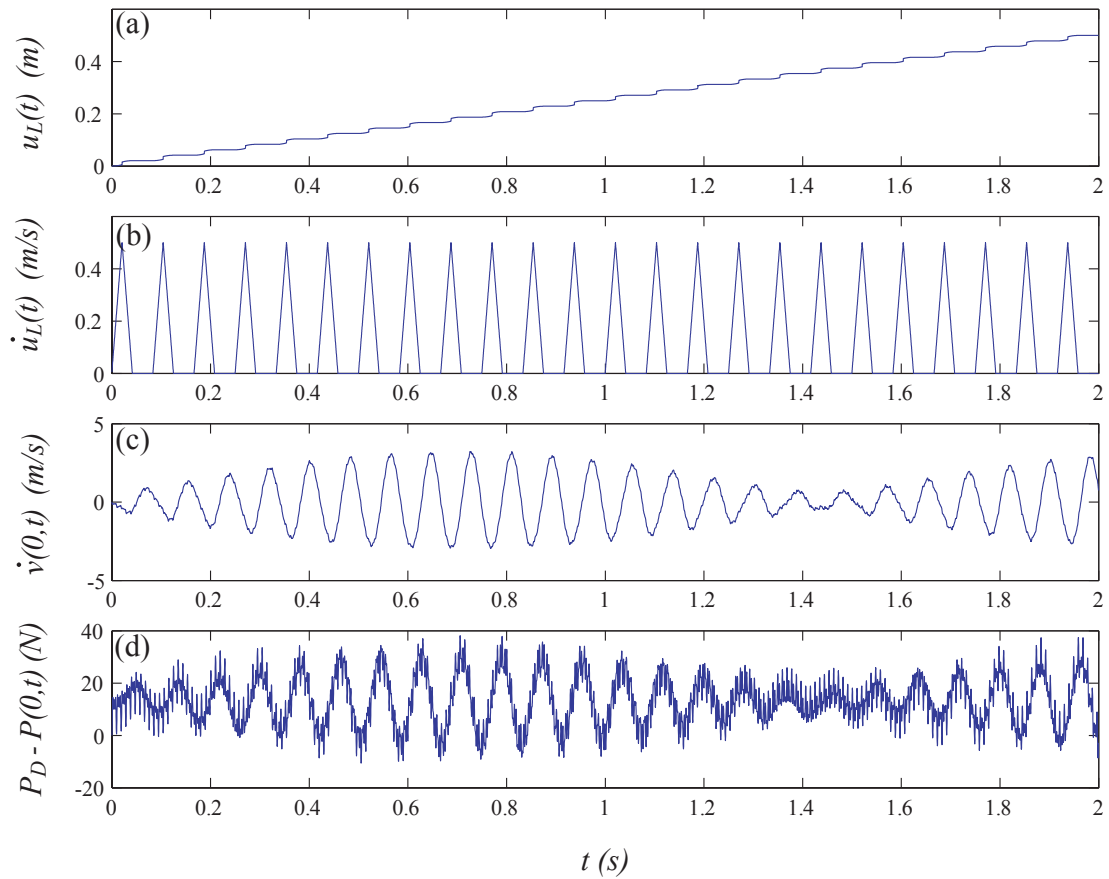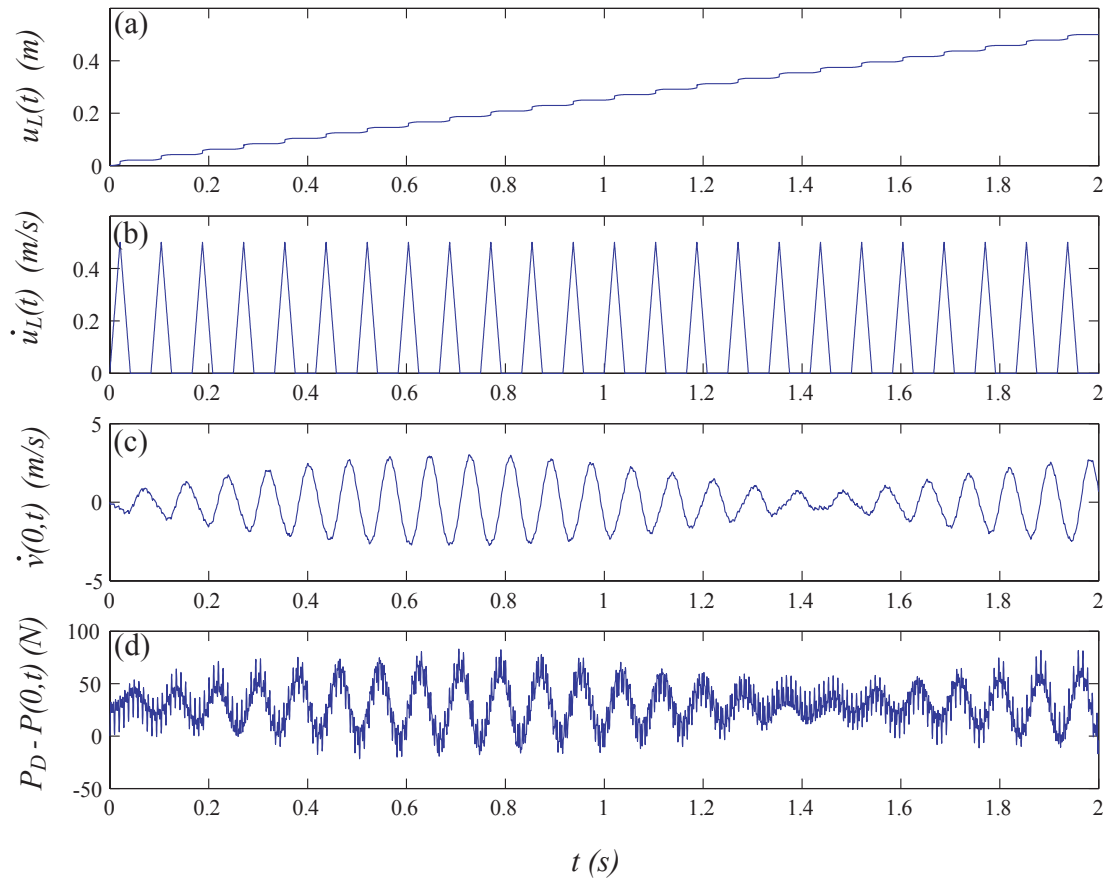
Fig. A.5. Open loop response of the system for case 3: (a) Disturbance position, $u_L(t)$, (b) Disturbance velocity, $\dot{u}_L(t)$, (c) Velocity error, $\dot{v}(0,t)$, and (d) Tension error, $P_D - P(0,t)$.
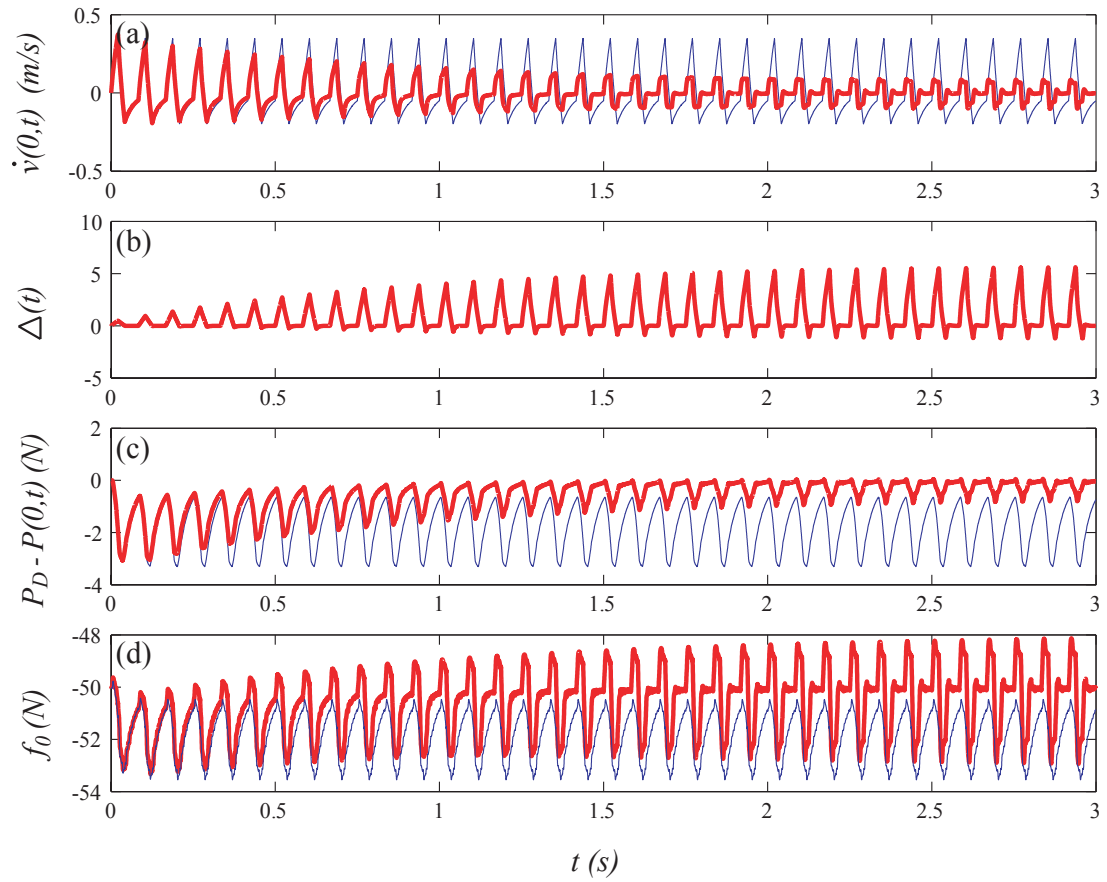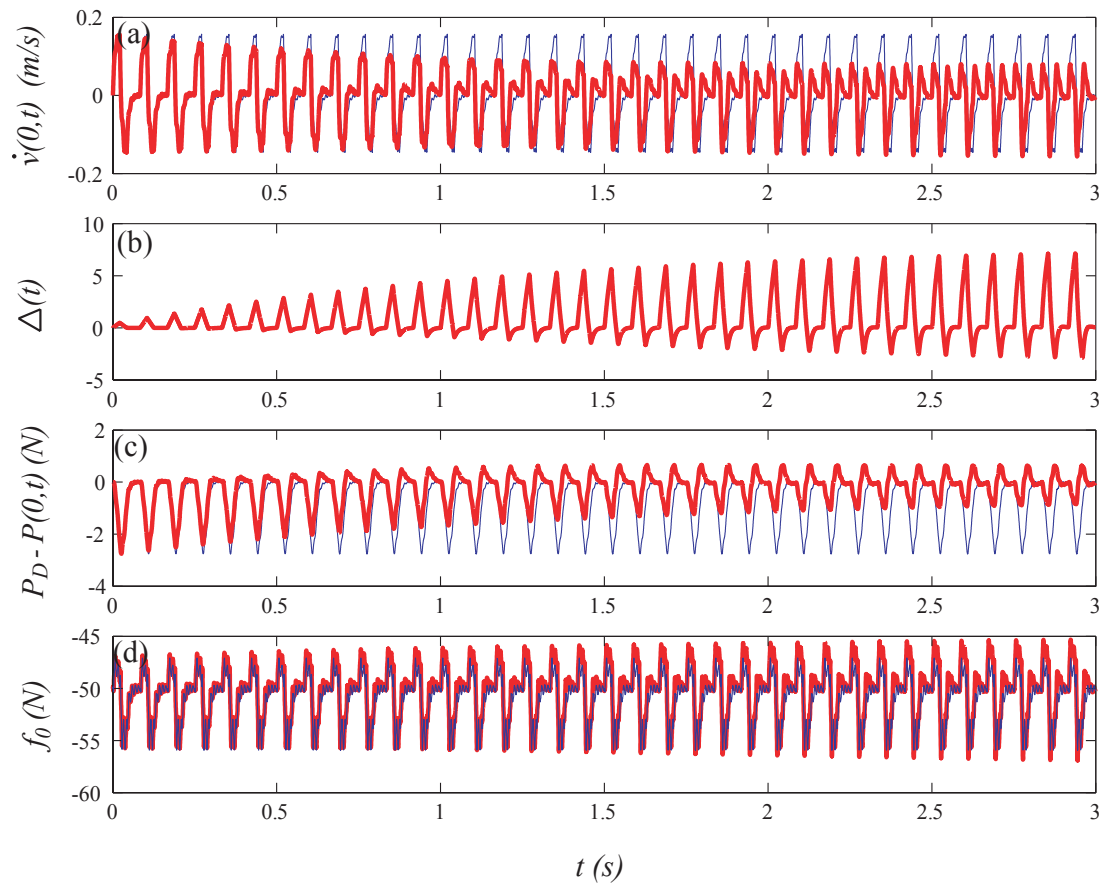
Fig. A.6. Closed loop response of the system for case 3 under PD (thin) and ILC (thick) control: (a) Velocity error, $\dot{v}(0,t)$, (b) Learning term, $\Delta(t)$, (c) Tension error, $P_D - P(0,t)$, and (d) Control effort, $f_0(t)$.

Fig. A.7.   Open loop response of the system for case 4: (a) Disturbance position, $u_L(t)$, (b) Disturbance velocity, $\dot{u}_L(t)$, (c) Velocity error, $\dot{v}(0,t)$, and (d) Tension error, $P_D - P(0,t)$.

Fig. A.8. Closed loop response of the system for case 4 under PD (thin) and ILC (thick) control: (a) Velocity error, $\dot{v}(0,t)$, (b) Learning term, $\Delta(t)$, (c) Tension error, $P_D - P(0,t)$, and (d) Control effort, $f_0(t)$.
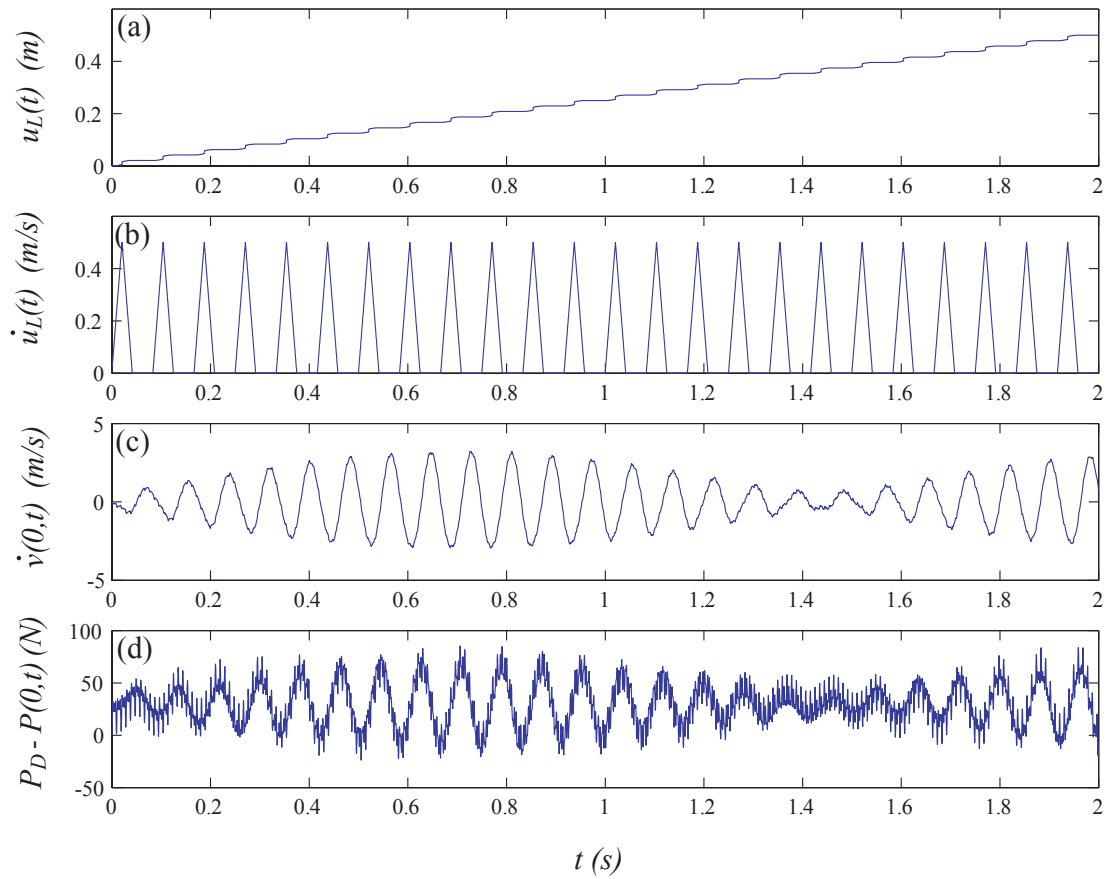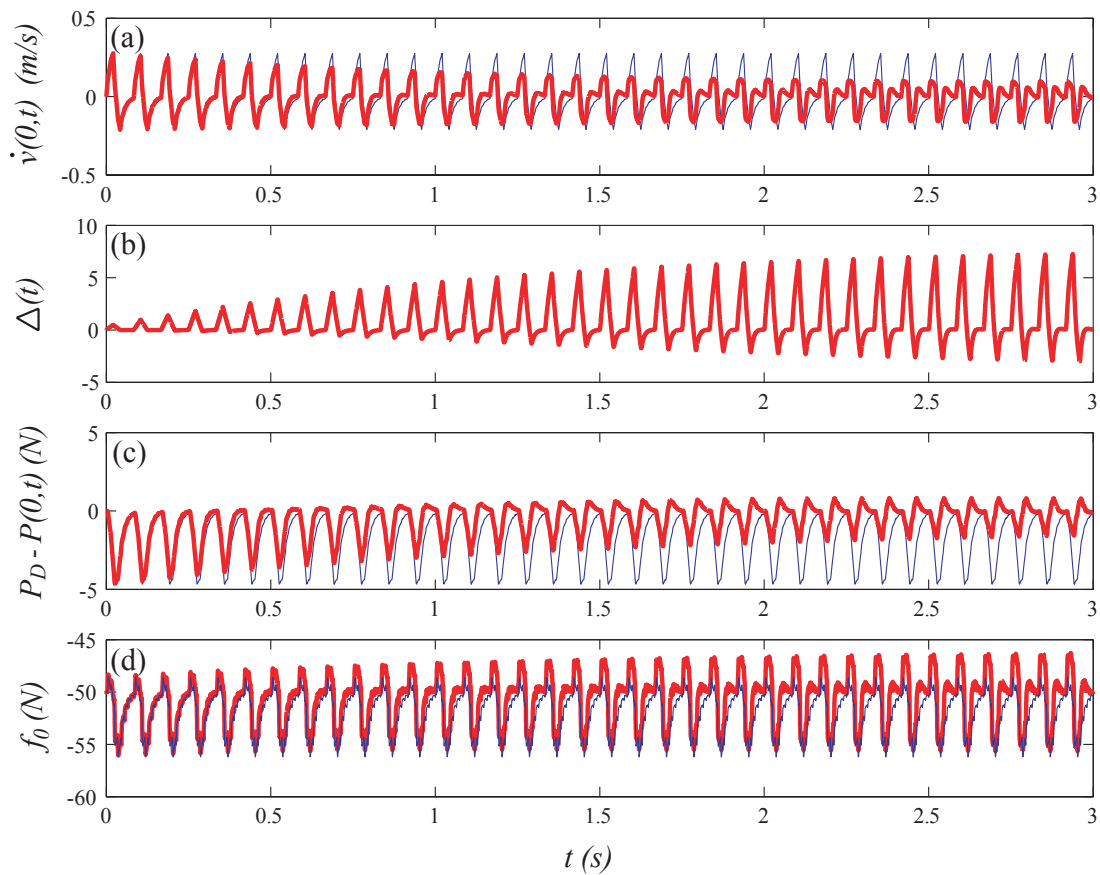
Appendix B

Lemmas for Repetitive Contact Imaging Proofs

Lemma 1: Given the model Eqs. (5.5) – (5.7), Lyapunov functional (5.10), and the control law (5.9), $\dot{V} \leq -\lambda V + \varepsilon$, where λ, $\varepsilon > 0$.

Proof: The time derivative of Eq. (5.11)

$$
\begin{aligned}
\dot{E}_s &= \beta_s \left(\int_0^L \dot{\omega} f \, dx - b \int_0^L \dot{\omega}^2 dx - EI \int_0^L \dot{\omega} \omega_{xxxx} \, dx + EI \int_0^L \dot{\omega}_{xx} \omega_{xx} \, dx \right) \\
&\leq \beta_s \left[-\left(b - \delta_1 \right) \int_0^L \dot{\omega}^2 dx + \frac{1}{\delta_1} \int_0^L f^2 dx - EI \dot{\omega}_x (0,t) \, \omega_{xx} (0,t) \right] \\
&= \beta_s \left\{ -\left(b - \delta_1 \right) \int_0^L \dot{\omega}^2 dx + \frac{1}{\delta_1} \int_0^L f^2 dx \right. \\
&\quad -EI \left[\left(\frac{1}{2\kappa} - \delta_6 \right) \dot{\omega}_x^2 (0,t) + \left(\frac{\kappa}{2} - \delta_7 \right) \omega_{xx}^2 (0,t) \right. \\
&\quad \left. \left. -\frac{1}{2\kappa} \eta^2 (t) + \left(\frac{\kappa}{2} - \frac{1}{\delta_6} - \frac{\kappa^2}{\delta_7} \right) \left(\frac{M_0}{EI} \right)^2 \right] \right\}
\end{aligned}
$$

using Eq. (5.8).

The time derivative of Eq. (5.12) simplifies to

$$
\begin{aligned}
\dot{E}_c &= \beta_c \rho \int_0^L \dot{\omega}^2 \, dx + \beta_c \int_0^L \omega \left(f - b\dot{\omega} - EI\omega_{xxxx} \right) \, dx \\
&= \beta_c \rho \int_0^L \dot{\omega}^2 \, dx + \dot{E}_{c1} + \dot{E}_{c2} + \dot{E}_{c3}.
\end{aligned} \tag{B.1}
$$

The terms in (B.1) simplify as follows

$$\dot{E}_{c1} = \beta_c \int_0^L \omega f \, dx \le \beta_c \delta_2 L^4 \int_0^L \omega_{xx}^2 \, dx + \frac{\beta_c}{\delta_2} \int_0^L f^2 dx. \tag{B.2}$$

$$\dot{E}_{c2} = -\beta_c b \int_0^L \omega \dot{\omega} \, dx \le \beta_c \delta_3 b L^4 \int_0^L \omega_{xx}^2 \, dx + \frac{\beta_c b}{\delta_3} \int_0^L \dot{\omega}^2 dx. \tag{B.3}$$

The third term

$$
\begin{aligned}
\dot{E}_{c3} &= -\beta_c EI \int_0^L \omega \omega_{xxxx} \, dx \\
&\le -\beta_c EI \left(1 - L\delta_4\right) \int_0^L \omega_{xx}^2 \, dx + \frac{\beta_c EI}{\delta_4} \omega_{xx}^2 \, (0,t) \tag{B.4}
\end{aligned}
$$

using the boundary conditions and inequality (2.8).

The time derivative of the final term in Eq. (5.10)

$$
\begin{aligned}
\frac{d}{dt}\left(\frac{1}{2} J \eta^2\right) &= \eta \left\{ -k_s \left\{ \dot{\omega}_x \, (0,t) - \kappa \left[\omega_{xx} \, (0,t) - \frac{M_0}{EI}\right]\right\} \right. \\
&\quad\quad\quad -EI\omega_{xx}(0,t) + J\kappa\dot{\omega}_{xx} \, (0,t) - \frac{k_s}{L} \dot{\upsilon}_L(t) \\
&\quad\quad\quad \left. +EI\omega_{xx}(0,t) - J\kappa\dot{\omega}_{xx} \, (0,t) - \frac{J}{L}\ddot{\upsilon}_L(t) \right\} \\
&= -k_s \eta^2 - \eta q(t), \tag{B.5}
\end{aligned}
$$

using Eqs. (5.4), (5.6), (5.8), and (5.9), where

$$q\left(t\right) = \frac{1}{L} \left[k_s \dot{\upsilon}_L(t) + J\ddot{\upsilon}_L(t) \right]. \tag{B.6}$$

The time derivative of the functional $V(t)$

$$
\begin{aligned}
\dot{V} \leq & -\left[\beta_s\left(b - \delta_1\right) - \beta_c\left(\rho + \frac{b}{\delta_3}\right)\right]\int_0^L \dot{\omega}^2 dx \\
& -\beta_c\left[EI\left(1 - L\delta_4\right) - \left(\delta_2 + \delta_3 b\right)L^4\right]\int_0^L \omega_{xx}^2 dx \\
& +\left(\frac{\beta_s}{\delta_1} + \frac{\beta_c}{\delta_2}\right)\int_0^L f^2 dx - \left(k_s - \delta_5 - \frac{\beta_s EI}{2\kappa}\right)\eta^2 + \frac{1}{\delta_5}q^2(t) \\
& -\left(\frac{1}{2\kappa} - \delta_6\right)\beta_s EI \dot{\omega}_x^2(0,t) - EI\left[\beta_s\left(\frac{\kappa}{2} - \delta_7\right) - \frac{\beta_c}{\delta_4}\right]\omega_{xx}^2(0,t) \\
& -\frac{\beta_s}{EI}\left(\frac{\kappa}{2} - \frac{1}{\delta_6} - \frac{\kappa^2}{\delta_7}\right)M_0^2 \\
\leq & -\lambda V + \varepsilon, \quad\quad\quad\quad\quad\quad\quad\quad\quad\quad\quad\quad\quad\quad\quad\quad\quad\quad (B.7)
\end{aligned}
$$

where, for sufficiently small β_s, β_c, δ_1, δ_2, δ_3, δ_4, δ_5, δ_6, and δ_7,

$$
\begin{aligned}
\varepsilon = & \left(\frac{\beta_s}{\delta_1} + \frac{\beta_c}{\delta_2}\right)\max_{t\in[0,\infty)}\int_0^L f^2 dx + \frac{1}{\delta_5}\max_{t\in[0,\infty)}\left[q^2(t)\right] \\
& +\frac{\beta_s}{EI}\left(\frac{1}{\delta_6} + \frac{\kappa^2}{\delta_7}\right)M_0^2 < \infty, \quad\quad\quad\quad\quad\quad\quad (B.8)
\end{aligned}
$$

$$
\varepsilon_1 = \beta_s\left(b - \delta_1\right) - \beta_c\left(\rho + \frac{b}{\delta_3}\right) > 0, \quad\quad\quad\quad\quad (B.9)
$$

$$
\varepsilon_2 = \beta_c\left[EI\left(1 - L\delta_4\right) - \left(\delta_2 + \delta_3 b\right)L^4\right] > 0, \quad\quad\quad (B.10)
$$

$$
\varepsilon_3 = k_s - \delta_5 - \frac{\beta_s EI}{2\kappa} > 0, \quad\quad\quad\quad\quad\quad\quad\quad (B.11)
$$

$$
\frac{1}{2\kappa} \geq \delta_6, \quad\quad\quad\quad\quad\quad\quad\quad\quad\quad\quad\quad\quad\quad (B.12)
$$

$$
\beta_s\left(\frac{\kappa}{2} - \delta_7\right) \geq \frac{\beta_c}{\delta_4}, \quad\quad\quad\quad\quad\quad\quad\quad\quad\quad (B.13)
$$

and

$$\lambda_3 = \frac{\min\left(\varepsilon_1, \varepsilon_2\right)}{\max\left(\rho, EI\right)},$$

$$\lambda = \frac{\min\left(\lambda_3, \varepsilon_3\right)}{\max\left(\lambda_3, \frac{J}{2}\right)}.$$

$\square$

Lemma 2: Given the model Eqs. (5.5) – (5.7), Lyapunov functional (5.10), and the control law (5.17) – (5.19) $\dot{V} \leq -\lambda V + \varepsilon + \eta\left[\triangle\left(t\right) - q\left(t\right)\right]$, where λ, $\varepsilon > 0$ and $q\left(t\right) = \frac{1}{L}\left[k_s \dot{v}_L(t) + J\ddot{v}_L(t)\right]$.

Proof: The time derivative of the boundary term

$$
\begin{aligned}
\frac{d}{dt}\left(\frac{1}{2}J\eta^2\right) &= \eta\left\{-k_s\left\{\dot{\omega}_x\left(0,t\right) - \kappa\left[\omega_{xx}\left(0,t\right) - \frac{M_0}{EI}\right]\right\}\right. \\
&\quad -EI\omega_{xx}\left(0,t\right) + J\kappa\dot{\omega}_{xx}\left(0,t\right) - \frac{k_s}{L}\dot{v}_L(t) + \Delta\left(t\right) \\
&\quad \left. +EI\omega_{xx}\left(0,t\right) - J\kappa\dot{\omega}_{xx}\left(0,t\right) - \frac{J}{L}\ddot{v}_L(t)\right\} \\
&= -k_s\eta^2 + \eta\left[\Delta\left(t\right) - q(t)\right], \qquad\qquad\text{(B.14)}
\end{aligned}
$$

using Eqs. (5.4), (5.6), (5.8), and (5.17).

The time derivative of Lyapunov functional

$$
\begin{aligned}
\dot{V} \;\leq\; & -\left[\beta_s\left(b-\delta_1\right)-\beta_c\left(\rho+\frac{b}{\delta_3}\right)\right]\int_0^L \dot{\omega}^2 dx \\
& -\beta_c\left[EI\left(1-L\delta_4\right)-\left(\delta_2+\delta_3 b\right)L^4\right]\int_0^L \omega_{xx}^2\, dx \\
& -\left(k_s-\frac{\beta_s EI}{2\kappa}\right)\eta^2-\left(\frac{1}{2\kappa}-\delta_6\right)\beta_s EI\dot{\omega}_x^2\,(0,t) \\
& -EI\left[\beta_s\left(\frac{\kappa}{2}-\delta_7\right)-\frac{\beta_c}{\delta_4}\right]\omega_{xx}^2\,(0,t)+\left(\frac{\beta_s}{\delta_1}+\frac{\beta_c}{\delta_2}\right)\int_0^L f^2 dx \\
& -\frac{\beta_s}{EI}\left(\frac{\kappa}{2}-\frac{1}{\delta_6}-\frac{\kappa^2}{\delta_7}\right)M_0^2+\eta\left[\Delta\left(t\right)-q(t)\right] \\
\;\leq\; & -\lambda_3 E+\varepsilon+\eta\left[\Delta\left(t\right)-q(t)\right] \\
\;\leq\; & -\lambda E+\varepsilon+\eta\left[\Delta\left(t\right)-q(t)\right]
\end{aligned}
$$

where, for sufficiently small β_s, β_c, δ_1, δ_2, δ_3, δ_4, δ_6, and δ_7,

$$
\begin{aligned}
\varepsilon \;=\; & \left(\frac{\beta_s}{\delta_1}+\frac{\beta_c}{\delta_2}\right)\max_{t\in[0,\infty)}\int_0^L f^2 dx+\frac{\beta_s}{EI}\left(\frac{1}{\delta_6}+\frac{\kappa^2}{\delta_7}\right)M_0^2<\infty, \\
\varepsilon_1 \;=\; & \beta_s\left(b-\delta_1\right)-\beta_c\left(\rho+\frac{b}{\delta_3}\right)>0, \\
\varepsilon_2 \;=\; & \beta_c\left[EI\left(1-L\delta_4\right)-\left(\delta_2+\delta_3 b\right)L^4\right]>0, \\
\varepsilon_3 \;=\; & k_s-\frac{\beta_s EI}{2\kappa}>0, \\
\frac{1}{2\kappa} \;\geq\; & \delta_6, \\
\beta_s\left(\frac{\kappa}{2}-\delta_7\right) \;\geq\; & \frac{\beta_c}{\delta_4},
\end{aligned}
$$

and

$$\lambda_3 = \frac{\min\left(\varepsilon_1, \varepsilon_2\right)}{\max\left(\rho, EI\right)},$$

$$\lambda = \frac{\min\left(\lambda_3, \varepsilon_3\right)}{\max\left(\lambda_3, \frac{J}{2}\right)}.$$

□

Appendix C

Additional Repetitive Contact Imaging Experiment

Another case is discussed for repetitive contact imager in order to show general applications. The profile of the object is steeper (see Fig. C.1) and the desired moment is $M_0 = 0.08$ Nm.

The yaw motor sweeps sinusoidally back and forth across the object under PID control at 0.1 Hz. The pitch axis is controlled using either the PDM control algorithm (5.9) or the RLC algorithm (5.17) – (5.19) with the control gains in Table C.1.

Table C.1.   Control Gains

Parameters	Values
k_s	0.0015
κ	200000
σ	2000

The yaw angle (Fig. C.2(a)) sweeps sinusoidally between 0 and 40 degrees. During the first 20 seconds, PDM control is applied. The maximum moment error (Fig. C.2(c)) is 0.016 Nm and the pitch axis (Fig. C.2(b)) does not move to accurately track the object shape. After $t = 20$ s, the RL controller is applied. The learning term $\Delta(t)$ for the period 20 s $\leq t \leq 30$ s uses error data from the previous period. The learning
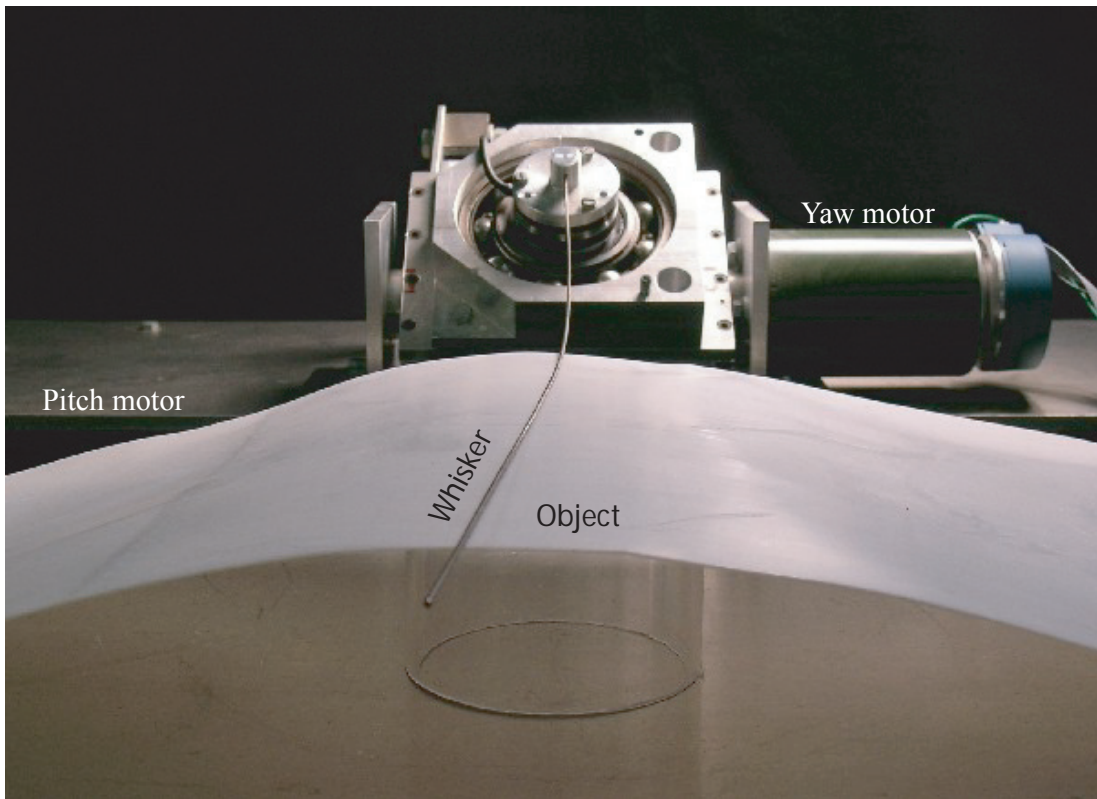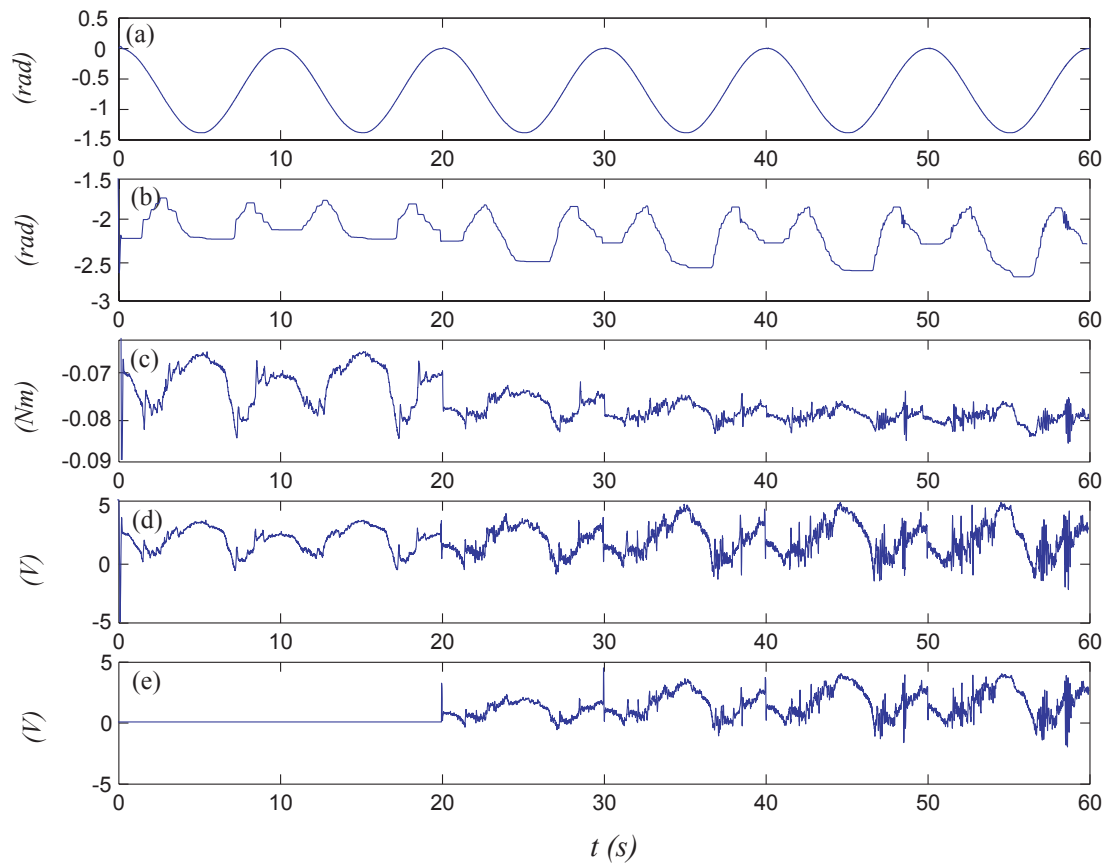
Fig. C.1.   Repetitive contact imaging experiment.

Fig. C.2.   Experiment results: (a) Yaw angle, (b) Pitch angle, (c) Hub bending moment $EIw_{xx}(0,t)$, (d) Control voltage, and (e) Learning term Δ.

term converges after a few cycles, the control voltage adjusts accordingly, and the moment error reduces to 0.005 Nm. The object profile can be discerned from the pitch trajectory.

The object in Fig. C.3, for example, had contact at the midpoint of the whisker. The stability and convergence of the response is unaffected by contact point location in these cases.
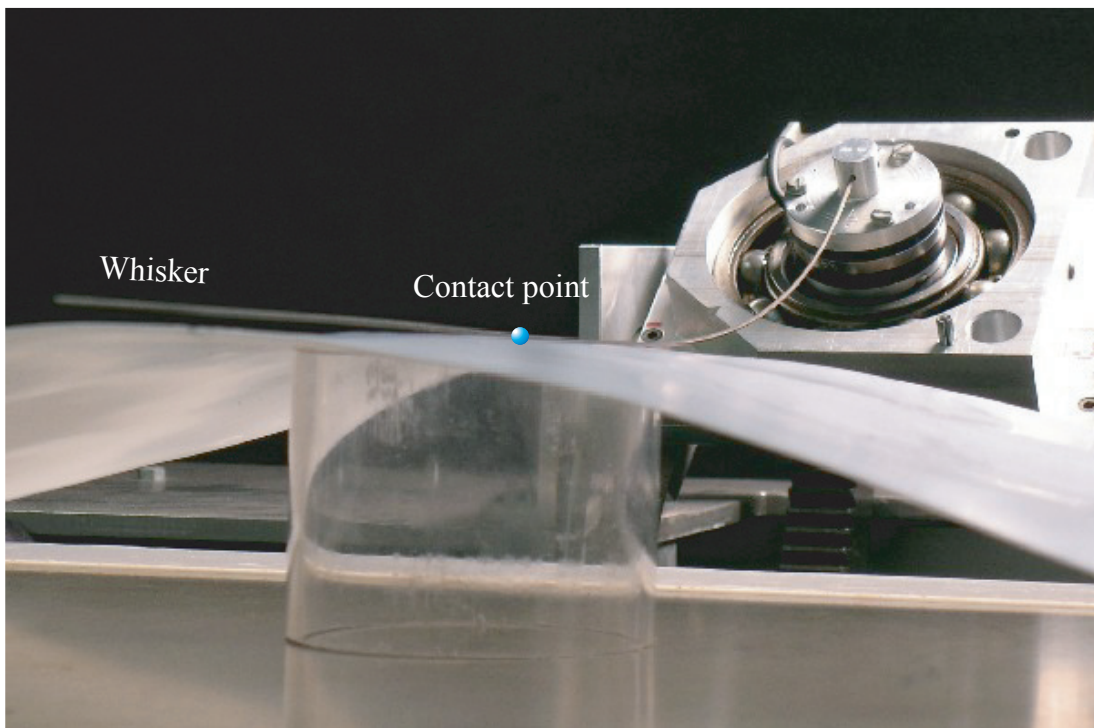
Fig. C.3.   Contact point.

References

[1] M. Al-Qassab and S. Nair. Wavelet-galerkin method for free vibrations of elastic cable. *Journal of Engineering Mechanics*, 129(3):350–357, 2003.

[2] T. AL-Towaim, A.D. Barton, P.L. Lewin, E. Rogers, and D.H. Owens. Iterative learning control - 2d control systems from theory to application. *Int. J. Control*, 77(9):877–893, 2004.

[3] K. Atkinson and W. Han. *Theoretical Numerical Analysis-A Functional Analysis Framework*. Springer, 2001.

[4] C.F. Baicu, C.D. Rahn, and B.D. Nibali. Active boundary control of elastic cables: Theory and experiment. *Journal of Sound and Vibration*, 198:17–26, 1996.

[5] M.J. Balas. Modal control of certain flexible dynamic systems. *SIAM Journal of Control and Optimization*, 16:450–462, 1978.

[6] A. Balogh, W.J. Liu, and M. Krstic. Stability enhancement by boundary control in 2-d channel flow. *IEEE Transactions on Automatic Control*, 46:1696–1711, 2001.

[7] B. Bamieh, F. Paganini, and M.A. Dahleh. Distributed control of spatially invariant systems. *IEEE Transactions on Automatic Control*, 47:1091–1107, 2002.

[8] H.T. Banks and D.J. Inman. On damping mechanisms in beams. *Journal of Applied Mechanics*, 58:716–723, 1999.

[9] M.D. Baumgart and L.Y. Pao. Robust control of tape transport systems with no tension sensor. *Proceedings of the IEEE Conference on Decision and Control*, 4:4342–4349, 2004.

[10] A. Baz. Boundary control of beams using active constrained layer damping. *Journal of Vibration and Acoustics*, 119(2):166–172, 1997.

[11] G.S. Bereksi. Implementation of a nonlinear control law for the magnetostrictive beam vibrations by an amplifier of current to current. *Proc. of Int. Conf. Modeling and Simulation of Microsystems, NanoTech2002*, 1:275–278, 2002.

[12] S. Biswas and N. Ahmed. Stabilization of a class of hybrid systems arising in flexible spacecraft. *Journal of Optimization Theory and Applications*, 50:83–108, 1986.

[13] B. Boulter and Z. Guo. A novel approach for on-line self-tuning web tension regulation. *Proceedings of the 4th IEEE Conference on Control Applications*, pages 91–98, 1995. Albany, NY.

[14] S. Burke and J. Hubbard. Distributed actuator control design for flexible beams. *Automatica*, 24(5):619–627, 1988.

[15] H. Canbolat, D. Dawson, C. Rahn, and P. Vedagarbha. Boundary control of a cantilevered flexible beam with point-mass dynamics at the free end. *Mechatronics*, 8:163–186, 1998.

[16] M. Cavalcanti and H. Oquendo. Frictional versus viscoelastic damping in a semilinear wave equation. *SIAM J. Control Optim.*, 42(4):1310–1324, 2003.

[17] C.T. Chen. *Linear System Theory and Design*. Oxford University, New York, third edition, 2000.

[18] A. Cheng and K. Morris. Well-posedness of boundary control systems. *SIAM J. Control Optim.*, 42(4):1244–1265, 2003.

[19] T.N. Clements and C.D. Rahn. Three-dimensional contact imaging with an actuated whisker. *2005 IROS*, pages 2587–2592, 2005.

[20] A. Collenz, F. De Bona, A. Gugliotta, and A. Soma. Large deflections of microbeams under electrostatic loads. *Journal of Micromech. Microeng*, 14:365–373, 2004.

[21] D.M. Dawson, M. Agarwal, and F. Zhang. daptive nonlinear boundary control of a flexible link robot arm. *IEEE Transactions of Robotics and Automation*, 15:779–787, 1999.

[22] F. dell'Isola, C. Maurini, and M. Porfiri. Passive damping of beam vibrations through distributed electric networks and piezoelectric transducers: Prototype design and experimental validation. *Smart Materials and Structures*, 13:299–308, 2004.

[23] W.E. Dixon, E. Zergeroglu, D.M. Dawson, and B.T. Costic. Repetitive learning control: A lyapunov-based approach. *IEEE Transactions on Systems, Man, and Cybernetics - Part B: Cybernetics*, 32(4):1019–1026, 2002.

[24] N. Ebler, R. Arnason, G. Michaelis, and N. D'Sa. Tension control: Dancer rolls or load cells. *IEEE Transactions on Industry Applications*, 29(4):727–739, 1993.

[25] R.F. Fung, J.W. Wu, and S.L. Wu. Exponential stabilization of an axially moving string by linear boundary feedback. *Automatica*, 35:177–181, 1999.

[26] W. Gawronski. *Dynamics and Control of Structures a Modal Approach.* Springer-Verlag, New York, 1998.

[27] A. Guesmia. A new approach of stabilization of nondissipative distributed systems. *SIAM J. Control Optim.*, 42(1):24–52, 2003.

[28] J.K. Hale and S.M.V. Lunel. *Introduction to Functional Differential Equations.* Springer-Verlag, New York, 1993.

[29] F. Hildebrand. *Advanced Calculus for Applications.* Prentice-Hall, Inc., New Jersey, 1976.

[30] G. Hillerstrom. Adaptive suppression of vibrations - a repetitive control approach. *IEEE Transactions on Control Systems Technology*, 4(1):72–78, 1996.

[31] P.C. Hughes. *Spacecraft Attitude Dynamics.* John Wiley & Sons, 1996.

[32] E.S. Hung and S.D. Senturia. Generating efficient dynamical models for microelectromechanical systems from a few finite-element simulation runs. *IEEE Journal of Microelectromechanical Systems*, 8:280–289, 1999.

[33] S. Joshi and C.D. Rahn. Position control of a flexible gantry crane: Theory and experiment. *Proceedings of American Control Conference*, pages 2820–2824, 1995.

[34] J. Jost. *Partial Differential Equations.* Springer, 2002.

[35] M. Kaneko, N. Kanayama, and T. Tsuji. Active antenna for contact sensing. *IEEE Transactions on Robotics and Automation*, 14(2):278–291, 1998.

[36] H.K. Khalil. *Nonliear Systems*. Prentice-Hall, Inc., New Jersey, third edition, 2002.

[37] H. Koc, D. Knittel, M. de Mathelin, and G. Abba. Modeling and robust control of winding systems for elastic webs. *IEEE Transactions of Control Systems Technology*, 10(2):197–208, 2002.

[38] V. Komornik. *Exact Controllability and Stabilization - the Multiplier Method*. John Wiley & Sons, 1994.

[39] S. Krylov and R. Maimon. Pull-in dynamics of an elastic beam actuated by continuously distributed electrostatic force. *Journal of Vibration and Acoustics*, 126:332–342, 2004.

[40] J.E. Lagnese. *Boundary Stabilization of Thin Plates*. SIAM, Philadelphia, third edition, 1989.

[41] T. Lam and R.B. Darling. Physical modeling of mems cantilever beams and the measurement of stiction force. *Proc. of Int. Conf. Modeling and Simulation of Microsystems, NanoTech2001*, 1:418–421, 2001.

[42] H. Laousy, C.Z. Xu, and G. Sallet. Boundary feedback stabilization of a rotating body-beam system. *IEEE Transactions of Automatic Control*, 41:241–244, 1996.

[43] Y. Li. *Adaptive Isolations of Vibration and Noise*. Clemson University, 2000.

[44] A.Q. Liu, X.M. Zhang, C. Lu, and Z.S. Liu. Optical and mechanical models for a variable optical attenuator using a micromirror drawbridge. *Journal of Micromech. Microeng*, 13:400–411, 2003.

[45] Y. Lu and W.C. Messner. Robust servo design for tape transport. *Proceedings of the 2001 IEEE International Conference on Control Applications*, 5-7:1014–1019, 2001.

[46] Z. Luo, B. Guo, and O. Morgul. *Stability and Stabilization of Infinite Dimensional Systems with Applications*. Springer, 1999.

[47] S.E. Lyshevski. *MEMS and NEMS, Systems, Devices, and Structures*. CRC Press, Washington DC, 2002.

[48] D. Mead. *Passive Vibration Control*. John Wiley & Sons, England, 1998.

[49] L. Meirovitch. *Principles and Techniques of Vibrations*. Prentice Hall, Upper Saddle River, New Jersey, 1997.

[50] S. Nagarkatti, F.Zhang, C. Rahn, and D. Dawson. Tension and speed regulation for axially moving materials. *Journal of Dynamic Systems, Measurement, and Control*, 122:445–453, 2000.

[51] P.R. Pagilla, I. Singh, and R.V. Dwivedula. Robust servo design for tape transport. *Proceedings of the 2001 IEEE International Conference on Control Applications*, 126(3):453–461, 2004.

[52] S. Pamidighantam, R. Puers, K. Baert, and H.A.C. Tilmans. Pull-in voltage analysis of electrostatically actuated beam structures with fixed-fixed and fixed-free end conditions. *Journal of Micromech. Microeng*, 12:458–464, 2002.

[53] J.A. Pelesko and D.H. Bernstein. *Modeling MEMS and NEMS*. Chapman & Hall/CRC, Washington DC, 2003.

[54] Z. Qu. *Robust Control of Nonlinear Uncertain Systems*. Wiley Interscience, New York, 1998.

[55] Z. Qu. An iterative learning algorithm for boundary control of a stretched moving string. *Automatica*, 38:821–827, 2002.

[56] C.D. Rahn. *Mechatronic Control of Distributed Vibration and Noise*. Springer, 2001.

[57] R.A. Russell. Using tactile whiskers to measure surface contours. *IEEE International Conference on Robotics and Automation*, 2:1295–1299, 1992.

[58] G.R. Scholz and C.D. Rahn. Profile sensing with an actuated whisker. *IEEE/ASME Transactions on Mechatronics*, 20(1):124–127, 2004.

[59] S.D. Senturia. *Microsystem Design*. Kluwer Academic Publishers, Massachusetts, 2001.

[60] I. Shames and C. Dym. *Energy and Finite Element Methods in Structural Mechanics*. Hemisphere Publishing Corporation, New Jersey, si units edition, 1991.

[61] N. Ueno, M. Svinin, and M. Kaneko. Dynamic contact sensing by flexible beam. *IEEE/ASME Transactions on Mechatronics*, 3(4):2354–264, 1998.

[62] H. Yang, J. Hong, and Z. Yu. Dynamics modelling of a flexible hub-beam system with a tip mass. *Journal of Sound and Vibration*, 266(4):759–774, 2003.

[63] S.M. Yang, J.A. Jeng, and Y.C. Liu. Controller desigh of a distributed slewing flexible structure - a frequency domain approach. *Journal of Dynamic Systems, Measurement, and Control*, 119:809–814, 1997.

[64] S.M. Yang and Y.C. Liu. Frequency domain control of single input/single output distributed parameter systems. *Journal of Guidance, Control, and Dynamics*, 19(3):736–738, 1996.

[65] S.M. Yang and C.D. Mote. Active vibration control of the axially moving string in the s domain. *ASME Journal of Applied Mechanics*, 58:189–196, 1991.

[66] H. Zhao and C. Rahn. On the boundedness of damped strings and beams with boundary and distributed inputs. *Proceedings of the 43rd IEEE Conference on Decision and Control*, 5:5077–5082, Dec. 2004.

[67] H. Zhao and C. Rahn. Stability of damped membranes and plates with distributed inputs. *Proceedings of the 24th American Control Conference*, pages 756–761, June 2005.

[68] H. Zhao and C. Rahn. Iterative learning velocity and tension control for axially moving materials. *Proceedings of ASME IDETC*, September 2005.

[69] H. Zhao, C. Rahn, and H. Canbolat. Repetitive control for an electrostatic micro-bridge actuator. *Proceedings of ASME IMECE*, Nov. 2005.

Vita

Haiyu Zhao received his BS degree in Engineering Physics and MS degree in Measuring and Testing Technology and Instruments at Tsinghua University in 1998 and 2001, respectively. In August 2001, he enrolled in the graduate program in Mechanical Engineering at the Pennsylvania State University and began to pursue his PhD. His research interests include vibration control, structural and system dynamics, and mechatronics. He is a member of IEEE and ASME and a member of Tau Beta Pi.